UNIVERSITY OF CALIFORNIA, SAN DIEGO

Mechanism-Based Inhibitors as Probes of Aerobic Flavoenzyme Activity

A Dissertation submitted in partial satisfaction of the
requirements for the degree
Doctor of Philosophy

in

Chemistry

by

Ian Phillip McCulloch

Committee in charge:

Professor Michael Burkart, Chair
Professor Nathan Gianneschi
Professor Elizabeth Komives
Professor Bradley Moore
Professor Charles Perrin

2016

The Dissertation of Ian Phillip McCulloch is approved, and it is acceptable in quality and form for publication on microfilm and electronically:

_____

_____

_____

_____

_____

Chair

University of California, San Diego

2016

DEDICATION

To my loving, supportive family members who instilled in me the gift of dogged stubbornness and a love of education.

EPIGRAPH

An expert is a person who has made all the mistakes

that can be made in a very narrow field.

—Niels Bohr

TABLE OF CONTENTS

LIST OF FIGURES

ACKNOWLEDGEMENTS

I would like to acknowledge Prof. Michael Burkart and Dr. James La Clair for their guidance and support. In addition to being an excellent advisor and committee chair, Prof. Burkart has overseen my growth as a scientist and has fostered an exceptional environment in which to conduct research. He also makes a tasty smoked brisket. Additionally, Dr. La Clair has helped mentor me in organic synthesis and has given me helpful personal motivational speeches, both stern and kind. I also thank my fellow members of the Burkart laboratory for their contribution to a harmonious, productive work environment. Additionally, I acknowledge my partner, Ryan Welsh, for his unwaivering support and encouragement throughout the tumult of my graduate school experience.

Chapter 4 entitled, "Fluorescent mechanism-based inhibitors of aerobic flavoenzymes," in full, is currently in review for publication of the material. The following authors contributed to this material: McCulloch, Ian; La Clair, James; Jaremko, Matt; Burkart, Michael. The dissertation author was the primary investigator and author of this material.

Chapter 5 entitled "Dissecting modular synthases: a complementary chemical and genetic approach," in full, is currently being prepared for submission for publication of the material. The following authors contributed to this material: McCulloch, Ian; Vickery, Christopher; Beld, Joris; Sonnenschein, Eva; Noel, Joseph; Burkart, Michael. The dissertation author was a primary co-investigator and co-author of this material.

VITA

2010	Bachelor of Arts in Chemistry, Reed College, Portland
2010-2016	Graduate Teaching Assistant, Department of Chemistry and Biochemistry, University of California, San Diego
2013	Masters of Science in Chemistry, University of California, San Diego
2016	Doctor of Philosophy in Chemistry, University of California, San Diego

PUBLICATIONS

McCulloch, Ian; La Clair, James; Jaremko, Matt; Burkart, Michael "Fluorescent mechanism-based probes of aerobic flavoenzyme activity," 2016, in review for publication.

ABSTRACT OF THE DISSERTATION

Mechanism-Based Inhibitors as Probes of Aerobic Flavoenzyme Activity

by

Ian Phillip McCulloch

Doctor of Philosophy in Chemistry

University of California, San Diego, 2016

Professor Michael Burkart, Chair

Aerobic flavoenzymes are flavin-dependent enzymes that use oxygen to catalyze a diverse set of redox reactions, and they are essential to the proper function of biosynthetic secondary metabolism. Along with other enzymatic domains found in biosynthesis, flavoenzyme domains are attractive targets to investigate, owing to their role in processing substrates within modular synthases and with other protein domains. In this dissertation, a review of flavoenyzmes in biosynthesis and applications in chemical biology is presented. Additionally, we report the successful development of mechanism-based inhibitors and probes of aerobic flavoenzyme activity.

Chapter 1

Introduction to Aerobic Flavoenzymes

1.1 Significance of Flavoenzymes in Metabolism

Flavin-dependent enzymes, or flavoenzymes, are an integral component of metabolism for all living organisms. Plants, fungi, and bacteria can regularly produce flavin metabolites, but higher order eukaryotes require it from their diet or from microbiotic symbionts.[1] In fact, the essential provision of flavin molecules in human nutrition is exemplified by the commonly known name of the metabolic precursor, riboflavin, as vitamin B2 that is a ubiquitous component of many food sources and dietary supplements. Flavins are coenzymes, meaning they are non-protein organic molecules that are required for enzymatic activity. While essential to the proper function of primary metabolism, or metabolic activity needed to sustain life, the flavin coenzyme also plays a pivotal role in facilitating secondary metabolism,[2] which is metabolic activity that not necessary for life but may impart a competitive or evolu-

tionary advantage within the ecosystem of the given organism.

Secondary metabolism propagates a diverse array of chemical small molecules, including polyketide, nonribosomal peptide, terpenoid, and alkaloid secondary metabolites; these molecules have provided immense utility to humans for medicinal and commercial purposes,[3] at which point they are often called natural products or biosynthetic metabolites. The focus of our research in this dissertation is to develop molecular tools to target the enzyme activity of flavoenzymes in secondary metabolism. The strategy centers on the development of novel mechanism-based inhibitors as probes to elucidate the activity, structural properties, and interaction with protein partners of flavoenzymes, a strategy consistently employed by the Burkart research group with a number of biosynthetic domains, including carrier protein (CP),[4] ketosynthase (KS),[5] dehydratase (DH),[6] and enoyl reductase (ER) domains.[7] With a better understanding of the structure-activity relationship that guides the role of flavoenzyme domains in the biosynthesis of natural products, we can endeavor to manipulate or engineer these pathways to our advantage.

1.2 Properties of Flavins as Coenzymes

The physical and chemical properties of flavin molecules provide a rationale for why these coenzymes are so crucial for metabolism. By visible light, flavins and flavoenzymes that harbor the flavin coenzyme are strikingly yellow in appearance. In fact, the name, flavin, originates from the Latin word *flavus*, meaning yellow, owing to the characteristic fluorescent yellow color that fully oxidized flavin molecules assume. The yellow color stems from the complex electron distribution consisting of conjugated p-orbitals as a redox-active quinone, which is responsible for the catalytic activity of

the flavin.

Flavin molecules are redox-active catalytic coenzymes of enzymatic activity. They comprise a nested set of small molecules, including flavin adenosine dinucleotide (FAD) and flavin mononucleotide (FMN), both metabolically derived from riboflavin (Figure 1.1).[8] Each of these molecules contains an identical tricyclic ring structure, dimethyl isoalloxazine, that may exist in five accessible protonation and redox states under physiological conditions.[9] These states include the oxidized quinone (Fl_{OX}), the anionic semiquinone ($Fl^{\cdot -}$, ASQ,), the neutral semiquinone ($FlH^{\cdot}$, NSQ), the anionic hydroquinone (FlH^{-}, AHQ) and the fully protonated, reduced hydroquinone (FlH_2) (Figure 1.2). The fully-conjugated quinone species may spontaneously undergo reduction in a one electron manifold with an electron donor resulting in a semiquinone species either as the ASQ or the NSQ species, depending on protonation state within the enzyme pocket. The ASQ state harbors a radical at the N5 position and an anion at the N1 position, whereas radical electron density resides primarily at the C4a position for the NSQ state. Reduction by an additional electron results in the fully reduced hydroquinone state.

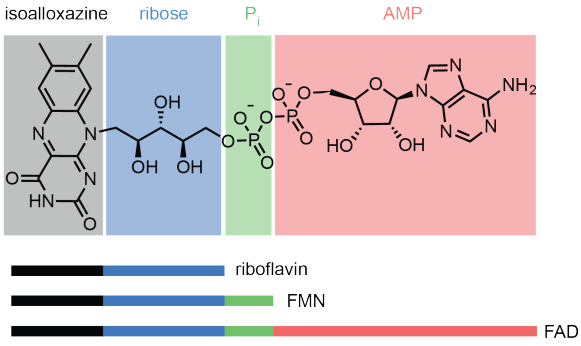

Figure 1.1: Structures of flavins and their color-coded constituent substructures. Individual components are the isoalloxazine ring (black), ribose (blue), phosphate (P_i, green), and adenosine monophosphate (AMP, red). Flavin molecular structures include riboflavin (black, blue), FMN (black, blue, green), and FAD (black, blue, green, red).

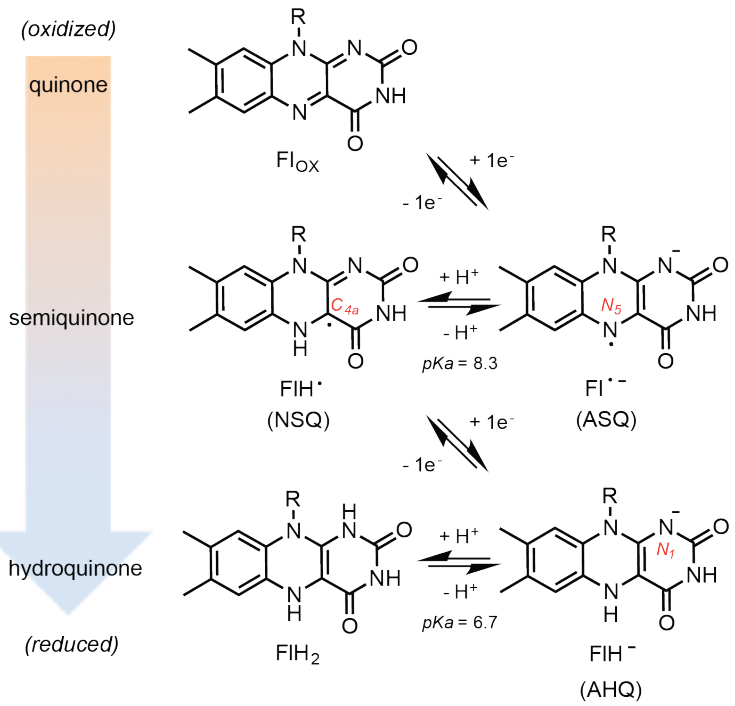

Figure 1.2: Redox and protonation states of the isoalloxazine ring in flavin molecules. The quinone may be reduced by 1 electron transfer to access the anionic semiquinone (ASQ), the neutral semiquinone (NSQ), or the anionic hydroquinone (AHQ) state. Full reduction and protonation affords the hydroquinone state.

The accessibility of redox and protonation states allows flavin coenzymes to facilitate one and two electron reduction and oxidation chemistry on a variety of enzyme substrates. The catalytic cycle of flavoenzymes is often initiated by the reductive half reaction, where the Fl_{OX} quinone participates in the addition of various substrates by electron donors (Figure 1.3). A two electron transfer from a hydride which adds to the N5 atom is a common motif, where the hydride transfer may be accomplished by reactive nicotinamide coenzymes (NAD(P)H). Typical of anabolic pathways, numerous examples of flavoenzyme activity have demonstrated similar or slightly higher affinity of NADPH over NADH, but both coenzymes are typically functional. The Flox species may also directly act with the enzyme substrate in a

redox-coupled reaction (Figure 1.4), where a substrate donates an acidic proton as a hydride to Fl_{OX}, oxidizing the substrate in turn. This reactivity initiates a reductive half reaction in the catalytic cycle typical of dehydrogenases, a subclass of oxidase flavoenzymes, whereas the reverse reaction is typical of reductase flavoenzymes. The N5 position is also known to be the site of addition for carbanions, which is consistent with nitroethane adducts to **D**-amino acid oxidase.[10] The second site of addition to the Fl_{OX} quinone takes place at the C4a bridgehead, where soft nucleophile heteroatoms such as sulfides have demonstrated addition.[11]

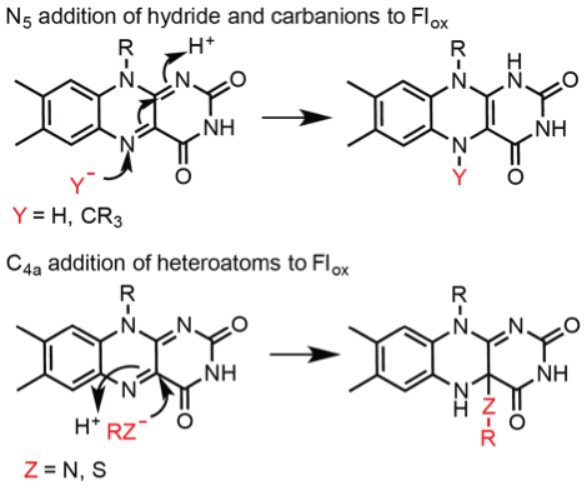

Figure 1.3: Addition of substrates to the fully oxizided quinone. Additions proceed by substrate addition to either N5 or C4a position of the Flox scaffold.

On the other hand, the reoxidative half reaction also plays a crucial role in flavoenzyme catalysis. Of particular interest is the reaction of FlH_2 with dioxygen, which may react in one of two pathways. In the first pathway, dioxygen is converted to superoxide by transfer of an electron from FlH_2 to afford the accessible NSQ state after the loss of one proton (Figure 1.5). Radical addition at the NSQ C4a bridgehead with superoxide gives the C4a flavin peroxide (Fl-C4a-OO^-) and a flavin hydroperoxide conjugate acid (Fl-C4a-OOH) with a pKa of 10. In second pathway,

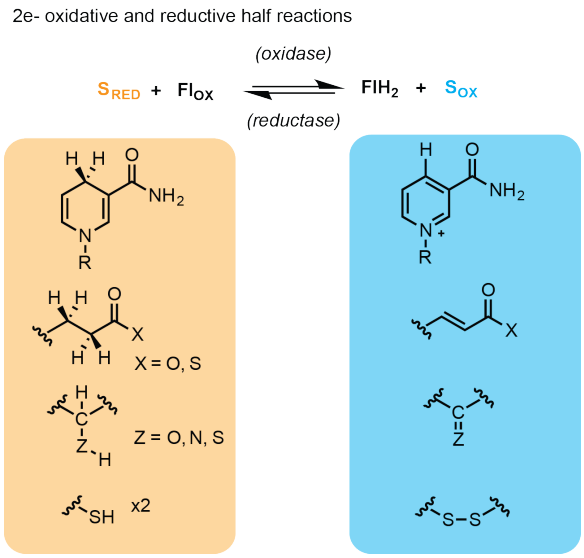

Figure 1.4: Oxidative and reductive half reactions with various flavoenzyme substrates.

the same superoxide is generated by donation of one electron from FlH_2. However, loss of two protons furnishes the ASQ species (Figure 1.6), which reacts with superoxide at the N5 position to give a transient N5 flavin hydroperoxide (Fl-N5-OOH). The N5 hydroperixde releases water by an umpolung-like mechanism to afford the more stable oxoammonium (Fl-N5-O) species. Flavoenzymes that react with dioxygen in either of these pathways are given the term *aerobic* flavoenzymes, as they require molecular oxygen to perform catalysis.

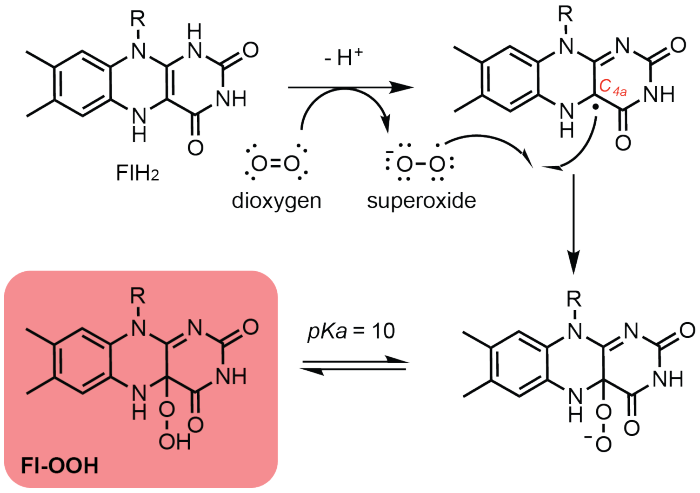

Figure 1.5: Formation of Fl-C4a-OOH by 1e- mechanism with dioxygen.

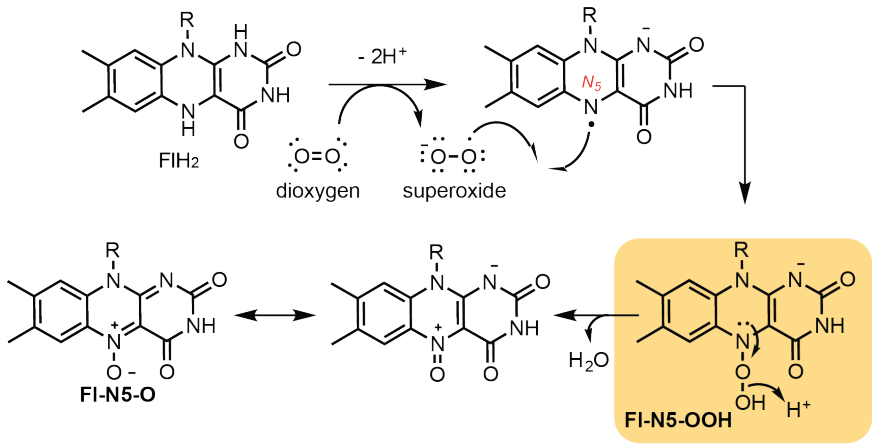

Figure 1.6: Formation of Fl-N5-OOH by 1e- mechanism with dioxygen.

1.3 Aerobic Flavoenyzmes in Biosynthesis

Aerobic flavoenzymes have a wide variety of enzymatic activity and substrates on which they act. They are sometimes simply called, "tailoring enzymes," which belies the robust and highly coordinated repertoire of their activity in modular biosynthetic processes. True to their aerobic name, they all incorporate dioxygen by reaction with the reduced hydroquinone state to access a reactive flavin hydroperoxide state (Fl-OOH). In these processes, their catalytic cycles are generally consistent with three distinct types: oxidases, monooxygenases, and halogenases (Figure 1.7). While there may be some variation in exact chronological sequence of substrate and flavin reactivity, the majority of examples in secondary metabolite biosynthesis fall into this classification scheme.

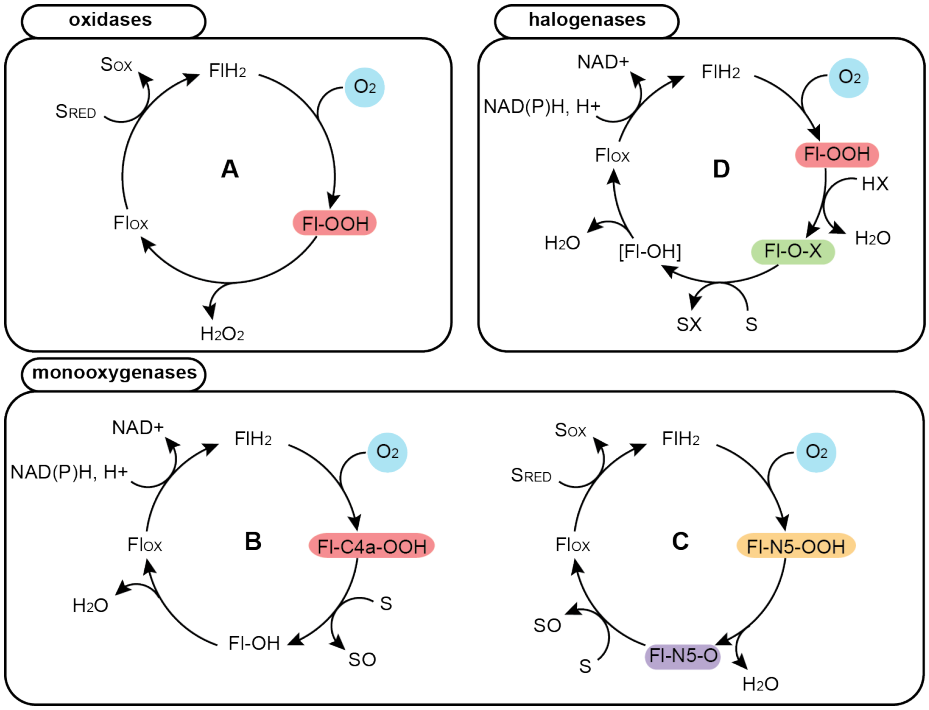

Figure 1.7: Catalytic cycles of aerobic flavoenzymes for oxidases, monooxygenases, and halogenases. A) The oxidase cycle incorporates dioxygen (cyan) to form Fl-OOH (red). B) Monooxygenases.

First among them is the oxidase type, (Figure 1.7a) previously mentioned, which uses the redox-coupled reductive half reaction of Flox to accept a hydride from a substrate (S_{RED}), allowing oxidation of said substrate (S_{OX}) and providing the FlH_2 hydroquinone. The hydroquinone then may react with dioxygen in a reoxidative half reaction to furnish a flavin peroxide species, which may release hydrogen peroxide to reestablish the Flox state. In the biosynthesis of secondary metabolites, examples of this enzyme type include desaturases, amine oxidases, alcohol oxidases and thiol oxidases. The oxidase flavoenzyme activity is notably featured in the biosynthesis of indigoidine by blue pigment synthase A (BpsA), a nonribosomal peptide synthetase (NRPS) endogenous to *Streptomyces lavendulae* (Figure 1.8). The oxidase domain in BpsA desaturates a glutamine tethered to a thiolation (T) domain by phosphopantheine, which cyclizes by a TE domain to give a monomeric unit. Autooxidation or enzyme assisted oxidation of this unit gives the blue pigment, indigoidine. A total synthesis of indigoidine has demonstrated that autooxidation is possible with precursor monomer units.[12] A chemical and genetic investigation into the activity of these enzymatic domains is provided in Chapter 5.

The second type of aerobic flavoenzymes in secondary metabolite biosynthesis is the monooxygenase class (Figure 1.7). Monooxygenases initiate catalysis by the reoxidative half reaction with dioxygen, to give a reactive flavin peroxide intermediate either as the Fl-C4a-OOH (Figure 1.7b) or Fl-N5-OOH species (Figure 1.7c). For the Fl-C4a-OOH monooxygenase pathway, the flavin peroxide itself directly reacts to transfer the terminal oxygen atom of the peroxide to the substrate, also called monooxygenation of that substrate, rendering the flavin as a hydroxy-C4a-species (Fl-OH). Protonation and release of the hydroxyl group as water gives

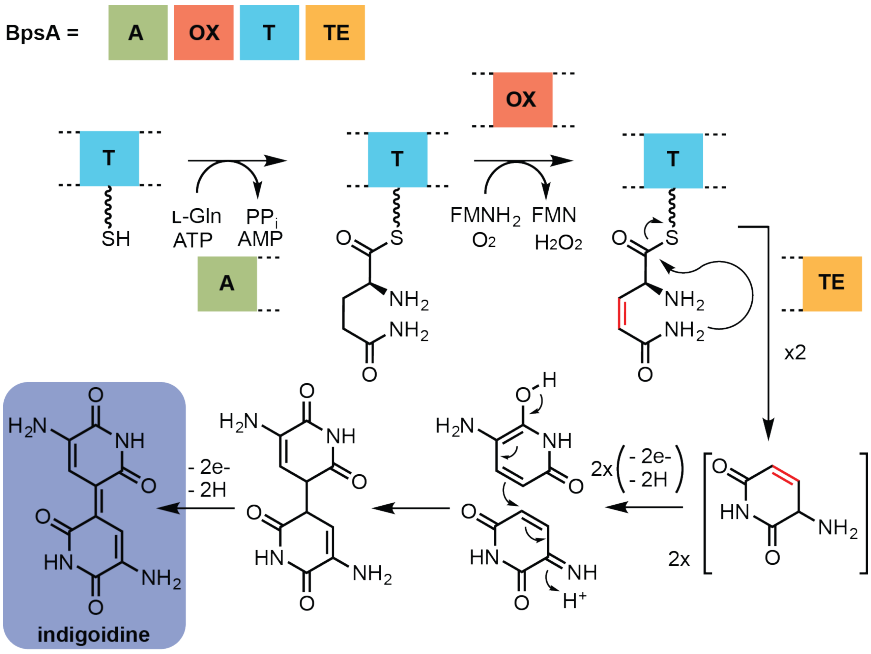

Figure 1.8: Modular biosynthesis of indigoidine with BpsA. The adenylation (A) domain loads L-glutamine onto the thiolation (T) domain. The oxidase (OX) domain desaturates the tethered cargo, and thioesterase (TE) domain condenses it into a reactive monomer that oxidizes to form indigoidine.

the oxidized flavin, which may undergo reduction with NAD(P)H to return to the hydroquinone state. Monooxygenase flavoenzymes can perform an impressive list of diverse chemical reactions, including hydroxylation of aromatic and unsaturated substrates,[13] Baeyer-Villiger with carbonyl-containing substrates,[14] epoxidation of unsaturated compounds,[15] and monooxidation of soft nucleophiles such as amines and thiols (typically performed as catabolic processes in liver tissue).[16] A notable example is cyclohexanone monooxygenase (CHMO), which performs a Baeyer-Villiger reaction on cyclic ketones to yield cyclic esters (Figure 1.9a).[14a]

For the Fl-N5-OOH pathway, the fate of the peroxy species is quickly resolved to the more stable Fl-N5-O state that contains an oxoammonium ion at N5 (Figure 1.6). This reoxidative half reaction is consistent with the flavoenzyme, EncM, in the biosynthesis of enterocin (Figure 1.9b), an antibiotic isolated from various

streptomycetes.[17] EncM reacts with a triketone portion of a polyketide substrate, where the enolate at C12 attacks the oxoammonium FAD-N5-O species, and the oxygen attached to N5 is released with the substrate to obtain a hydroxyl group at C12 and the FADox state of the coenzyme. Interestingly, EncM does not bear a nicotinamide coenzyme binding site, unlike many monooxygenases, and instead abstracts an acidic hydride from C12 of the substrate to regenerate the reduced hydroquinone. A Favorskii-type rearrangement then occurs to lead to enterocin scaffold. This dual oxidation pattern of the flavin puts EncM in a class of its own, where it has the oxidative half reaction of a monooxygenase and the reductive half reaction of an oxidase.

The last type of aerobic flavoenzyme is the halogenase (Figure 1.7d). The halogenase follows a very similar catalytic pathway to the Fl-C4a-OOH monooxygenase pathway. The notable difference is the facilitation of halogen anions such as chloride and bromide, to displace the terminal oxygen of the peroxide species creating a reactive hypohalite (Fl-OX) species. Flavin-dependent halogenases include chlorinases and brominases, but exclude rarely encountered fluoridases that are only known to be mediated by other cofactors.[18] A notable example of a halogenase is a chlorinating flavoenzyme, PltA, in the biosynthesis of the antifungal compound, pyoluteorin (Figure 1.10a), which is produced by *Pseudomonas fluorescens* Pf-5.[19] Pyluteorin is biosynthesized, in part, by the loading of **L**-proline to PltL, a peptidyl carrier protein (PCP), and desaturation by the flavin-dependent oxidase, PltE, to afford a tethered pyrrole. Subsequent chlorination by the chlorinase PltA provides the bischloropyrrole moiety that leads to pyoluteorin. In the PltA active site (Figure 1.10b), a lysine residue proximal to the flavin (10 Å) receives the halogen after nucleophilic attack

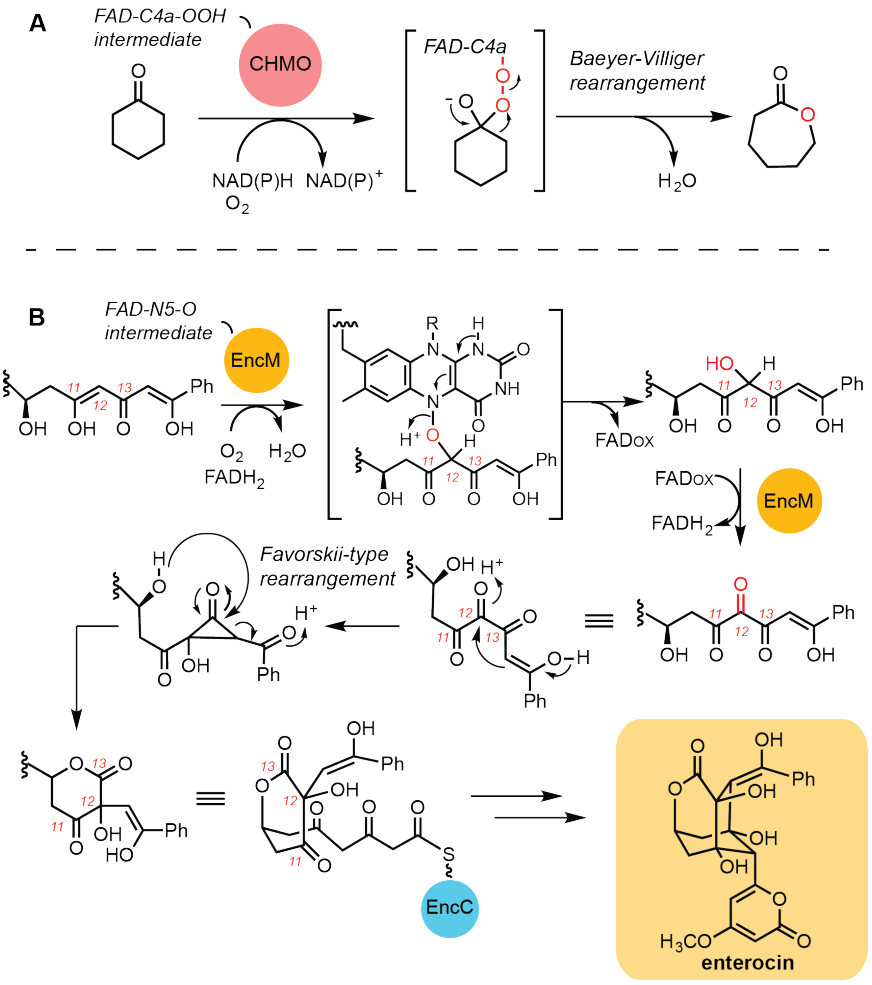

Figure 1.9: Monooxygenase pathways for Fl-C4a-OOH and Fl-N5-OOH intermediates.

of a released hypochlorious acid from the reactive FAD-O-Cl species.[20] This tradeoff of electrophilic chloride affords a long-lived ($t_{1/2}$ = 63 h at 4°C) lysine chloramine (Lys-εNH-Cl) intermediate, the stability of which has been demonstrated in similar chlorinase structures, such as RebH in the biosynthesis of rebeccamycin.[21] Halogenation then procedes by electrophilic aromatic substitution, owing to the electrophilicity of the lysine chloramine species with aromatic substrates.

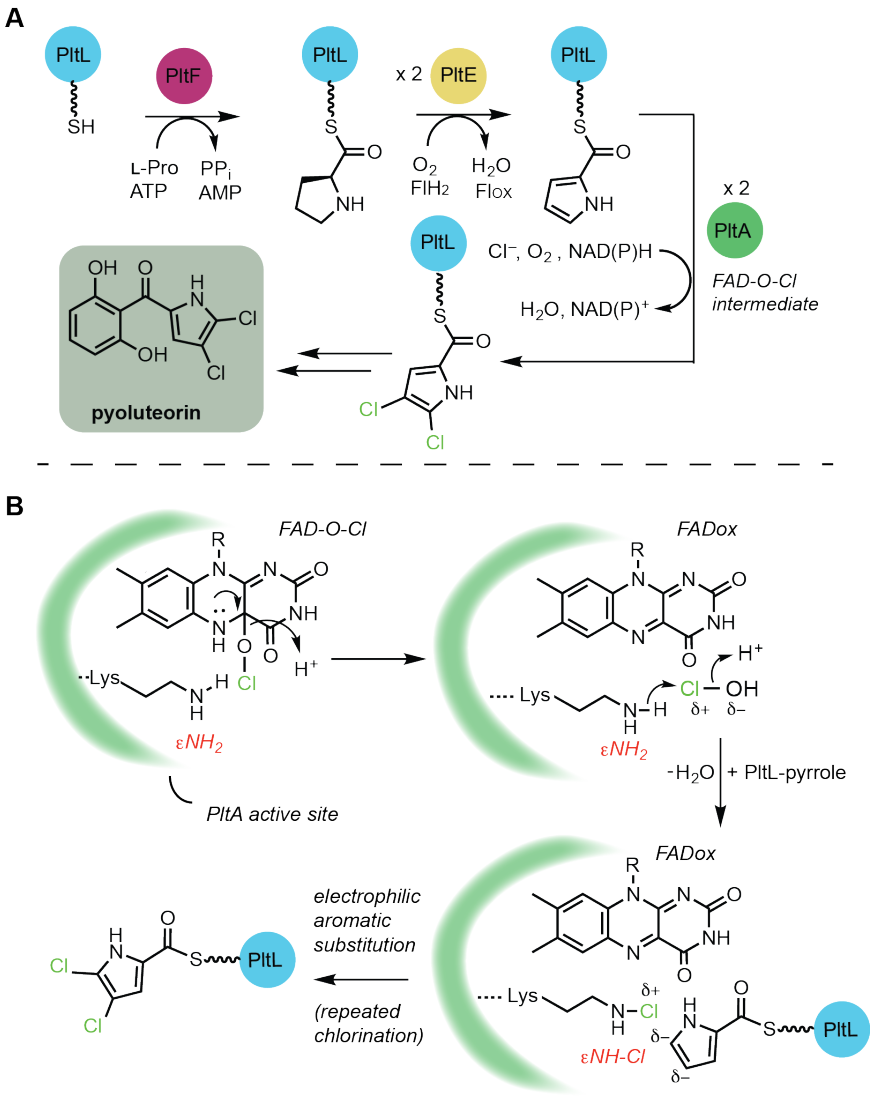

Figure 1.10: Biosynthesis of pyoleuteorin by chlorination of a tethered pyrrole.

1.4 Concluding Remarks

Aerobic flavoenzymes contribute to a vast array of natural product biosynthetic pathways, many of which produce small molecules of considerable interest to human utility. Featured in this chapter was a discussion of the most exhaustive classification of various aerobic flavoenzymes that are prominent in biosynthesis. Also featured, were relevant examples of their vast array of activity. The subsequent chapter of this dissertation will review current applications of flavoenzymes from a chemical biology perspective.

1.5 References

1. Barile, M.; Anna Giancaspero, T.; Brizio, C.; Panebianco, C.; Indiveri, C.; Galluccio, M.; Vergani, L.; Eberini, I.; Gianazza, E., *Curr. Pharm. Des.* **2013**, *19* (14), 2649-2675.

2. Walsh, C. T.; Wencewicz, T. A., *Nat. Prod. Rep.* **2013**, *30* (1), 175-200.

3. Dewick, P. M., Medici "Natural Products: A Biosynthetic Approach, Second Edition." 2001.

4. (a) Worthington, A. S.; Rivera, H.; Torpey, J. W.; Alexander, M. D.; Burkart, M. D., *ACS Chem. Biol.* **2006**, *1* (11), 687-91; (b) Worthington, A. S.; Burkart, M. D., *Org. Biomol. Chem.* **2006**, *4* (1), 44-6.

5. (a) Worthington, A. S.; Porter, D. F.; Burkart, M. D., *Org. Biomol. Chem.* **2010**, *8* (8), 1769-72; (b) Worthington, A. S.; Hur, G. H.; Meier, J. L.; Cheng, Q.; Moore, B. S.; Burkart, M. D., *ChemBioChem* **2008**, *9* (13), 2096-103.

6. (a) Nguyen, C.; Haushalter, R. W.; Lee, D. J.; Markwick, P. R.; Bruegger, J.; Caldara-Festin, G.; Finzel, K.; Jackson, D. R.; Ishikawa, F.; O'Dowd, B.; McCammon, J. A.; Opella, S. J.; Tsai, S. C.; Burkart, M. D., *Nature* **2014**, *505* (7483), 427-31; (b) Ishikawa, F.; Haushalter, R. W.; Lee, D. J.; Finzel, K.; Burkart, M. D., *J. Am. Chem. Soc.* **2013**, *135* (24), 8846-9; (c) Ishikawa, F.; Haushalter, R. W.; Burkart, M. D., *J. Am. Chem. Soc.* **2012**, *134* (2), 769-72.

7. Tallorin, L.; Finzel, K.; Nguyen, Q. G.; Beld, J.; La Clair, J. J.; Burkart, M. D., *J. Am. Chem. Soc.* **2016**.

8. (a) Pedrolli, D.; Langer, S.; Hobl, B.; Schwarz, J.; Hashimoto, M.; Mack, M., *FEBS J.* **2015**, *282* (16), 3230-42; (b) Fischer, M.; Bacher, A., *Nat. Prod. Rep.* **2005**, *22* (3), 324-50.

9. Kao, Y. T.; Saxena, C.; He, T. F.; Guo, L.; Wang, L.; Sancar, A.; Zhong, D., *J. Am. Chem. Soc.* **2008**, *130* (39), 13132-9.

10. Porter, D. J. T.; Voet, J. G.; Bright, H. J., *J. Biol. Chem.* **1973**, *248* (12), 4400-4416.

11. Thorpe, C.; Williams, C. H., Jr., *J. Biol. Chem.* **1976**, *251* (23), 7726-8.

12. Kuhn, R.; Bauer, H.; Knackmus, H-j, *Ber. Dtsch. Chem. Ges.* **1965**, *98* (7), 2139.

13. (a) Entsch, B.; Massey, V.; Ballou, D. P., *Biochem. Biophys. Res. Commun.* **1974**, *57* (4), 1018-25; (b) Massey, V.; Strickland, S.; Mayhew, S. G.; Howell, L. G.; Engel, P. C.; Matthews, R. G.; Schuman, M.; Sullivan, P. A., *Biochem. Biophys. Res. Commun.* **1969**, *36* (6), 891-7.

14. (a) Yachnin, B. J.; Sprules, T.; McEvoy, M. B.; Lau, P. C.; Berghuis, A. M., *J. Am. Chem. Soc.* **2012**, *134* (18), 7788-95; (b) Mihovilovic, M. D.; Muller, B.; Stanetty, P., *Eur. J. Org. Chem.* **2002**, (22), 3711-3730; (c) Sheng, D.; Ballou, D. P.; Massey, V., *Biochemistry* **2001**, *40* (37), 11156-67.

15. (a) Thibodeaux, C. J.; Chang, W. C.; Liu, H. W., *Chem. Rev.* **2012**, *112* (3), 1681-709; (b) Huff, M. W.; Telford, D. E., *Trends Pharmacol. Sci.* **2005**, *26* (7), 335-40; (c) Nagumo, A.; Kamei, T.; Sakakibara, J.; Ono, T., *J. Lipid Res.* **1995**, *36* (7), 1489-97.

16. Krueger, S. K.; Williams, D. E., *Pharmacol. Ther.* **2005**, *106* (3), 357-87.

17. Teufel, R.; Miyanaga, A.; Michaudel, Q.; Stull, F.; Louie, G.; Noel, J. P.; Baran, P. S.; Palfey, B.; Moore, B. S., *Nature* **2013**, *503* (7477), 552-6.

18. O'Hagan, D.; Schaffrath, C.; Cobb, S. L.; Hamilton, J. T.; Murphy, C. D., *Nature* **2002**, *416* (6878), 279.

19. Nowak-Thompson, B.; Chaney, N.; Wing, J. S.; Gould, S. J.; Loper, J. E., *J. Bacteriol.* **1999**, *181* (7), 2166-74.

20. Pang, A. H.; Garneau-Tsodikova, S.; Tsodikov, O. V., *J. Struct. Biol.* **2015**, *192* (3), 349-57.

21. Yeh, E.; Blasiak, L. C.; Koglin, A.; Drennan, C. L.; Walsh, C. T., *Biochemistry* **2007**, *46* (5), 1284-92.

Chapter 2

The Chemical Biology of Flavoenzymes

2.1 Introduction

To grasp the current state of chemical biology for flavoenzyme biochemistry, it is incumbent to consider the enzyme pocket and physiological conditions in which the flavin resides at a molecular level. While last chapter focused primarily on the reactivity of flavins and their role in promoting catalysis of biosynthetic processes, this chapter reviews the modality of flavin binding and its significance, the types of inhibitors and inhibitor mechanisms for flavoenzymes, and the applications brought to bear on flavoenzymes using these inhibitor motifs within a complex milieu.

2.2 Binding Modality of Flavins

To harness the redox activity of these coenzymes, flavoenzymes bind flavins in their active sites by either post-translational covalent linkage or tight intermolecular interactions that bind with a dissociation constant (K_d) typically in the micromolar to picomolar range. Most flavoenzymes have a dissociable FAD or FMN coenzyme, however, only approximately 10% of cellular FAD in humans, for example, is covalently bound to flavoenzymes including succinate dehydrogenase[1] and monoamine oxidase.[2] Flavoenzymes may covalently bind a flavin molecule at the *C8α* methyl group with cysteine, histidine, or tyrosine and the *C6* position with cysteine. The most prevalent mechanism of covalent linkage, or flavinylation, is proposed to proceed by a quinone methide mechanism at the *C8α* position (Figure 2.1), at which the nucleophilic side chain residues of the enzyme may covalently attach.[3] Deprotonation at the *C8α* position by a basic residue is facilitated by its acidity due to the electron withdrawing capability of a conjugated carbonyl, which is enhanced by electrostatic interactions with a positively charged, cationic arginine at the distal end of the conjugated system. A less common binding motif is the Fl-C6-*S*-Cys linkage, found in trimethylamine dehydrogenase[4] for example, occurs by aromatic substitution at *C6* with the terminal thiol side chain of cysteine.

Covalent flavinylation imparts a couple advantages to flavoenzymes. Covalently-bound flavins typically maintain a higher reduction potential than their noncovalent counterparts, which promotes catalysis at a lower energy of activation. Covalent linkage with electron withdrawing residues, especially aromatic examples including C8α-N3-histidyl FAD, lowers the thermodynamic energy level of the hydroquinone state. For example, wild type vanillyl-alcohol oxidase,[5] which has C8α-N3-histidyl

FAD bound, benefits by covalent flavinylation with a $FAD_{ox}/FADH_2$ reduction potential of +55 mV over noncovalent alanine mutants that have a -113 mV reduction potential. The second advantage to covalent flavinylation is that some flavoenzymes, such as human sarcosine oxidase,[6] have a significantly lower affinity for the Flox state than for FlH_2 state, which would allow the coenzyme to disassociate between catalytic cycles and hinder catalytic efficiency. Covalently flavinylated enzymes benefit by efficiently keeping the coenzyme bound at all redox states.

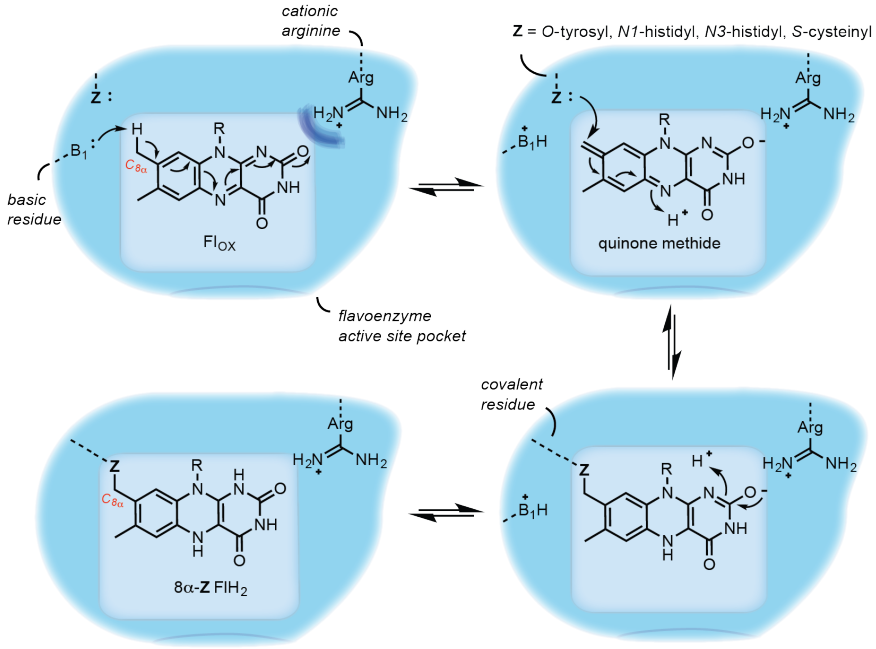

Figure 2.1: The quinone methide mechanism of covalent flavinylation. Assisted by a general base and a cationic arginine in the active site pocket, tyrosine, histidine, and cysteine residues covalently add to the C8α position.

2.3 Covalent inhibitors

Flavoenzymes have been the target of numerous inhibitor applications that take advantage of the binding modality of the flavin ligand. The most studied applications focuses on targeting the approximate 10% of human flavoenzymes that have

a covalently-bound flavin ligand, including monoamine oxidases, which have been popular drug targets. Other flavoenzymes of general mechanistic interest have also been studied with covalent inhibitors, both as flavin adducts and as indirect adducts to nucleophilic active site residues. Aside from human targets, covalent inhibitors have also been reported for targeting flavoenzymes in *Mycobacterium tuberculosis*, the causative pathogen of tuberculosis (TB).

2.3.1 Covalent Monoamine Oxidase Inhibitors

Historically, inhibition of human monoamine oxidases (MAOs), which contain a FAD-N5-His flavin linkage, has been one the most attractive targets of this research because of the therapeutic effects MAO inhibitors (MAOIs) have on depression,[7] anxiety, hypertension, and Parkinson's[8] and Alzheimer's[9] diseases. Two types of MAO isoforms exist in humans, MAO-A and MAO-B, which are primarily expressed in the nervous system and anchored in the outer mitochondrial membrane. MAOs function to oxidatively deaminate phenethylamine neurotransmitters such as dopamine, norepinephrine, and serotonin to their corresponding aldehyde catabolites. Inhibitors that target MAOs have an antagonistic effect on neurotransmitter degradation, promoting greater potentiation effects of these neurotransmitters in neuron synapses.

The first types of MAOIs developed were irreversible, mechanism-based inhibitors that covalently bind to FAD within the MAO active site. Inhibitors belonging to this irreversible inhibitor class historically earned the name, suicide inhibitor, to acknowledge the self-destructive mechanism by which inhibitors inactivate an enzyme via covalent attachment.[10] Canonical irreversible MAOIs are comprised of three classes: propargylamines, cyclopropylnamines, and hydrazines (Figure 2.2).

The class was the first discovered of these irreversible inhibitors, was the hydrazine class, which are generally non-selective MAO-A and MAO-B inhibitors. The entry of this class was marked by the discovery of iproniazid in 1952, which contains a reactive hydrazide moiety.[11] Iproniazid maintained a presence as a pharmaceutical in the treatment of depression, but was withdrawn from the market in 1961 because of its hepatoxicity and other side effects.[12] However, inhibitors in the propargylamine class have greater selectivity for MAO-B. While propargyline inhibitors have generally been phased out in the treatment of depression (e.g. pargyline), derivatives such as selegiline, rasagiline, deprenyl, and ladostigil have enjoyed a resurgence of this motif as selective inhibibitors of MAO-B for current treatment of Parkinson's and Alzheimer's diseases.[13] Tranylcypromine, a cyclopropanamine, comprises the last of the covalent inhibitor types as a nonselective MAO-A and MAO-B inhibitor. It should be noted that these inh nibitor classes also have crossover inhibitory effects on flavin-dependent histone *N*-methyl-lysine demethylases, especially derivatives of tranylcypromine[14] and phenelzine.[15]

These inhibitors contain electrophiles that, when oxidized, primarily bind to the nucleophilic N5 or radical C4a portion of the bound flavin (Figure 2.3). Hydrazines, such phenelzine, decompose to nitrogen gas and alkyl radicals when oxidized by Fl_{ox}; these alkyl radicals subsequently react with the neutral semiquinone, Fl-C4a, to form an inactivating adduct with the flavin (Figure 2.3a). Tranylcypromine, a cyclopropanamine, reacts in a similar fashion, alkylating at the *C4a* position as well (Figure 2.3b). In contrast, propargylamines form adducts at the *N5* position of the flavin. The propargylamine warhead is activated by oxidation of the amine to imine, forming an electrophilic conjugated iminium complex and a reduced anionic hydro-

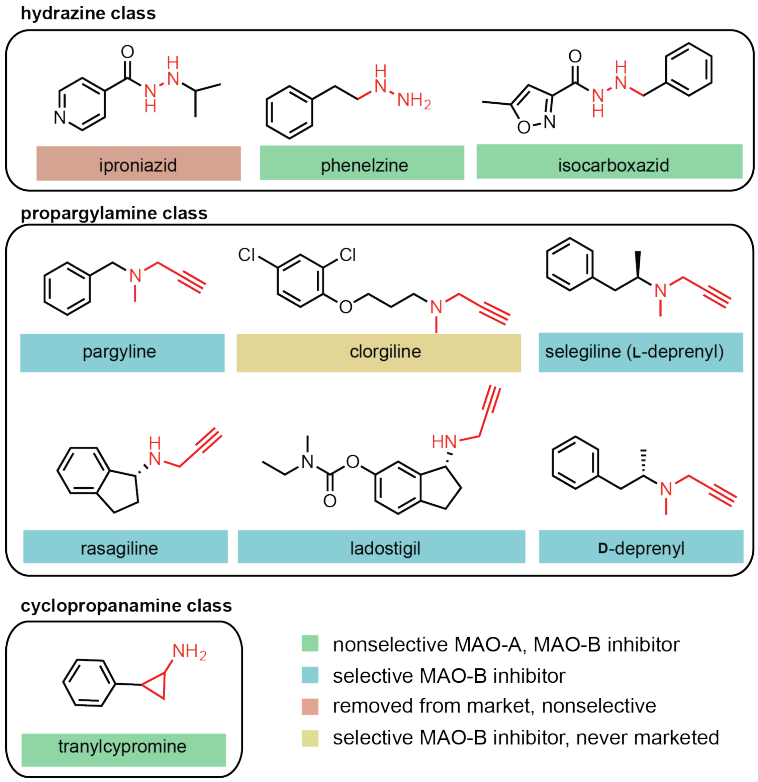

Figure 2.2: MAOI classes and common covalent inhibitors thereof.

quinone (Figure 2.3c). The lone pair of the *N5* atom then adds to the terminus of the alkyne by a Michael-type addition, yielding a covalent conjugated iminium-flavin adduct.[16]

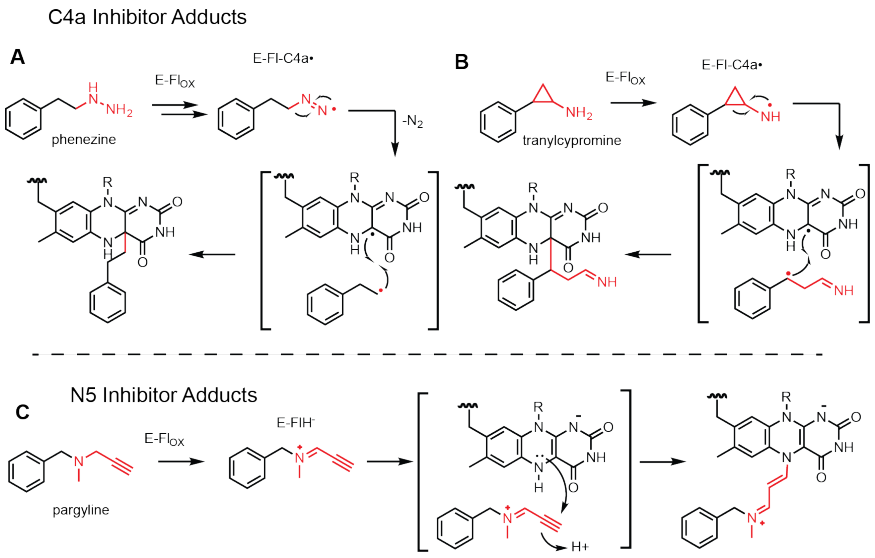

Figure 2.3: Inhibition mechanisms of representative MAO covalent inhibitors.

2.3.2 Additional Covalent Flavoenzyme Inhibitors

Covalent inhibitors have also been discovered for other flavoenzyme targets of interest. Similar to MAOIs developed as drugs, some of these other covalent inhibitors also bind as covalent adducts to the flavin molecule, while some bind to indirect nucleophilic targets in the enzyme pocket (Figure 2.4).

An interesting example of a naturally-occuring covalent inhibitor is the toxin, hypoglycin A, which is the causative agent of Jamaican vomiting sickness and is isolated from the unripened fruit of the Ackee tree.[17] Hypoglycin A is an amino acid derivative that inhibits the beta oxidation of fatty acids, causing severe hypoglycemia in humans who ingest it.[18] The mechanism of inhibition proceeds by a series of catabolic processing, including transamination to an alpha-keto species and ligation to CoA by CoA ligase to form a CoA thioester (Figure 2.5a). The flavoenzyme, isovaleryl CoA dehydrogenase, abstracts an acidic proton and activates a cyclopropane ring-opening cascade, whereby nucleophilic attack of the flavin at the *C4a* or *C6* position leads to an inactivated flavin adduct. Hypoglycine A inactivation of medium-chain acyl-CoA dehydrogenase has also demonstrated there may be additional routes of inactivation, whereby hypoglycine oxidation by Fl-OOH may activate it as an electrophile for nucleophilic attack by side-chain residues.[19]

Another well-studied flavin adduct inhibitor is 2-hydroxy-3-butynoatic acid, which inhibits lactate dehydrogenase.[20] The mechanism of inhibition initiates similar to that of hypogylcin A, where an acidic alpha proton is abstracted. Generation of the enolate propagates a reactive allene intermediate that is proposed to form an adduct at the *N5* and either *C6* or *C4a* position of the flavin (Figure 2.5b). While no crystal structures have elucidated the structure of the flavin adduct, it has been

proposed that **L**/**D** enantiomers of 2-hydroxy-3-butynoic acid may have differential regioselectivity in covalent attachment to the flavin.[10,21] Spectrophotometric analysis of adduct formation with L-2-hydroxy-3-butynoic acid demonstrates "bleaching" of *C4a* peaks in the UV absorbance spectrum, suggesting that the **L** enantiomer binds to the *C4a* position.[20]

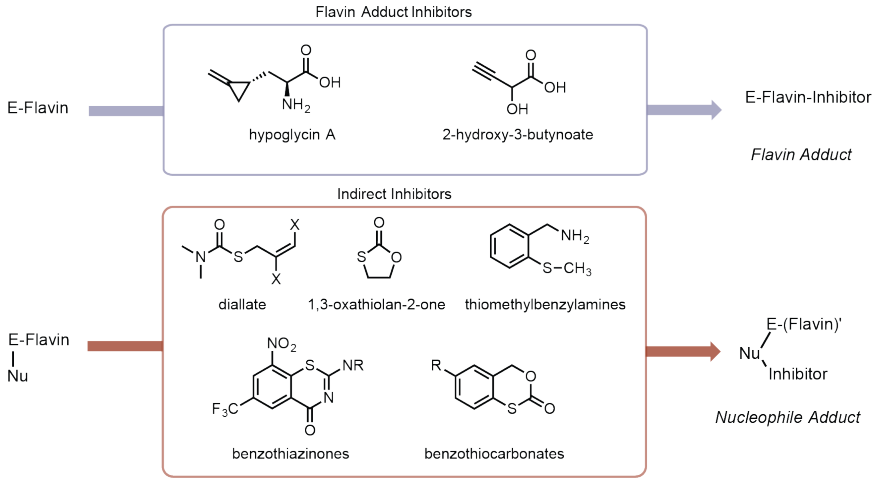

Figure 2.4: Adduct formation of exemplary flavin inhibitors and indirect inhibitors.

Covalent inhibitors that indirectly bind to residues in the active site after flavin activation have also received a great amount of investigation. Nearly all of these inhibitors take advantage of the redox ability of sulfur- or nitro-containing compounds (Figure 2.4). A practical example of this class of molecules, includes the herbicide, diallate. Diallate is composed of a thiocarbamate that, when oxidized to a sulfoxide by the Fl-OOH species of the flavoenzymes, undergoes a [2,3]-sigmatropic rearrangement, or Misolow-Evans-type rearrangement, with the adjacent vicinal dichloroallyl group (Figure 2.6a).[22] Subsequent elimination affords the reactive electrophiles, thiocarbamoyl chloride and 2-chloroacrylaldehyde, which react with nucleophilic residues and cause inactivation of the enzyme. Another example includes

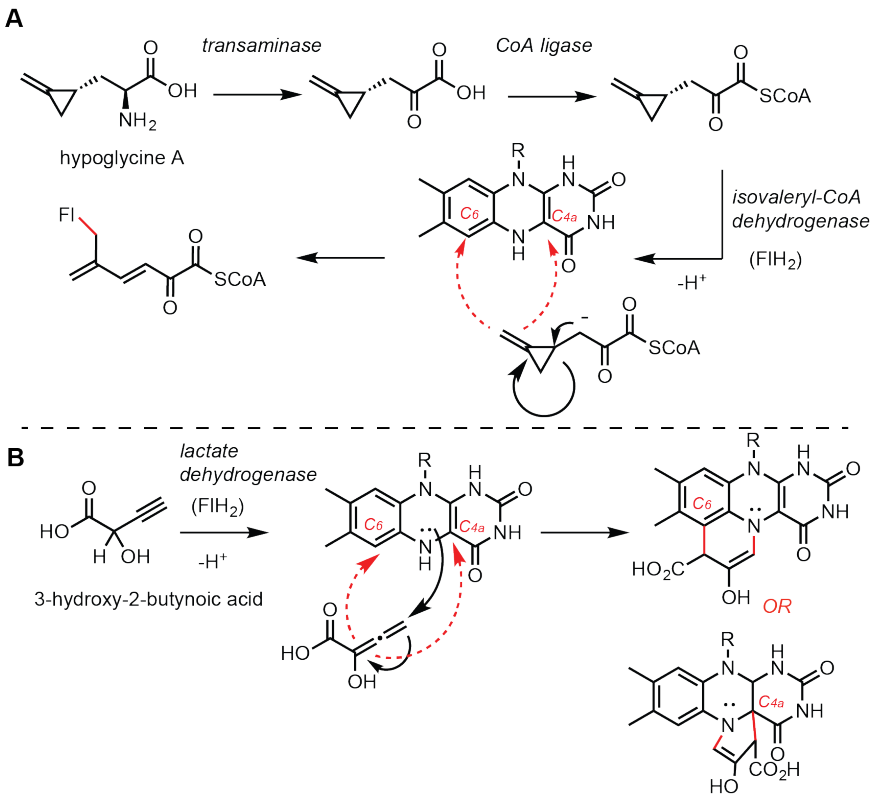

Figure 2.5: Covalent flavin adduct formation mechanisms. Representative examples include hypoglycine A (A) and 3-hydroxy-2-butynoic acid (B).

o- and *p*-thiomethylbenzylamine, which are inhibitors of MAO-B.[23] These inhibitors work by Fl_{OX} forming an imine at the benzyl position, an alkylation by a nucleophilic residue, and disulfide formation with cysteine residues within the enzyme pocket (Figure 2.6b).

Some of these indirect nucleophile motifs, including benzothiazinones, have provided promise as a pharmaceutical in the treatment of TB, particularly for inhibitors of DprE1.[24] DprE1 is a crucial flavoenzyme used for cell wall construction in mycobacteria. Benzothiazinones contain a redox-reactive aryl-nitro group that is reduced to a nitroso group in the presence of FlH_2. The nitroso group acts as an electrophile with a specific neighboring cysteine, forming a stable adduct with the enzyme. The inhibitor adduct has been demonstrated by X-ray crystallization of the

DprE1 complex to Cys394.[25] The specific mode of inhibibition to form a cysteine adduct provides a rationale for why TB-resistance can occur, as Cys394Ser DprE1 mutants are significantly less inhibited by this inhibitor.

The last category of these flavin-reactive indirect inhibitors, are the thiocarbonates. Thiocarbonates. such as 1,3-oxathian-2-one[26] and benzothiocarbonates (Figure 2.4), have been demonstrated as general inhibitors of aerobic flavoenzymes, specifically enzymes that have the Fl-OOH intermediate as part of their catalytic cycle. Similar to the mechanism of diallate, these inhibitors are activated by oxidation of the sulfur atom to a sulfoxide or sulfenic anhydride (Figure 2.6d). Potential nucleophilic attack of this reactive intermediate in either of two electrophilic regions renders the enzyme inactive by formation of an adduct.[27] Chapters 3 and 4 of this dissertation will address the synthesis of benzothiocarbonates and their inhibition of aerobic flavoenzymes.

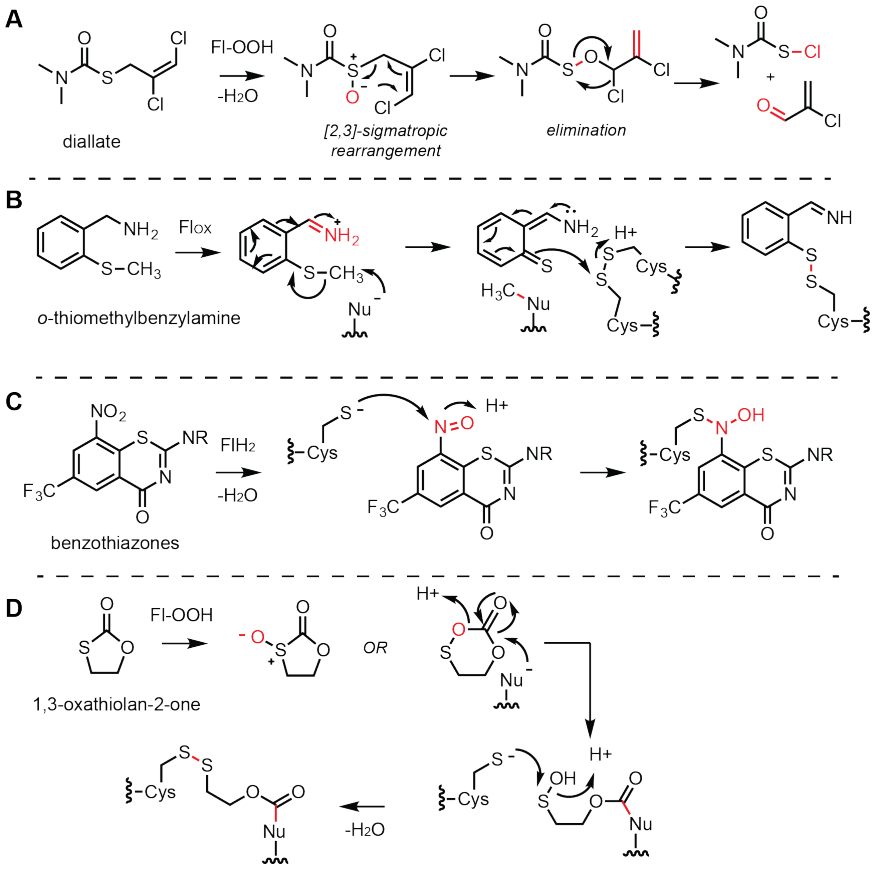

Figure 2.6: Representative indirect inhibitor mechanisms of flavoenzymes.

2.4 Applications with Covalent Inhibitors

From a chemical biology perspective, inhibitors that selectively form covalent adducts with the enzyme or with a covalent flavin impart advantages for tagging and manipulating the corresponding flavoenzyme. For example, since MAOs harbor a covalently-bound flavin, the advantage of using irreversible inhibitors that form covalent adducts to the flavin provide a means to label and identify MAO enzymes from a complex environment. Alternatively, since most flavins in flavoenzymes are not covalently bound, probes derived from indirect inhibitors provide distinct utility in this respect.

Fluorescently-tagged inhibitors of these types have allowed selective activity-based proteomic profiling (ABPP) of flavoenzymes. ABPP is a technique whereby mechanism-based inhibitors are tagged with fluorescent moieties and used as probes for visualization and analysis by denaturing gels and mass spectrometry (Figure 2.7).[28] The provision of a covalent adducts of the probe with flavoenzymes makes these analysis techniques possible, as noncovalent probes disassociate and make poor tags.

This type of labeling application has been demonstrated for targeting DprE1 with probes containing the benzothiazinone inhibitor and a TAMRA fluorophore (Figure 2.8a).[29] This probe was demonstrated as an indicator of activity for WT DprE1 versus various mutants, whereas WT labels well and the Cys394Ser mutation abolishes inhibition and probe labeling. The probe was further extended for use in visualizing the DprE1 protein in *Mycobacterium smegmatis* cells, which demonstrated localization of the protein near cell walls.

Additionally, multiple studies have focused on tagging MAO-B with covalent

fluorescent probes. The first of these studies utilized a pargyline-like inhibitor with an alkyne at the other terminus (Figure 2.8b).[30] This terminal alkyne handle provided a means to tag inhibited proteins with a TAMRA-azide moiety in a two-step process by a click reaction under aqueous conditions. A similar probe was generated with reported greater selectivity for MAO-B, also with an alkyne handle for fluorophore installation, which was demonstrated to label MAO-B within lysates for proteomic profiling and within HepG2 cells (Figue 2.8c).[31] The last of these applications for MAO-B employs use of a simple terminal alkyne tethered to a number of fluorescent coumarin ether derivatives (Figure 2.8d).[32] The authors of that study demonstrated greater selectivity of MAO-B over MAO-A when the probe contained certain R groups.

The last example features a probe that generally targets aerobic flavoenzymes (Figure 2.8e), and it is the topic of Chapter 4 of this dissertation. This probe contains a benzothiocarbonate inhibitor and a dimethylaminocoumarin fluorescent reporter, which are adjoined by a "clicked" linker portion. The probe was used to specifically tag a variety of aerobic flavoenzymes, including an oxidases, monooxygenase, and halogenase, which facilitate crucial oxidative reactions in biosynthetic processes.

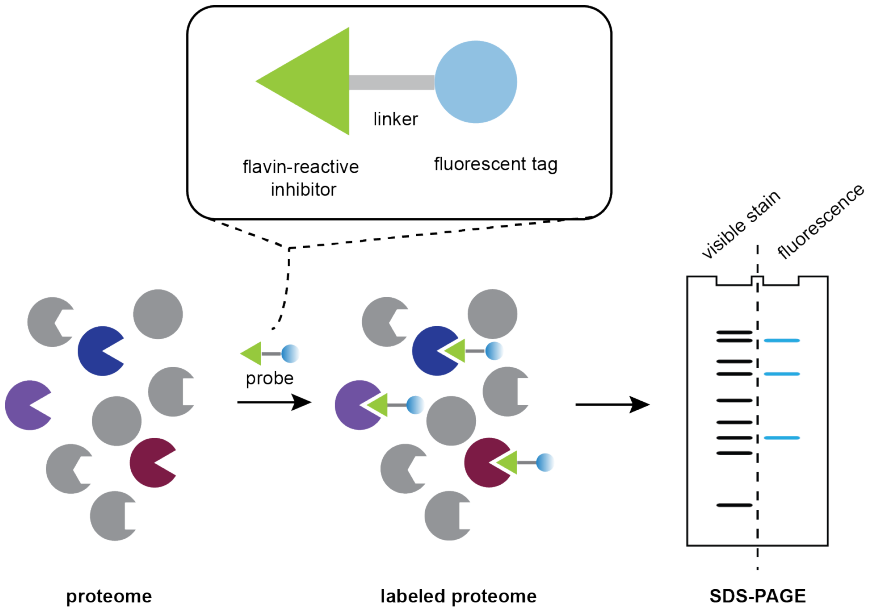

Figure 2.7: Scheme of activity-based proteomic profiling.

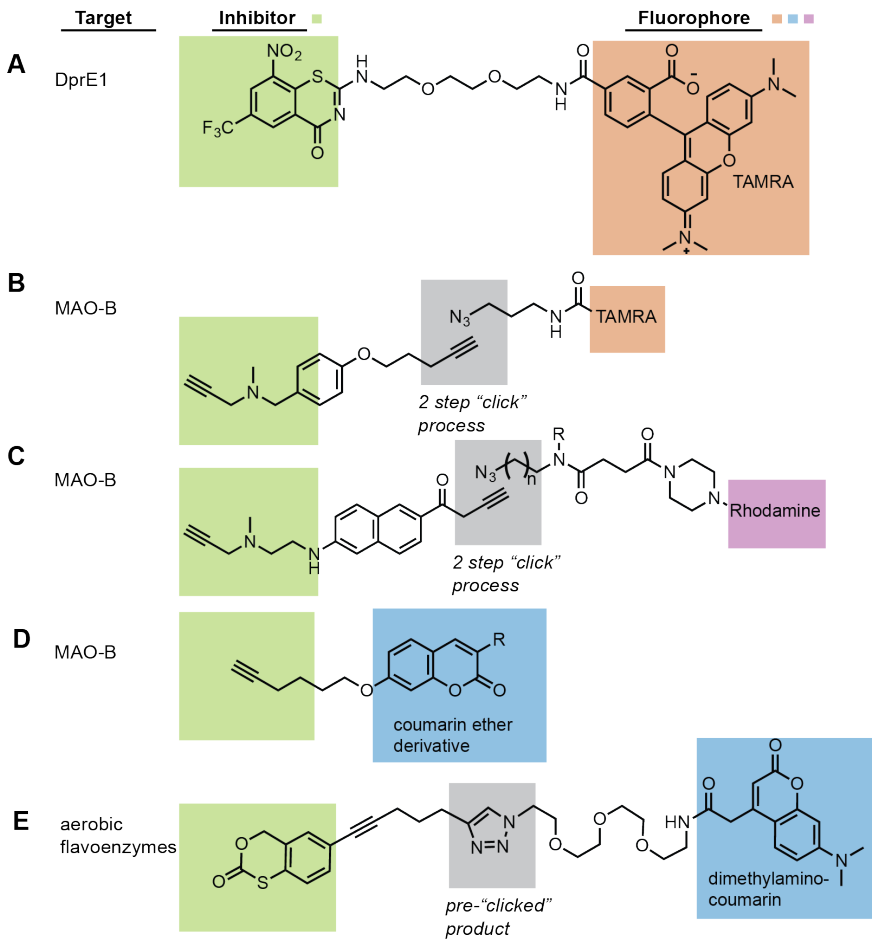

Figure 2.8: Fluorescent probes used for activity-based proteomic profiling of flavoenzymes.

2.5 Applications with Noncovalent Probes

Noncovalent probes play a significant role in activity assays of flavoenzymes. Among many applications, activity assays provide the tools to study potential inhibitors of target flavoenzymes,as well as image activity within complex environments. To date, there are a variety of colorometric,[33] luminometric,[34] and fluorometric[35] assays for detecting flavoenzyme activity.

For in vitro applications, a commercially-available, resorufin-based system is the most common assay used for oxidases (Figure 2.9).[35] The methodology involves a peroxidase enzyme-coupled assay that is an indirect measure of product formation. The assay proceeds by formation of hydrogen peroxide from the oxidase as a by-product after substrate oxidation, which is used by the peroxidase to oxidatively cleave an acyl group from the non-fluorescent resorufin dye, activating the fluorescent compound as resorufin.

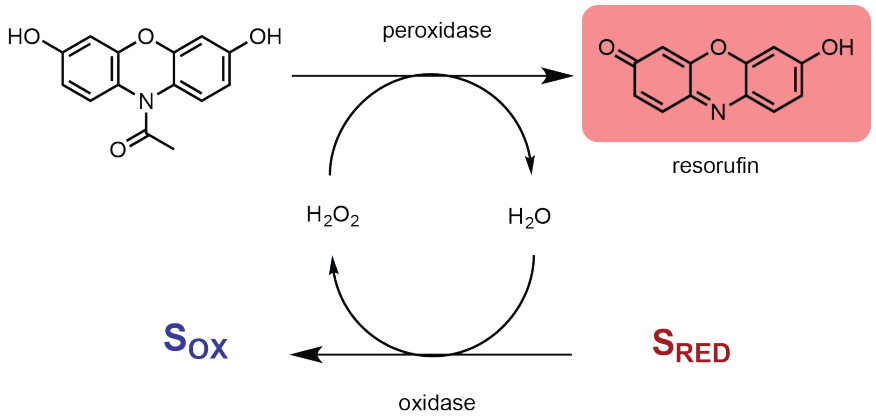

Figure 2.9: Enzyme-coupled assay for oxidase activity.

For *in vivo* applications, a more direct reporter assay of activity is required since the environment of a cell is not always amenable to the addition of coupled enzymes. Along these lines, cell permeable dyes have been used for the detection of

MAO-B activity within cells. These dyes are masked fluorophores, such as resorufin[36] and fluorescein[37] derivatives, which contain an amine portion that becomes labile after oxidation by MAO-B (Figure 2.10). Elimination of these amine-based masks enables detection of the free fluorphore, enabling fluorescent imaging *in vivo*.

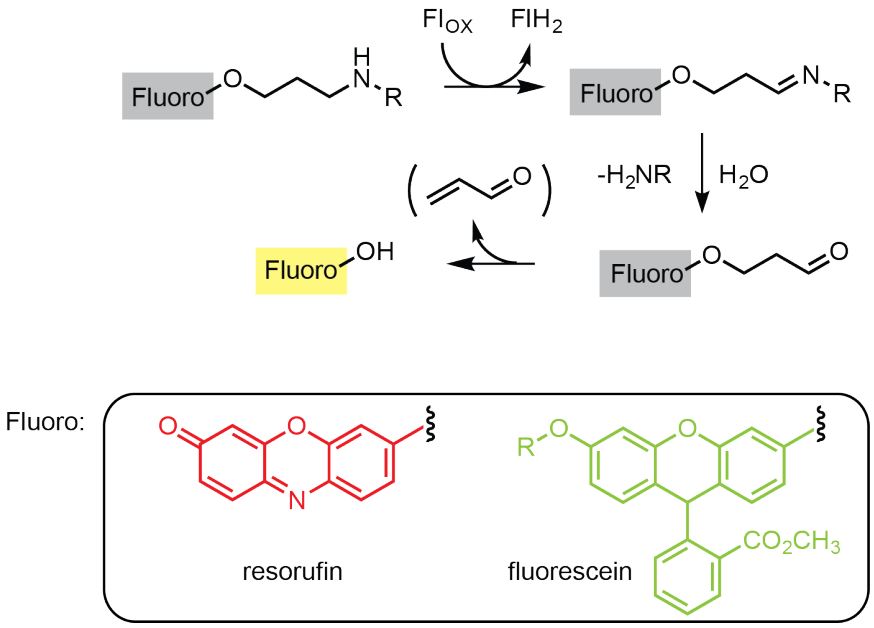

Figure 2.10: Direct activity assays using masked fluorophores that are activated by MAOs.

2.6 Affinity Applications

Owing to the robust affinity of the flavin as a ligand for noncovalently-bound flavoenzymes, various affinity applications have been used to target and harness the reactivity of specific flavoenzymes. This principle has been exploited to isolate and immobilize apo-flavoenzymes on derivatized agarose resin (Figure 2.11), which has been demonstrated for phenylacetone monooxygenase and phosphite dehydrogenase.[38] This technique is enabled by functionalizing the *N6* moeity of the adenine ring in FAD with an *N*-succinimidyl ester. Coupling of the activated FAD with ethanolamine capped agarose resin forms a covalent FAD-resin adduct, whereby apo-protein flavoenzymes may be immobilized. Immobilized flavoenzymes demonstrated continuous activity after multiple rounds of catalysis, and some examples exhibited increased thermostability under these conditions, demonstrating their potential utility in biocatalysis.

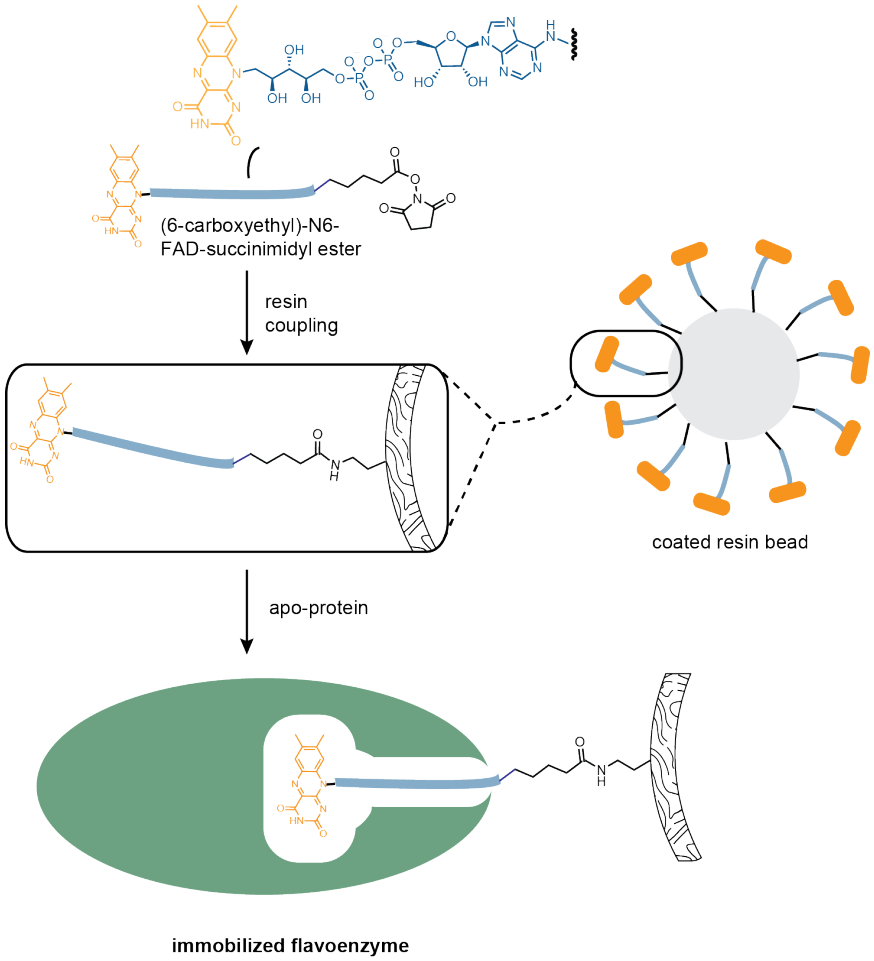

Figure 2.11: Immobilization scheme of flavoenzymes to resin for biocatalysis.

2.7 Concluding Remarks

While flavoenzymes are the nexus of many redox chemical reactions performed in a biosynthetic pathways, they are also interesting and useful targets of applications in the field of chemical biology. What is notably missing from the field is a system to crosslink flavoenzymes with their partner domains. As these protein-protein interactions are critical for the formation of many natural products, very little is understood about how individual flavoenzyme domains recognize cognate domains to facilitate processing of substrates. This investigation is most needed studying how flavoenzymes participate in processing when substrates are tethered to the ubiquitous carrier protein domain, such as in the biosynthesis of pyoluteorin.[39] This crosslinking ability is within the scope of current applications, as many of the inhibitor structures discussed may be used as the starting scaffolds for development of crosslinking agents. The outlook of this application is further discussed in Chapter 6.

2.8 References

1. Kim, H. J.; Winge, D. R., *Biochim. Biophys. Acta* **2013**, *1827* (5), 627-36.

2. Mewies, M.; McIntire, W. S.; Scrutton, N. S., *Prot. Sci.* **1998**, *7* (1), 7-20.

3. (a) Brandsch, R.; Bichler, V., *FEBS Lett.* **1985**, *192* (2), 204-208; (b) Kim, J.; Fuller, J. H.; Kuusk, V.; Cunane, L.; Chen, Z.; Matthews, F. S.; McIntire, W. S., *J. Biol. Chem.* **1995**, *270* (52), 31202-31209.

4. (a) Kenney, W. C.; McIntire, W.; Steenkamp, D. J., *FEBS Lett.* **1978**, *85* (1), 137-40; (b) Boyd, G.; Mathews, F. S.; Packman, L. C.; Scrutton, N. S., *FEBS Lett.* **1992**, *308* (3), 271-6.

5. Fraaije, M. W.; van den Heuvel, R. H. H.; van Berkel, W. J. H.; Mattevi, A., *J. Biol. Chem.* **1999**, *274* (50), 35514-35520.

6. Hassan-Abdallah, A.; Zhao, G.; Jorns, M. S., *Biochemistry* **2006**, *45* (31), 9454-62.

7. Grady, M. M.; Stahl, S. M., *CNS Spectr.* **2012**, *17* (1), 2-10.

8. (a) Riederer, P.; Laux, G., *Exp. Neurobiol.* **2011**, *20* (1), 1-17; (b) Youdim, M. B.; Bakhle, Y. S., *Br. J. Pharmacol.* **2006**, *147* Suppl 1, S287-96.

9. Saura, J.; Luque, J. M.; Cesura, A. M.; Prada, M. D.; Chan-Palay, V.; Huber, G.; Löffler, J.; Richards, J. G., *Neuroscience* **1994**, *62* (1), 15-30.

10. Walsh, C., *Tetrahedron* **1982**, *38* (7), 871-909.

11. Griesemer, E. C.; Barsky, J.; Dragstedt, C. A.; Wells, J. A.; Zeller, E. A., *Proc. Soc. Exp. Biol. Med.* **1953**, *84* (3), 699-701.

12. Trehout, M.; Fedrizzi, S.; Loggia, G.; Lecardeur, L.; Nathou, C.; Dollfus, S., *Rev. Med. Interne.* **2016**, *37* (2), 135-8.

13. Yamada, M.; Yasuhara, H., *Neurotoxicology* **2004**, *25* (1-2), 215-221.

14. (a) McAllister, T. E.; England, K. S.; Hopkinson, R. J.; Brennan, P. E.; Kawamura, A.; Schofield, C. J., *J. Med. Chem.* **2016**, *59* (4), 1308-29; (b) Mimasu, S.; Sengoku, T.; Fukuzawa, S.; Umehara, T.; Yokoyama, S., *Biochem. Biophys. Res. Commun.* **2008**, *366* (1), 15-22.

15. Prusevich, P.; Kalin, J. H.; Ming, S. A.; Basso, M.; Givens, J.; Li, X.; Hu, J.; Taylor, M. S.; Cieniewicz, A. M.; Hsiao, P. Y.; Huang, R.; Roberson, H.; Adejola, N.; Avery, L. B.; Casero, R. A., Jr.; Taverna, S. D.; Qian, J.; Tackett, A. J.; Ratan, R. R.; McDonald, O. G.; Feinberg, A. P.; Cole, P. A., *ACS Chem. Biol.* **2014**, *9* (6), 1284-93.

16. Binda, C.; Hubalek, F.; Li, M.; Herzig, Y.; Sterling, J.; Edmondson, D. E.; Mattevi, A., *J. Med. Chem.* **2004**, *47* (7), 1767-74.

17. (a) Golden, K. D.; Kean, E. A.; Terry, S. I., *Clin. Chim. Acta* **1984**, *142* (3), 293-8; (b) Feng, P. C.; Patrick, S. J., *Br. J. Pharmacol. Chem.* **1958**, *13* (2), 125-30.

18. Tanaka, K.; Miller, E. M.; Isselbacher, K. J., *Proc. Natl. Acad. Sci. USA* **1971**, *68* (1), 20-4.

19. Lai, M. T.; Li, D.; Oh, E.; Liu, H. W., *J. Am. Chem. Soc.* **1993**, *115* (5), 1619-1628.

20. Ghisla, S.; Ogata, H.; Massey, V.; Schonbrunn, A.; Abeles, R. H.; Walsh, C. T., *Biochemistry* **1976**, *15* (9), 1791-7.

21. Ghisla, S.; Wenz, A.; Thorpe, C., "Suicide Substrates as Irreversible Inhibitors of Flavoenzymes. First publ. in: Enzyme Inhibitors : proceedings of a meeting held in Basel, on 20 and 21 March 1980"/ ed. by Urs Brodbeck. Weinheim: Verl. Chemie,: 1980.

22. Schuphan, I.; Rosen, J.; Casida, J., *Science* **1979**, *205* (4410), 1013-1015.

23. Lu, X.; Rodriguez, M. A.; Gu, W.; Silverman, R. B., *Bioorg. Med. Chem.* **2003**, *11* (20), 4423-4430.

24. Batt, S. M.; Jabeen, T.; Bhowruth, V.; Quill, L.; Lund, P. A.; Eggeling, L.; Alderwick, L. J.; Futterer, K.; Besra, G. S., *Proc. Natl. Acad. Sci. USA* **2012**, *109* (28), 11354-9.

25. Trefzer, C.; Skovierova, H.; Buroni, S.; Bobovska, A.; Nenci, S.; Molteni, E.; Pojer, F.; Pasca, M. R.; Makarov, V.; Cole, S. T.; Riccardi, G.; Mikusova, K.; Johnsson, K., *J. Am. Chem. Soc.* **2012**, *134* (2), 912-5.

26. Latham, J. A.; Walsh, C., *J. Am. Chem. Soc.* **1987**, *109* (11), 3421-3427.

27. Minato, H.; Kodama, H.; Miura, T.; Kobayashi, M., *Chem. Lett.* **1977**, (4), 413-416.

28. Simon, G. M.; Cravatt, B. F., *J. Biol. Chem.* **2010**, *285* (15), 11051-11055.

29. Neres, J.; Pojer, F.; Molteni, E.; Chiarelli, L. R.; Dhar, N.; Boy-Rottger, S.; Buroni, S.; Fullam, E.; Degiacomi, G.; Lucarelli, A. P.; Read, R. J.; Zanoni, G.; Edmondson, D. E.; De Rossi, E.; Pasca, M. R.; McKinney, J. D.; Dyson, P. J.; Riccardi, G.; Mattevi, A.; Cole, S. T.; Binda, C., *Sci. Transl. Med.* **2012**, *4* (150), 150.

30. Krysiak, J. M.; Kreuzer, J.; Macheroux, P.; Hermetter, A.; Sieber, S. A.; Breinbauer, R., *Angew. Chem. Int. Ed.* **2012**, *51* (28), 7035-40.

31. Li, L.; Zhang, C. W.; Ge, J.; Qian, L.; Chai, B. H.; Zhu, Q.; Lee, J. S.; Lim, K. L.; Yao, S. Q., *Angew. Chem. Int. Ed.* **2015**, *54* (37), 10821-5.

32. Mertens, M. D.; Hinz, S.; Muller, C. E.; Gutschow, M., *Bioorg. Med. Chem.* **2014**, *22* (6), 1916-28.

33. (a) Tabor, C. W.; Tabor, H.; Rosenthal, S. M., *J. Biol. Chem.* **1954**, *208* (2), 645-61; (b) Weissbach, H.; Smith, T. E.; Daly, J. W.; Witkop, B.; Udenfriend, S., *J. Biol. Chem.* **1960**, *235*, 1160-3; (c) Houslay, M. D.; Tipton, K. F., *Biochem. J.* **1974**, *139* (3), 645-52; (d) Flaherty, P.; Castagnoli, K.; Wang, Y. X.; Castagnoli, N., Jr., *J. Med. Chem.* **1996**, *39* (24), 4756-61; (e) Bissel, P.; Bigley, M. C.; Castagnoli, K.; Castagnoli Jr, N., *Bioorg. Med. Chem.* **2002**, *10* (9), 3031-3041.

34. Zhou, W.; Valley, M. P.; Shultz, J.; Hawkins, E. M.; Bernad, L.; Good, T.; Good, D.; Riss, T. L.; Klaubert, D. H.; Wood, K. V., *J. Am. Chem. Soc.* **2006**, *128* (10), 3122-3.

35. Zhou, M.; Diwu, Z.; Panchuk-Voloshina, N.; Haugland, R. P., *Anal. Biochem.* **1997**, *253* (2), 162-8.

36. Albers, A. E.; Rawls, K. A.; Chang, C. J., *Chem. Commun.* **2007**, (44), 4647-9.

37. Li, X.; Zhang, H.; Xie, Y.; Hu, Y.; Sun, H.; Zhu, Q., *Org. Biomol. Chem.* **2014**, *12* (13), 2033-6.

38. Krzek, M.; van Beek, H. L.; Permentier, H. P.; Bischoff, R.; Fraaije, M. W., *Enzyme Microb. Technol.* **2016**, *82*, 138-43.

39. Dorrestein, P. C.; Yeh, E.; Garneau-Tsodikova, S.; Kelleher, N. L.; Walsh, C. T., *Proc. Natl. Acad. Sci. USA* **2005**, *102* (39), 13843-8.

Chapter 3

Synthesis of Benzothiocarbonate Inhibitors

3.1 Introduction and Purpose

The focus of research in this dissertation is toward the design, development, and application of mechanism-based inhibitors for aerobic flavoenzymes. The aim is to expand our existing inhibitor set to help elucidate the modular domain enzymology of certain biosynthetic FAD-dependent domains, such as BpsA in the biosynthesis of indigoidine. Against these domains, a mechanism-based inhibitor scaffold containing a reactive benzothiocarbonate moiety has been developed. This reactive moiety has demonstrated inhibition against the oxidase-containing flavoenzyme, BpsA, and other representative examples from the monooxygenase and halogenase classes (described in greater detail in Chapters 4 and 5). Generally speaking, this inhibitor scaffold was employed to study these flavoenzymes in three major areas: flavoenzyme mechanism, domain crosslinking, and fluorescent detection (Figure 3.1).

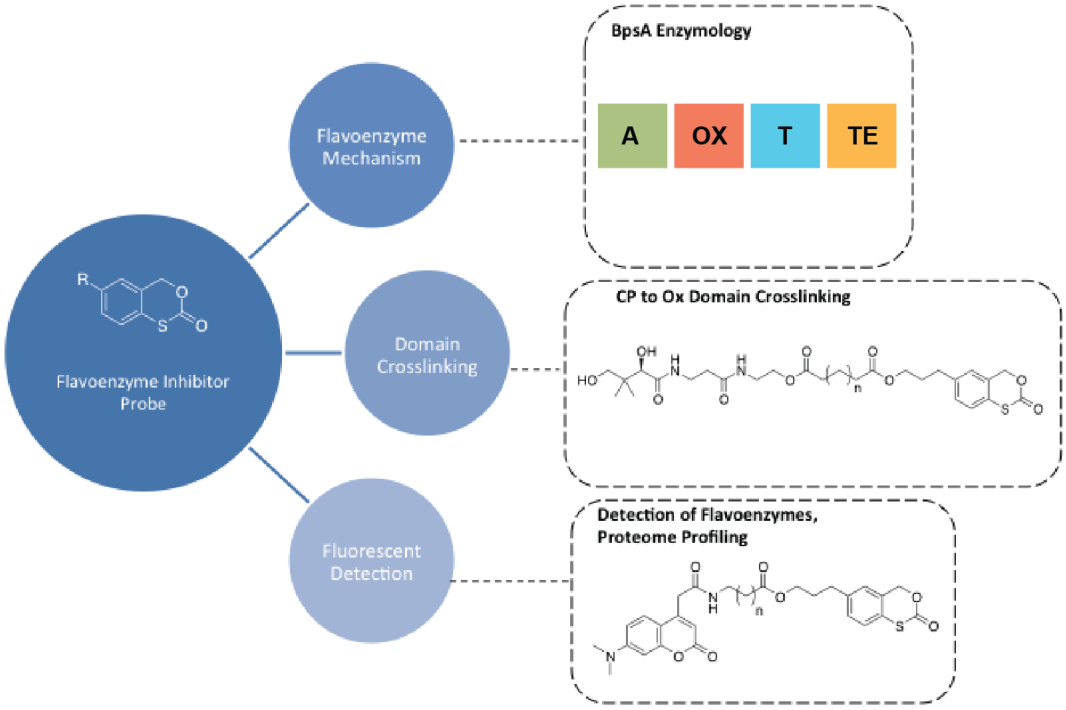

Figure 3.1: The flavoenzyme inhibitor scaffold can be used to probe flavoenzyme mechanism, domain crosslinking, and for fluorescent detection of flavoenzymes. Adjacent boxes include examples of applications in these areas.

These studies correspond appropriately to the work flow diagram of research in the Burkart laboratory (Figure 3.2). First among these objectives, is the design and synthesis of inhibitor probes that bind to these domains. Described in this chapter, are the efforts to accomplish objective 1, which was to synthetically elaborate on the current reactive benzothiocarbonate inhibitor scaffold, providing tools to advance in this work flow scheme. Full experimental conditions and characterization of select compounds are provided in Chapter 4.

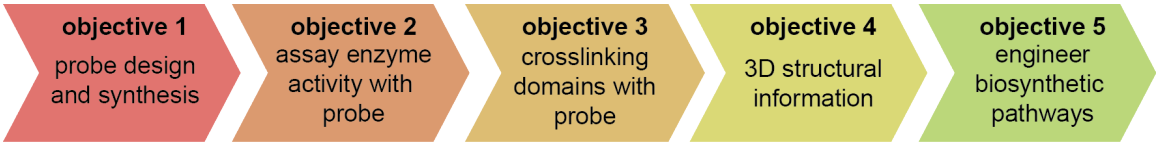

Figure 3.2: Work flow diagram of objectives toward probe design and applications in the Burkart laboratory.

3.2 Benzothiocarbonate Inhibitor Design and Synthesis

The concept of the benzothiocarbonate inhibitor was based upon the 1,3-oxathian-2-one inhibitor motif, described by Latham and Walsh in 1987.[1] Given the reactivity of their inhibitor with cyclcohexanone monooxygenase (CHMO), we hypothesized that this scaffold could be extended to inhibit a variety of flavoeyznes that contain the reactive flavin peroxide species, owing to the oxophilic tendencies of the sulfur atom in the thiocarbonate moiety.

To validate that benzothiocarbonates could sustain these types of broad inhibitory properties on all aerobic flavoenzymes, we focused on the synthesis of the basic thiocarbonate scaffold, **1** (Figure 3.3) The synthesis of **1** was achieved in a two-step, back-to-back process, which included reduction of thiosalicylic acid with lithium aluminum hydride (LAH) and subsequent treatment with carbonyl diimidazole (CDI). While **1** is not a novel compound, it was only previously examined primarily for synthetic interest, and its bioactive properties were never reported.[2]

We envisioned that the inhibitory mechanism of benzothiocarbonates would be analogous to that proposed for 1,3-oxathian-2-one by Latham and Walsh (Figure 3.4).[1] Under this scheme, inhibitor **1** is oxidized by the Fl-OOH species of the aerobic flavoenzyme to generate either acyl sulfoxide **2** or sulfenic anhydride **3**. The

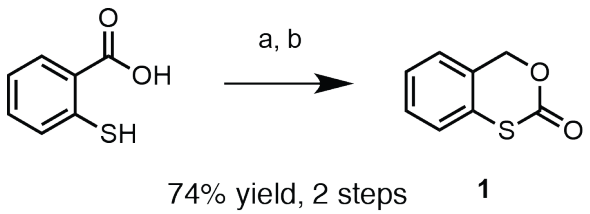

Figure 3.3: Synthesis of **1**. Reaction conditions: a) LAH, THF, 0°C to RT, 3 h; b) CDI, DCM, 3 h.

nucleophilic residues of the flavoenzyme are then acylated by addition to the carbonyl carbon (**4**) and potential disulfide linkage to the corresponding sulfur-containing moiety (**5**). The nascent inhibitor-enzyme adduct thus inactivates flavoenzyme activity by covalently binding within the active site and blocking substrate access.

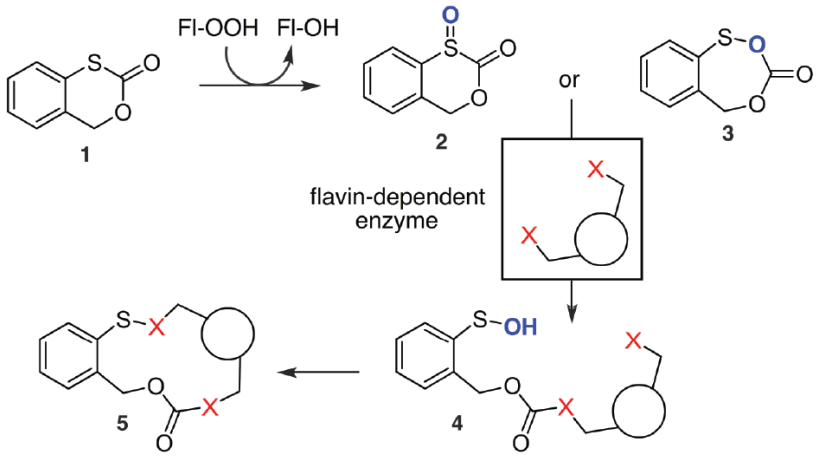

Figure 3.4: Inhibitor mechanism. Inhibitor **1** renders the enzyme inactive by covalent crosslinkage.

Compound **1** was then tested for its inhibitory properties of the oxidase-type domain, using BpsA as a reporter enzyme system. Since BpsA produces the blue pigment, indigoidine, inhibition could be easily measured as a function of its production of apparent product, both visually and spectrophotometrically at $\lambda_{abs} = 590$ nm. Enzymatic assays with BpsA in vitro, demonstrated that **1** was a potent covalent inhibitor with a $K_i = 46.9 \pm 3.1$ nM and $k_{inact} = 5.56 \pm 0.47 \times 10^3$ s^{-1} (Figure 3.5a-c).

Heterologous expression of BpsA and Sfp, an activating phosphopantotheinyl transferase, in *E. coli* allowed a visual means of assaying BpsA activity *in vivo*. Filter discs laden with increasing concentrations of **1** were placed on plates containing lawns of *E. coli* double transformants (Figure 3.5d). Treatment with **1** resulted in zones of white colonies, where BpsA was inhibited, but alive; increased ten-fold concentration of **1** resulted in a zone of antibiotic activity with a ring of white colony BpsA inactivation surrounding it. The combination of the quantitative *in vitro* and qualitative *in vivo* results, provided strong evidence for the inhibitory properties of **1** and the scaffolds' potential for probing this flavoenzyme activity.

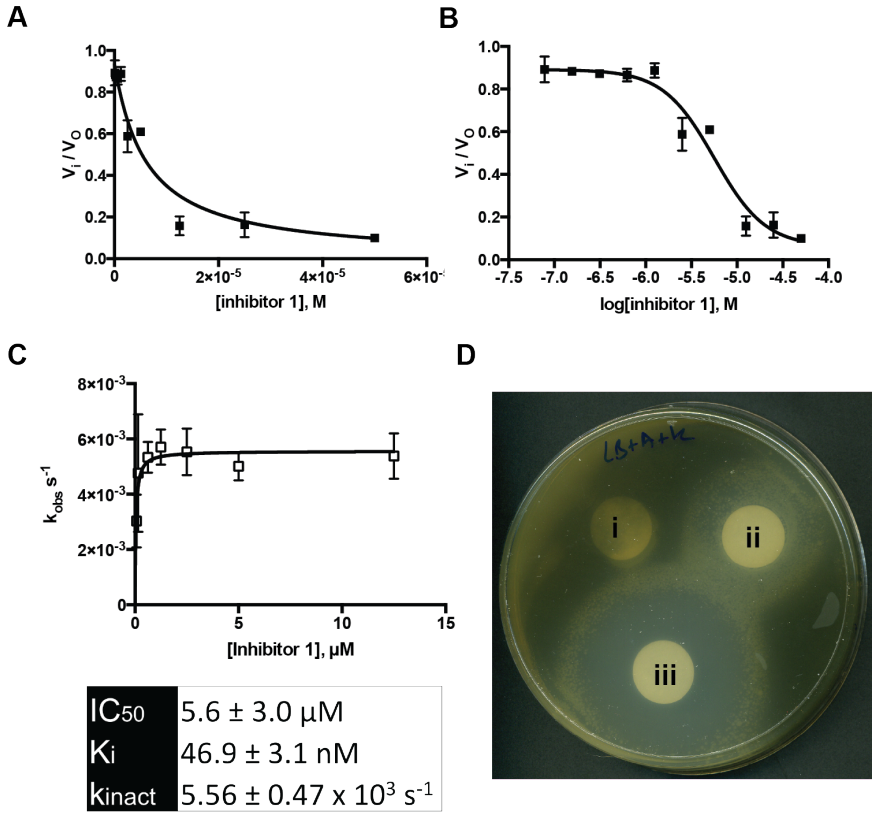

Figure 3.5: Inhibitory properties of **1** *in vitro* and *in vivo*. A)

3.3 Development of Fluorescent Inhibitor Probes

Development of fluorescent benzothiocarbonate inhibitors was pursued first among these areas in our scheme because it may be used to validate reactivity and selectivity of these probes. Such validation was key for demonstrating that this scaffold is active against other aerobic flavoenzyme domains than simply that of BpsA, as our preliminary results have shown.

3.3.1 Synthetic Route 1

The first synthetic route toward a fluorescent inhibitor probe was envisioned by accessing a functionalized handle appended to the benzothiocarbonate moiety (Scheme 2). This appendage could be installed by a Sonogashira coupling reaction of an aryl halide and alkyne. Additionally, the thiocarbonate could be installed from a phenol by a Miyazaki-Newman-Kwart reaction.[3] Hence, the functionalized inhibitor could be accessed from **7**, a commercially-available bromo methyl salicylate.

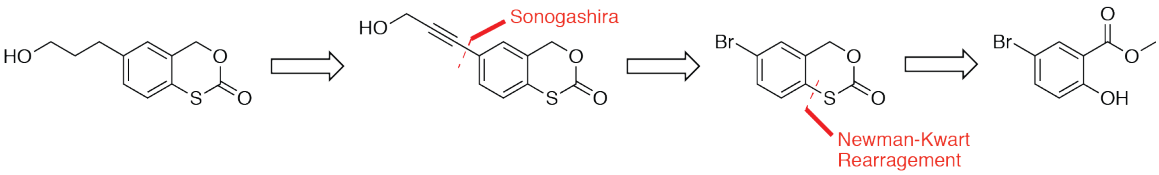

Figure 3.6: Retrosynthesis of the synthetic route 1 to obtain a functionalized benzothiocarbonate.

Compound **8** was obtained by reaction of **7** with dimethylthiocarboyl chloride and triethylamine with a yield of 67% (Figure 3.7). Yields of 8 could be improved to 92% by using DABCO instead of triethylamine. Thiocarbamate **9** was accessed by an intramolecular Miyazaki-Newman-Kwart rearrangement under 180°C and using bromobenzene as a heat transfer medium. The thiophenol 10 was obtained from

hydrolysis with 10% aq. NaOH. Compound **10** was then subjected first to reduction with lithium aluminum hydride, and the crude material was treated with carbonyl diimidazole to afford the bromo benzothiocarbonate **11**.

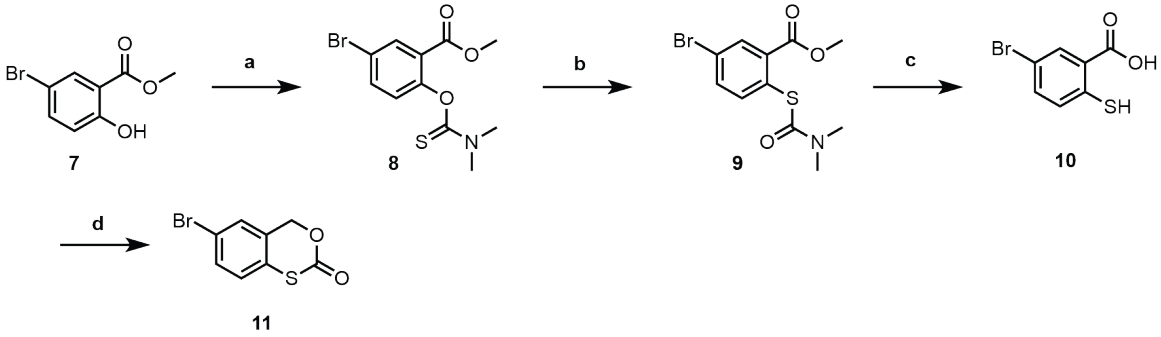

Figure 3.7: Synthesis of a bromothiocarbonate. Reaction conditions: a) Et_3N, $(CH_3)_2NCSCl$, DMF; 67% yield b) 180%C, bromobenzene c) 10% NaOH, H_2O d) 1. LAH, THF 2. CDI, DCM.

The Sonogashira coupling reaction was then attempted with **12** under twelve different conditions, varying alkyne, solvent, catalyst, base, and temperature (Figure 3.8). While some starting material had been recovered at each attempt, a majority had been lost to degradation an oligimerization. It was then hypothesized that the conditions for the Sonogashira coupling may be too harsh for the reactive thiocarbonate, or that the sulfur atom may be poisoning the palladium catalyst.

To address the reactivity issues of the thiocarbonate **12**, the Sonogashira reaction was attempted with the relatively less reactive thiocarbamate **9** (Figure 3.9), but to no avail. Nearly all starting material was recovered, however, indicating that the thiocarbamate was not sensitive to the Sonogashira conditions. Thus, it was then hypothesized that the aryl bromide was simply not reactive enough to undergo coupling with the alkyne under the conditions attempted.

The Sonogashira conditions were then performed on a more reactive aryl iodide to validate the activity of the catalysts and find optimal conditions for the reaction

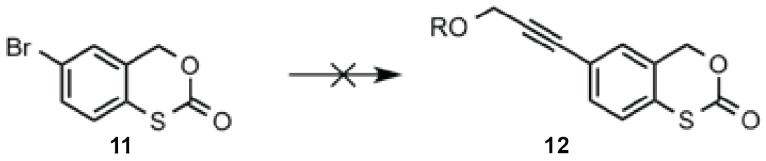

Entry	Alkyne	Solvent	Catalyst	Base	Temp (˚C)	
1	propargyl-OH	THF	Pd(PPh3)2Cl2	TEA	50	✗
2	TBSO-propyne	THF	Pd(PPh3)2Cl2	TEA	50	✗
3	TBSO-propyne	DMF	Pd(PPh3)2Cl2	TEA	50	✗
4	TBSO-propyne	DMF	Pd(PPh3)2Cl2	DBU	50	✗
5	TBSO-propyne	THF	Pd(PPh3)4	DBU	25	✗
6	TBSO-propyne	THF	Pd(PPh3)4	DIPEA	25	✗
7	TBSO-propyne	THF	Pd(PPh3)4	DBU	50	✗
8	TBSO-propyne	THF	Pd(PPh3)4	DIPEA	50	✗
9	TBSO-propyne	THF	Pd(PPh3)4	TEA	50	✗
10	TBSO-propyne	DMF	Pd(PPh3)2Cl2	DBU	25	✗
11	TBSO-propyne	DMF	Pd(PPh3)2Cl2	DIPEA	25	✗
12	TBSO-propyne	DMF	Pd(PPh3)2Cl2	TEA	25	✗

Figure 3.8: Conversion of **11** to **12** was attempted using Sonogashira reaction conditions by varying alkyne, solvent, catalyst, base, and temperature. Addition of CuI was held constant at 5 mol%. Red cross marks at right indicate no observation of **12**.

(Figure 3.10). The second attempt with tetrakis(triphenylphosphine)palladium(0), triethylamine, at 70°C with no co-solvent gave the Sonogashira product in 85% yield. The positive result supported attempting the synthesis with an aryl iodide instead of the bromo iodide.

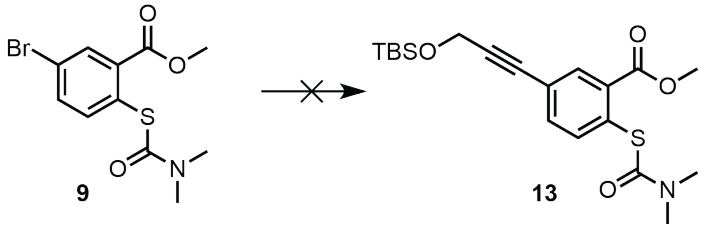

Figure 3.9: Conversion of **9** to **13** was attempted using Sonogashira reaction conditions (above).

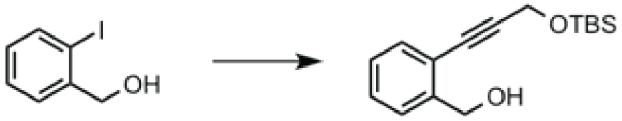

Entry	Alkyne	Solvent	Catalyst	Base	Temp (˚C)	
1	TBSO-propyne	DMF	Pd(PPh3)2Cl2	TEA	50	✗
2	TBSO-propyne	——	Pd(PPh3)4	TEA	70	✓

Figure 3.10: Conversion of aryl iodide was attempted using Sonogashira reaction conditions by varying alkyne, solvent, catalyst, base, and temperature. Addition of CuI was held constant at 5 mol%. Red cross marks at right indicate no observation of product; the green check mark indicates product was observed.

3.3.2 Synthetic Route 2

A new synthetic route was thus devised to incorporate the use of an aryl iodide as a coupling partner in the Sonogashira reaction (Figure 3.11). It was also devised such that the synthesis could be attempted by switching the order of reactions to afford flexibility in evading potential synthetic pitfalls.

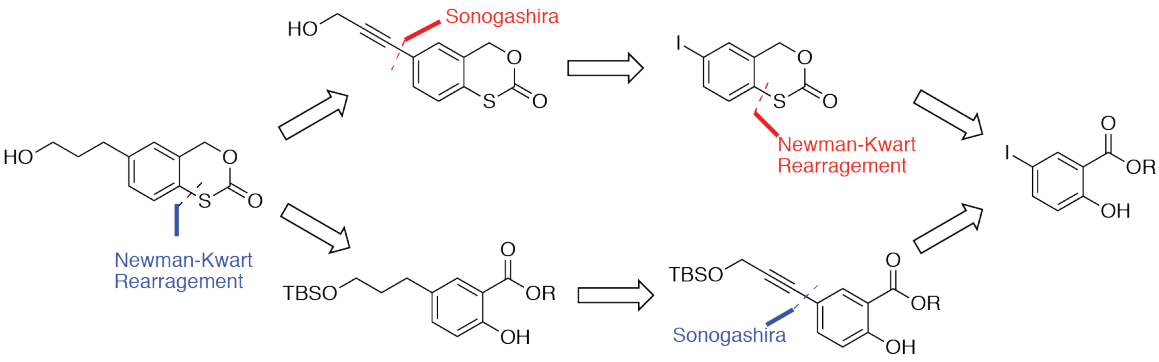

Figure 3.11: Retrosynthesis of the synthetic route 1 to obtain a functionalized benzothiocarbonate. Red and blue text indicate separate pathways.

The first pathway attempted was the red sequence indicated above. Unlike the aryl bromide **7**, the corresponding aryl iodide was not commercially available. However, the aryl iodide **15** could be prepared from commercially available **14** using chloramine-T and NaI (Figure 3.12). The reaction proceeds because, *in situ*, I-Cl is formed allowing electrophilic aromatic substitution at the most reactive and available para position. Compound **15** was treated under the sequence in synthetic route 1, where the addition of the thiocarbamate and subsequent Miyazaki-Newman-Kwart rearrangement provided 16 and 17, respectively.

The Sonogashira reaction was then attempted on compound **17** because of its relatively stable thiocarbamate compared to the final thiocabonate. The conditions were replicated from the positive result achieved with the model iodo compound

above, which fortunately gave the product **18** in 82% yield.

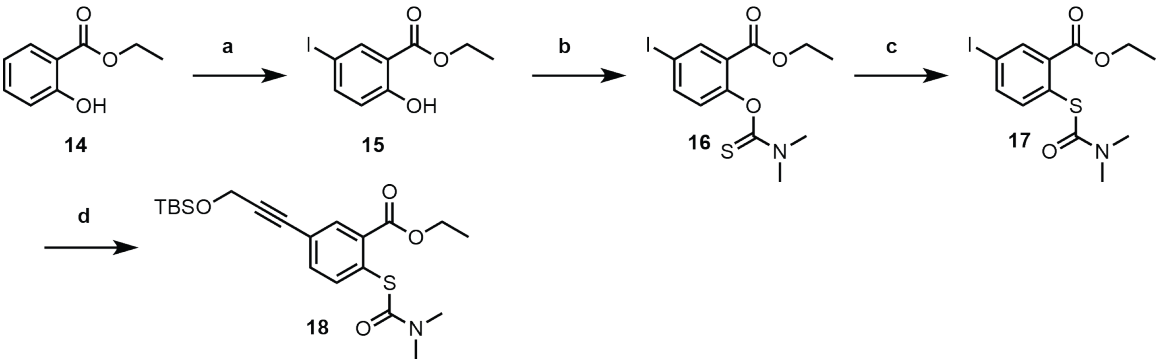

Figure 3.12: Synthesis of **18**. Reaction conditions: a) Chloramine-T, NaI, DMF b) Et_3N, $(CH_3)_2NCSCl$, DMF c) 180°C, bromobenzene d) TBSO-propyne, $Pd(PPh_3)_4$, CuI, Et_3N, 50°C.

Hydrogenation of alkyne **18** was then attempted with four catalyst conditions in an attempt to afford **19** (Figure 3.13). The reaction was monitored over 72 hours, during which the unreacted starting material **18** was observed until the unintended product**20** was observed after 48 hours. It was hypothesized that the sulfur or combination of polar groups were chelating the catalysts, thus poisoning the ability to hydrogenate. The slow pi-allyl elimination of TBSOH was hypothesized to occur, owing to the position of the propargyl group in relation to the conjugated system.

To avoid the elimination problem and perhaps encourage hydrogenation of the alkyne, the Sonogashira reaction was performed with TBSO-butyne to give **21** (Figure 3.14). The hydrogenation conditions were attempted with the same conditions as above. While no elimination of the TBSOH group was observed, product **22** was not formed. It was reasoned that the polar functionality might be the main problem in poisoning the hydrogenation catalyst reactivity.

Because the alkyne was not situated near the reactive inhibitor portion of the molecule, we hypothesized that the alkyne may have insignificant bearing on

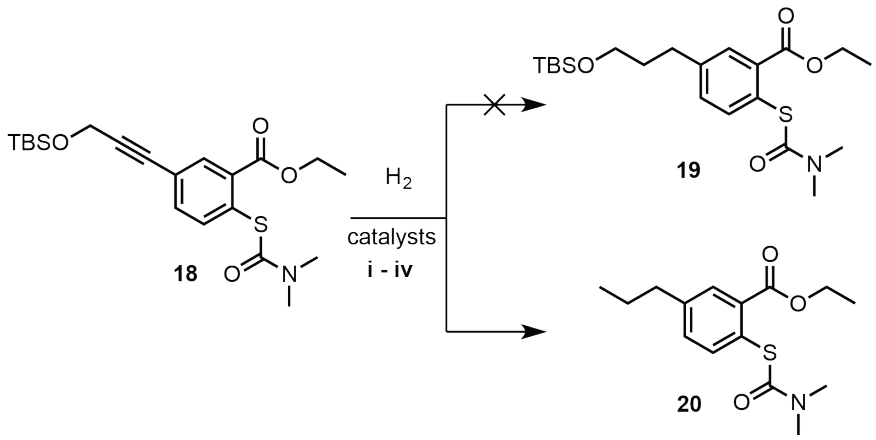

Figure 3.13: Hydrogenation attempts. Reaction of **18** under hydrogen gas and catalysts i-iv gave**20** instead of **19**. Catalysts conditions: i) 5% Pd on C ii) 10% Pd on C iii) 5% Pt on C iv) PtO_2 .

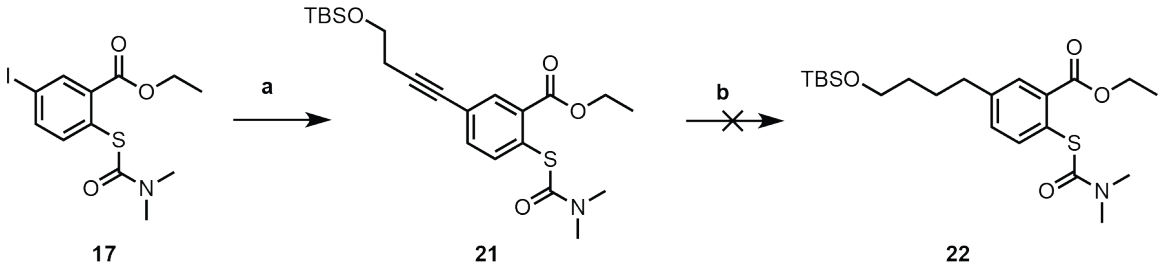

Figure 3.14: Hydrogenation attempts with TBSO-butyne. Reaction conditions: a) TBSO-butyne, $Pd(PPh_3)_4$, CuI, Et_3N, 50°C. b) H_2 , PtO_2.

the probe reactivity. Hence, the reaction sequence was continued leaving the alkyne intact. The same reduction with LAH and CDI carbonylation steps were used as in synthetic route 1, however the first step was modified so that it was quenched with neutral water instead of 3N HCl to avoid acidic deprotection of the TBS group. Instead of forming **23**, an oligomerized set of molecules (**24**) were observed by mass spectrometry, which suggested thiol dimerization. The thiol dimerization was likely due to a slightly basic or slow reaction conditions that allowed thiolates to dimerize rather than form thiocarbonates.

However, these conditions were optimized by using phosgene instead of CDI,

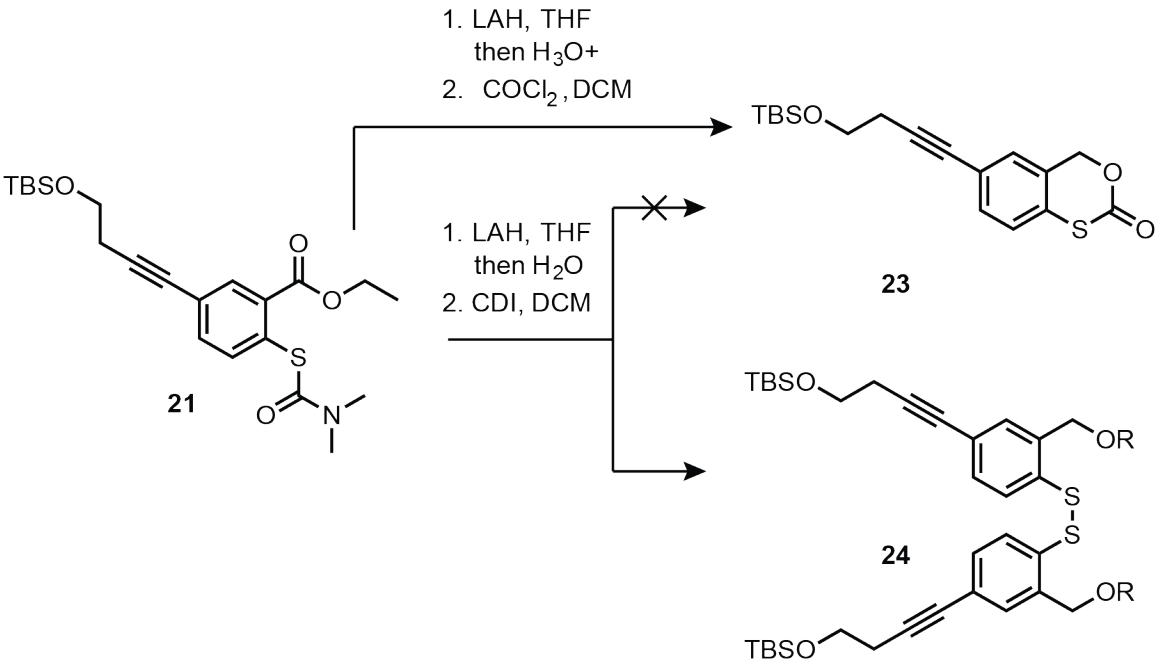

Figure 3.15: Reaction of **21** under reaction two conditions.

which acted faster and more selectively to give **23**, rather than the oligermized **24**. Acidifying work-up conditions with ammonium chloride also gave higher yields of **23**.

3.3.3 Synthetic Route 3

A final synthetic route was pursued that exploited the productive Sonogashira conditions of the previous two routes, but employed an alkyne that would accommodate functionalization, endure the reaction conditions needed to form the thiocarbonate moiety, and be amenable to modular installation to a variety of alternative linkers and fluorescent probes. Along those prerequisites, we attempted a reaction scheme whereby 17 could be coupled with hepta-1,6-diyne (Figure 3.16). Conversion from **17** to **21** proceeded by the same Sonogashira conditions, but singular crosscoupling of the alkyne to one equivalent of 21 was controlled stoichoimetrically by addition of two equivalents of hepta-1,6-diyne to the reaction mixture. Compound **21** was converted

to **23** directly by reduction with LAH and treatment with CDI or phosgene, and it was obtained indirectly by hydrolysis to obtain **22**, then treatment with the previous conditions. The indirect hydrolysis was performed to observe whether **23** could be obtained in higher yields if the more stable thiocarbamate were first converted to the thiophenol. While the non-reduced thiocarbamate was still observed after 3 hours as a minor product, in practice, the extra hydrolysis step did not significantly improve yields of **23**.

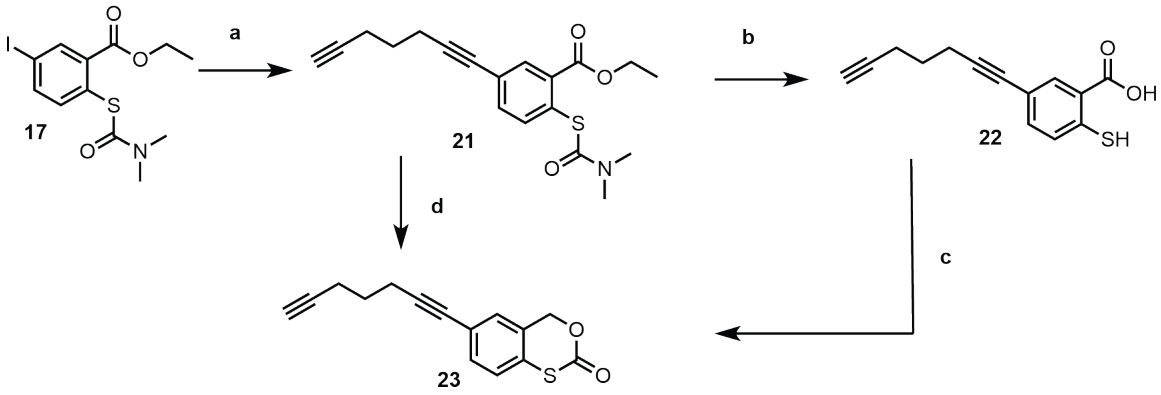

Figure 3.16: Synthesis of bisalkyne **23**. Reaction conditions: a) hepta-1,6-diyne (2 equiv.), $Pd(PPh_3)_4$, CuI, Et_3N, 50°C., b) 10% NaOH in 1:1:1 H_2O/MeOH/THF, c) and d) LAH, THF then $COCl_2$, DCM.

Compound **23** was then tested for its inhibitory properties of BpsA in vitro. By increasing concentration of **23** the activity of BpsA decreased, as measured by monitoring absorbance at 590 nm, with an observed IC_{50} 61 μM (Figure 3.17). While this result marks a decrease in inhibition compared to that of compound **1**, compound **23** was considered to be a good candidate for use as a probe of activity for *in vitro* applications.

Among several candidate fluorophores to couple to compound **23**, we decided upon the dimethylaminocoumarin containing compound **24**, which could undergo click conditions, or a Huisgen 1,3-dipolarcycloaddion, to afford a adjoined triazole

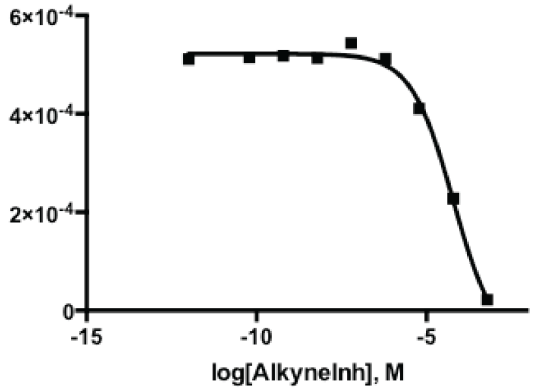

Figure 3.17: Dose-dependent inhibition of BpsA activity plotted against the log of concentration of inhibitor **23**.

adduct. Many conditions were attempted to give the clicked product **25** (Figure 3.18). The highest yielding conditions were those performed in 1:1 t-butanol/water with copper sulfate, sodium ascorbate, and TBTA as a ligand for stabilizing the reactive Cu(I) species.[4] The reaction could also be performed in organic conditions with toluene as solvent, copper(I) iodide, and three equivalents of diisopropylethylamine (DIPEA) to give **25** in decent yields.

With compound **25** in hand, we envisioned using it as a final flurourescent probe that could be amenable for further variation by modular installation of other azide partners (Figure 3.19). Chapter 4 provides our investigation into this topic.

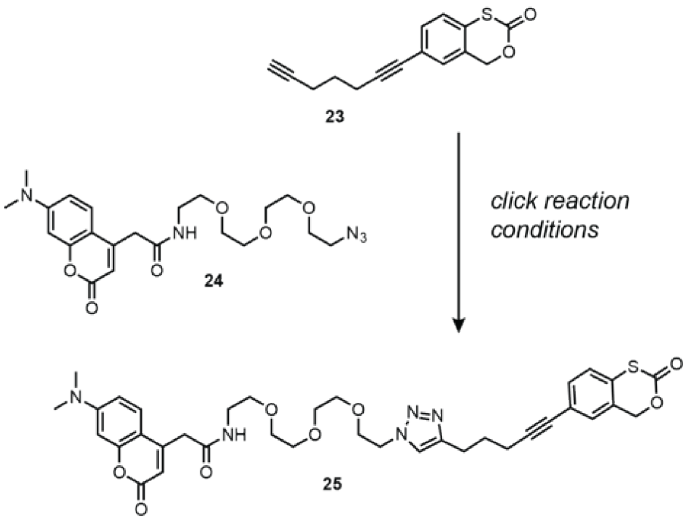

Entry	Cu(I) Source	Ligand Additive	Solvent	Yield
1	$Cu(PPh3)_3Br$	–	MeCN	–
2	$Cu(PPh3)_3Br$	–	1:1 t-butanol/H_2O	11%
3	$CuSO_4$ + NaAsc	–	1:1 t-butanol/H_2O	65%
4	$CuSO_4$ + NaAsc	TBTA	1:1 t-butanol/H_2O	73%
5	CuI	TBTA	1:1 t-butanol/H_2O	–
6	CuI	3 eq. DIPEA	toluene	62%
7	CuI	3 eq. DIPEA	THF	–

Figure 3.18: Click conditions attempted for synthesis of probe **25**.

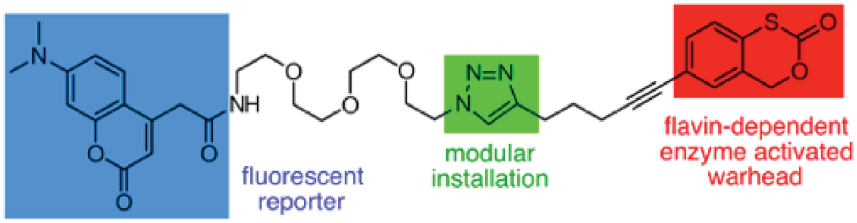

Figure 3.19: Structure of fluorescent probe with benzothiocarbonate warhead.

3.4 Synthesis of Benzothiocarbonate Variants

To investigate the limitations of positions that could be elaborated upon the original benzothiocarbonate scaffold and retain inhibitory properties, we undertook the synthesis of benzothiocarbonate variants that have substitutions at the benzyl position of **1**, which has been demonstrated synthetically by various groups.[5] First, we synthesized compound **27** from commercially-available **26** by treatment with sodium sulfate nonahydride and subsequent addition of acetic anhydride (Figure 3.20). Addition by n-butyllithium, and treatment with phosgene gave **28** as a racemic mixture. Similarly, treatment of **29** with methyllithium gave **30**, which could be protected with acetic anhydride to give **31**. Treatment with the same n-butyllithium and phosgene conditions gave racemic **32** (Figure 3.21). Compounds **28** and **32** were tested for their inhibition of BpsA with concentrations up to 100 mM. Unfortunately, no inhibition of BpsA of detected.

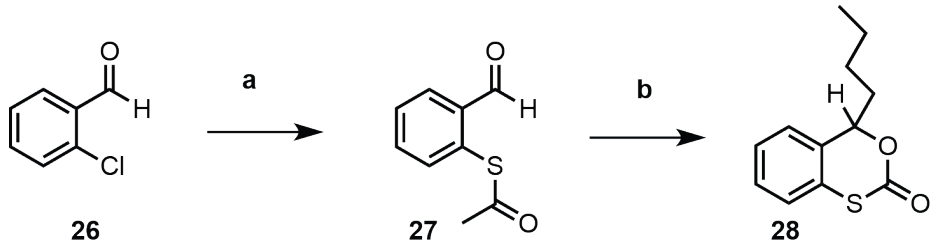

Figure 3.20: Synthesis of aldeyhyde-derived **28**, by alkyl lithium addition. Reaction conditions: a) $Na_2S{\cdot}9H_2O$, dimethylacetamide, 70°C, then acetic anhydride, b) nBuLi (3 equiv.), THF, at -70° then $COCl_2$.

Slightly more compact versions of this motif were envisioned by addition of an allyl Grignard reagent, instead of n-butyllithium. Treatment of **27** and **31** with the allyl Grignard reagent and phosgene gave **33** and **34**, respectively. Neither **33** or **34** exhibited inhibition of BpsA with concentrations up to 100 mM.

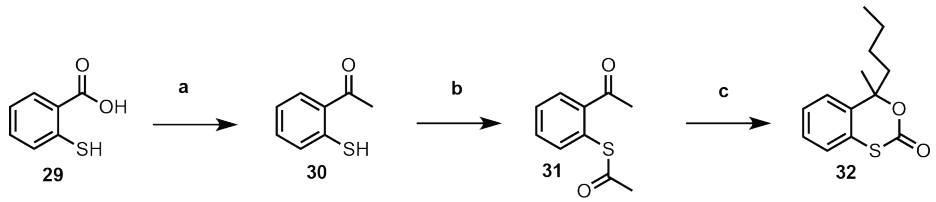

Figure 3.21: Synthesis of ketone-derived **32**, by alkyl lithium addition. Reaction conditions: a) MeLi (3 equiv.), THF, b) acetic anhydride, Et_3N, c) nBuLi (3 equiv.), THF, at -70° then $COCl_2$.

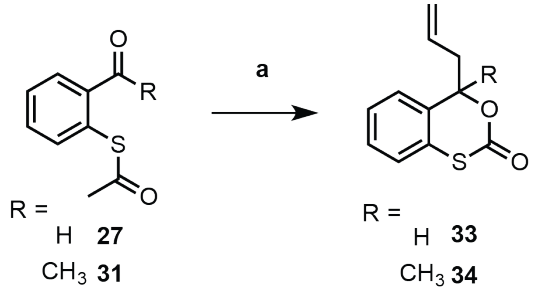

Figure 3.22: Synthesis of allyl thiobenzocarbonates. Reaction conditions: a) allylmagnesium bromide (3 equiv.), THF, -70°.

3.5 Concluding Remarks

Discussed in this chapter was the synthesis of tools for investigating flavoenzymes, including a reactive thiocarbonate inhibitor and a fluorescent thiocarbonate probe. Despite some noted setbacks, the goal was attained with a terminal alkyne linker that was amenable for modular installation of other potential chemical moieties of interest, including a possible pantetheine portion for crosslinking to carrier protein domains. Using these probes, in combination of co-crystallization studies, will hopefully advance our understanding of flavoenzyme domains and the metabolic processes in which they are involved.

3.6 References

1. Latham, J. A.; Walsh, C., *J. Am. Chem. Soc.* **1987**, *109* (11), 3421.

2. Meier, H.; Mayer, A., *Synthesis* **1996**, *1996* (03), 327.

3. (a) Miyazaki, K., *Tetrahedron Lett.* **1968**, (23), 2793; (b) Newman, M. S.; Karnes, H. A., *J. Org. Chem.* **1966**, *31* (12), 3980; (c) Kwart, H.; Evans, E. R., *J. Org. Chem.* **1966**, *31* (2), 410

4. Chan, T. R.; Hilgraf, R.; Sharpless, K. B.; Fokin, V. V., *Org. Lett.* **2004**, *6* (17), 2853.

5. Kamila, S.; Khan, O.; Zhang, H.; Biehl, E. R., *Synth. Commun.* **2006**, *36* (10), 1419.

Chapter 4

Fluorescent Mechanism-Based Inhibitors of Aerobic Flavoenzymes

4.1 Abstract

Diversity in non-ribosomal peptide and polyketide secondary metabolism is facilitated by interaction between biosynthetic domains with discrete monomer loading and their cognate tailoring enzymes, such as oxidation or halogenation enzymes. The cooperation between peptidyl carrier proteins and flavin-dependent enzymes offers a specialized strategy for monomer selectivity, which oxidizes small molecules from within a complex cellular milieu. In an effort to study this process, we have developed fluorescent probes to selectively label aerobic flavin-dependent enzymes. Here we report the preparation and implementation of these tools to label oxidase, monooxygenase and halogenase flavin-dependent enzymes.

4.2 Introduction

Natural product biosynthesis occurs through a cascade of enzymatic reactions that combine monomeric building blocks into complex chemical scaffolds.[1] Over the last decade, our laboratory has participated in a global effort to develop methods that discretely label enzymatic domains responsible for fatty acid, polyketide, and nonribosomal peptide biosynthesis.[2] A variety of tools now exist to selectively label domains containing activities of acyl and peptidyl carrier proteins,[3] ketosynthases,[4] dehydratases,[5] and thioesterases.[6] We now report efforts to deliver probes that label aerobic flavin-dependent enzymes, or flavoenzymes, as a first step in delivering selective probes for oxidative enzymes within carrier protein dependent pathways.

Aerobic flavoenzymes are oxygen-dependent and catalyze a variety of reactions in natural product biosynthesis, including desaturations, mono-oxygenations, and halogenations.[7] These enzymes are subcategorized by their use of catalytic cycle within three major classes: oxidases,[7] monooxygenases,[8] and halogenases[9] (Supporting Figure 4.18). Each cycle initiates with the oxidation of reduced flavin (FlH_2) with O_2 via a radical mechanism, forming the hydroperoxy-containing flavin (Fl-OOH) at the C(4a) position depicted in Figure 4.1.[10] The fate of the Fl-OOH species is resolved differently in each of the three flavoenzyme classes (Supporting Figure 4.18).

Mechanism-based inhibitors have been developed for the monoamine oxidase subset of flavin-dependent enzymes, where irreversible inhibitors containing *N*-propargylamine moieties, such as pargyline and clorgiline, are used to covalently react with the flavin via oxidation and Michael addition.[11] These inhibitors have been used to probe substrate specificities in the active sites of these enzymes, and fluorescent derivatives have been used as probes for targeting specific enzymatic activity.[12] How-

ever, no similar probes have yet been demonstrated for monooxygenases or halogenases.

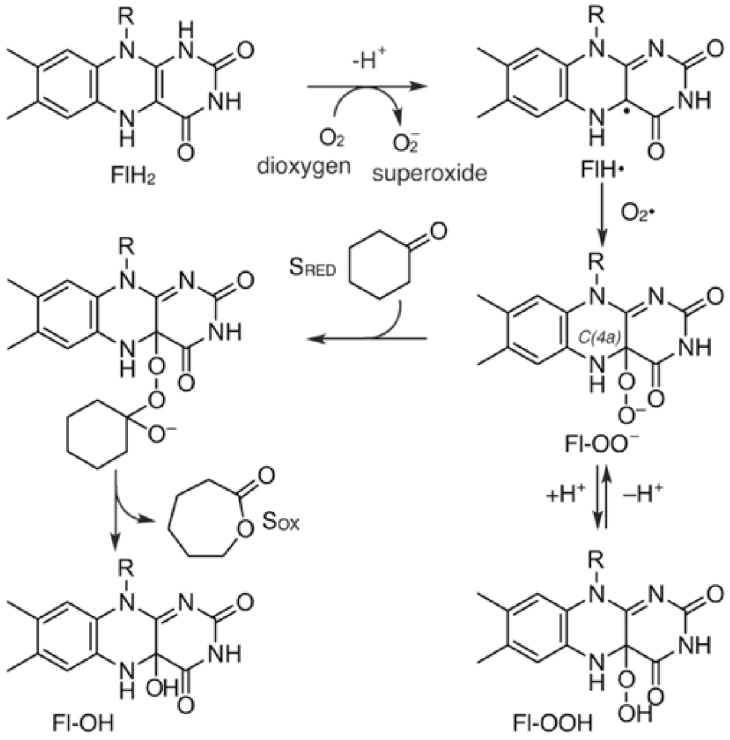

Figure 4.1: Action of a flavin-dependent enzymes as illustrated by the Baeyer-Villiger oxidation of cyclohexanone (S_{RED}) to caprolactone (S_{OX}).[10]

In 1987, Latham and Walsh reported mechanism-based inhibition of an *Acinetobacter*-derived cyclohexanone monooxygenase (CHMO) using a cyclic thiocarbonate.[13] They proposed that this motif, upon oxidation with the Fl-OOH species, became an electrophilic warhead for enzyme inactivation, but further studies were not pursued. To examine the potential of these agents, we turned our attention to compound **1** as an aromatic thiocarbonate core for installation of reporter motifs.[14] Here, exposure to Fl-OOH would result in the generation of either acyl sulfoxide **2** or sulfenic anhydride **3** (Figure 2). These reactive intermediates would then be susceptible to nucleophilic attack within the active site of the corresponding flavin-dependent enzyme, leading

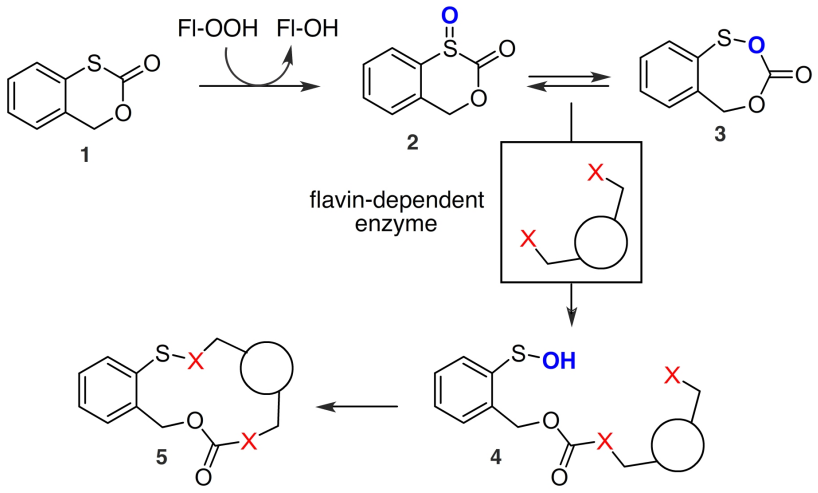

Figure 4.2: Proposed mechanism for the inhibition of flavin-dependent enzymes by **1**. The sphere represents a flavin-dependent enzyme, X (red) denotes nucleophilic residues within a flavin-dependent enzyme (in box) and O (blue) denotes oxygen atoms incorporated by the action of a flavin-dependent enzyme.

to covalently-linked protein **4** or the fully-crosslinked protein **5**.

4.3 Results and Discussion

We began by testing the inhibitory properties of **1** with a model flavin-dependent enzyme. We chose the BpsA oxidase (Ox) domain for a convenient colorimetric readout that had been previously employed for other non-ribosomal peptide synthetase (NRPS) associated enzymes.[15] As discrete domains within NRPSs, Ox domains catalyze the desaturation or dimerization of carrier protein-tethered substrates. BpsA-Ox catalyzes the desaturation of a piperidinedione intermediate, leading to the formation of indigoidine, a blue pigment (Supporting Figure 4.19).[16] Assays for *in vitro* inhibition of BpsA by compound **1** revealed an IC_50 value of 5.6 $\pm$ 3.0 μM, a K_i of 47 $\pm$ 3 nM, and a k_{inact} of 5.6 $\pm$ 0.5 ms^{-1} (Supporting Figure 4.20). The evidence

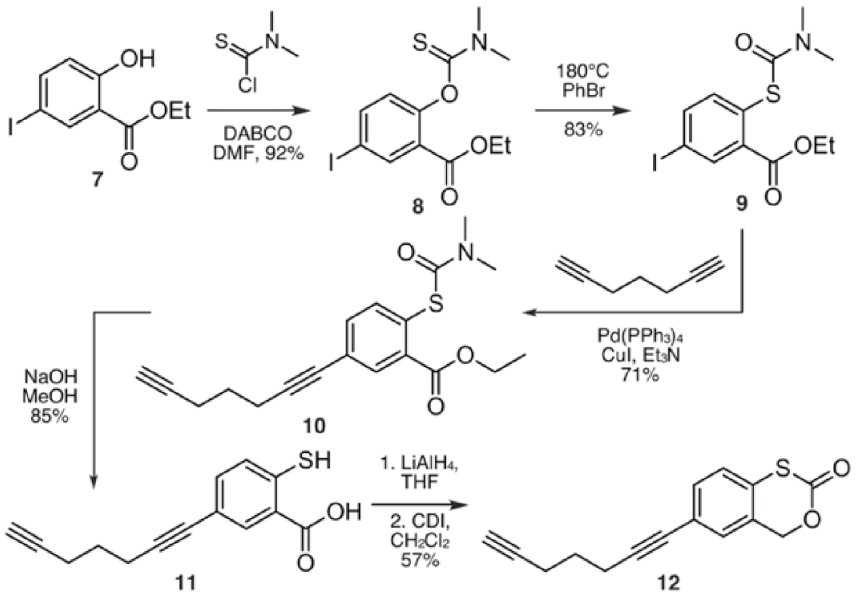

Figure 4.3: Probe **12** as prepared in 6 steps in an overall yield of 26% from ethyl 2-hydroxy-5-iodobenzoate (**7**)

of oxidase inhibition, along with previously demonstrated inhibition of CHMO by Latham and Walsh, highlighted the potential of these probes to target other aerobic flavoenzyme activities. We next turned our attention to elaborate **1** into a fluorescent reporter. As shown in Figure 4.3, we used the aryl-ring in **6** to regioselectively install a reporter in a position remote from the active moiety.

The synthesis of **6** began by converting ethyl 2-hydroxy-5-iodobenzoate (**7**) to its corresponding dimethylcarbamothioate **8**. Heating **8** in bromobenzene afforded an effective Miyazaki-Newman-Kwart rearrangement,[17] providing **9** in 76% yield from **7**. After exploring multiple options for Sonogashira coupling, we found the partner hepta-1,6-diyne offered a facile route to functionalization, offering access to **10** (Figure 3) with a terminal mono-substituted alkyne handle for reporter installation. The conversion of **10** to **12** required considerable optimization. We found that the most effective route to install the 1,3-oxathiin-2-one motif arose by hydrolysis of **10** to

afford **11**, which was immediately reduced and treated with CDI, to afford **12** in three back-to-back operations.[18]

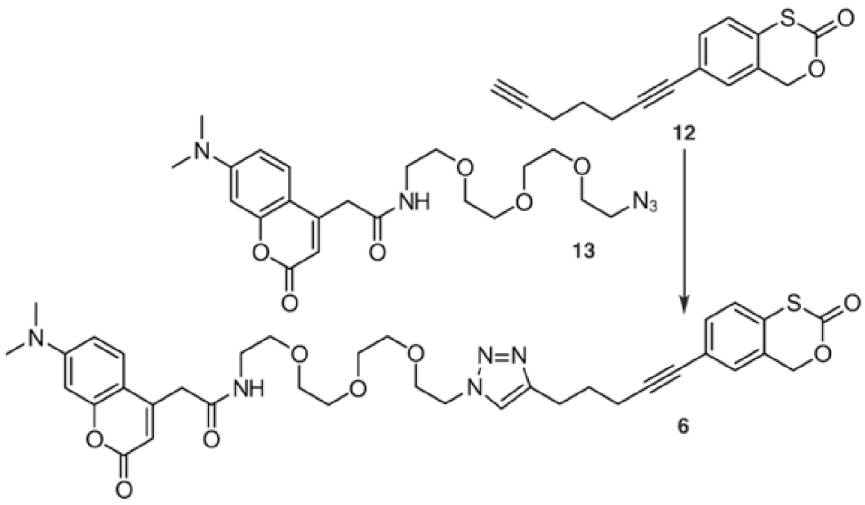

Figure 4.4: Reporter-labeling of probe **12** was achieved in aqueous (0.05 eq. $CuSO_4$ in 0.10 eq. sodium ascorbate) and anhydrous conditions (CuI, $EtNiPr_2$, toluene).

We then explored the incorporation of a reporter tag to **12** using conventional 1,3-dipolar cycloaddition chemistry.[19] We found that the blue fluorescent immunoaffinity azide tag **13**[20] could be installed to afford **6** under either aqueous conditions with 5% molar equivalents of $CuSO_4$ and aq. sodium ascorbate or anhydrous conditions with CuI and EtNiPr$_2$, respectively, in toluene (Figure 4.5)

As shown in Figure 4.6a, both apo-BpsA and holo-BpsA, generated *in vitro* by incubation with CoA and a 4'-phosphopantheinyl transferase, Sfp,[21] (Supporting Figure 4.21), were labeled with probe **6**. Furthermore, labeling of holo-BpsA occurred in both the presence and absence of ATP and glutamine (Figure 4.5a), indicating that BpsA was labeled without substrate dependency or 4'-phosphopantetheinylation.

Next, we expanded our panel of representative oxidative flavoenzymes to include the Baeyer-Villiger cyclohexanone monooxygenase (CHMO) from *Rhodococcus*

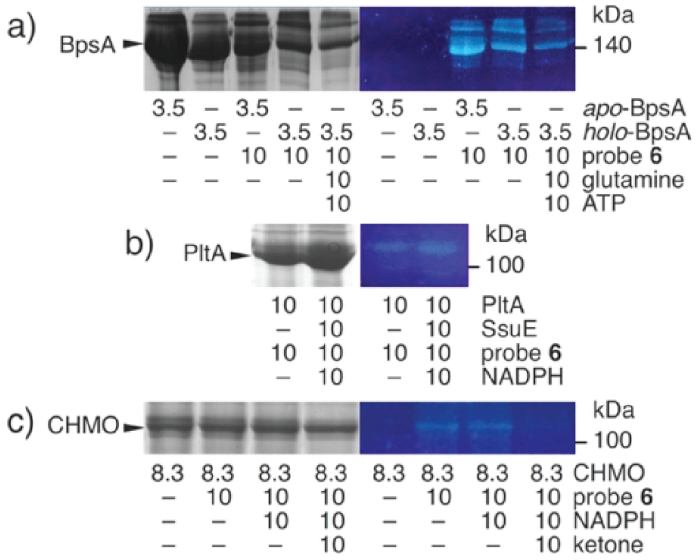

Figure 4.5: In-gel fluorescent SDS-PAGE analysis of protein labeling. Coomassie stained (left) and fluorescent (right) SDS-PAGE gels depicting the labeling of BpsA, PltA, or CHMO with probe **6**. a) The labeling of apo-BpsA or holo-BpsA with and without the presence of glutamine and ATP. b) The labeling of PltA with and without the presence of SsuE and NADPH. c) The labeling of CHMO with and without the presence of cyclohexanone (ketone) and NADPH. Concentrations are provided in μM. Full images of the gels are provided in Supporting Figure 4.22.

sp. HI-31, which can convert cyclohexanone to caprolactone (Figure 4.1);[8] and the NRPS halogenase PltA from *Pseudomonas fluorescens* responsible for dichlorination of a pyrrolyl-loaded carrier protein (pyrrolyl-PltL) substrate.[22]

We also found that **6** prepared *in situ* from **12** effectively labeled the halogenase, PltA (Figure 4.5b). While the addition of a partner enzyme SsuE, a flavin reductase compatible with PltA,[23] and NADPH increased labeling efficiency (Figure 4.5b), probe **6** labeled PltA without the need for addition of its associated partner enzyme or cofactors. In addition, we were able to demonstrate that the labeling of PltA with **6** occurred in a 1:1 stoichiometry via MALDI-MS analyses (Supporting Figure 4.24), suggesting that PltA was modified at a single site. Multiple attempts

were made to identify the modified residue in PltA using tryptic digestion followed by LC-MS-MS analysis. Unfortunately, we were not able to identify peptides bearing modifications by **6** or **1**, although superb peptide coverage was obtained. This observation was consistent with previous studies that used similar inhibitors,[13] suggesting that covalent linkages were not stable to either digestion or LC MS-MS analyses.

As shown in Figure 4.5c, CHMO also underwent labeling under identical conditions as BpsA or PltA with probe **6**. Interestingly, the addition of cyclohexanone and cofactor, NADPH, to CHMO diminished labeling with **6**, suggesting that **6** is a weak competitive inhibitor for CHMO compared to substrate under the assayed conditions. Interestingly, all three enzymes underwent labeling without the need of cofactors. This reactivity may be owed to relative abundance of these proteins in the C(4a)-hydroperoxide state, which is thought to predominate in the cell, as previous studies have demonstrated its relatively long-lasting stability by spectroscopic and crystallographic means.[24]

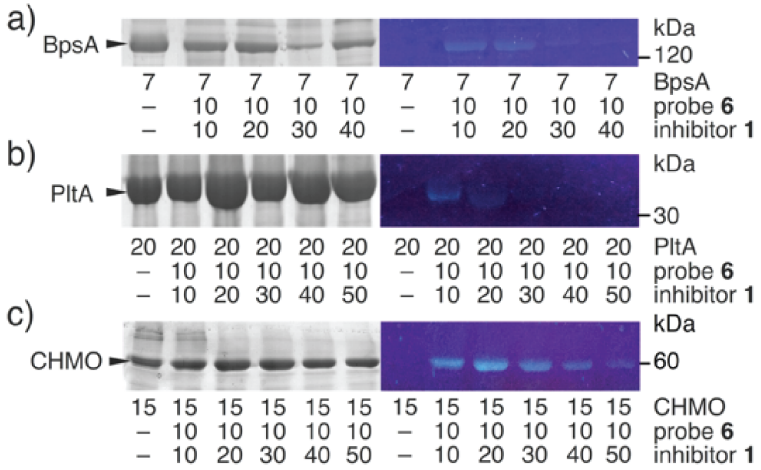

Figure 4.6: Competition experiments. Coomassie stained (left) and fluorescent (right) SDS-PAGE gels depicting the competition of **1** and **6** in labeling of: a) BpsA; b) PltA; or c) CHMO. Proteins were treated with 1 for 30 min then subjected to labeling with **6**. Concentrations are provided in μM. Full images of the gels are provided in Supporting Figure S6.

To further validate this activity, we turned to examine if these events were selective to the 1,3-oxathiin-2-one motif. As shown in Figure 4.6, the labeling of all three enzymes BpsA (Figure 4.7a), PltA (Figure 4.6b) and CHMO (Figure 4.6c) by **6** was reduced in a concentration-dependent manner when the enzymes were pre-incubated with **1**. In all examples, use of a 2 to 4 fold excess of **1** blocked labeling with **6**, suggesting a single site for inhibition for all three enzymes.

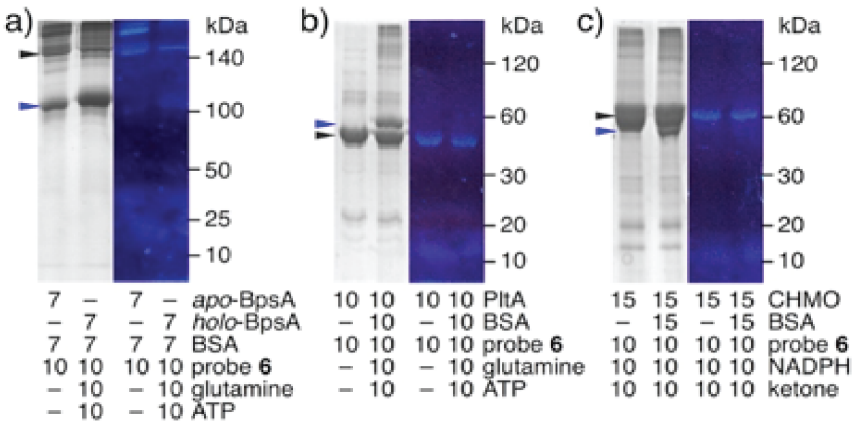

Figure 4.7: Selectivity analyses. Coomassie stained (left) and fluorescent (right) SDS-PAGE gels depicting the selective labeling of flavoenzymes BpsA, PltA, or CHMO (black arrows) in the presence of BSA (blue arrows). Gels depicting the labeling of: a) apo-BpsA/holo-BpsA; b) PltA; or c) CHMO. Concentrations are provided in μM.

Next, we tested selectivity of the probe for each flavoenzyme versus bovine serum albumin (BSA), a protein known for its binding to a variety small molecules including lipids, primary metabolites, natural products, synthetic drug leads and pharmaceuticals.[25] Upon incubation with probe **6**, BpsA (Figure 4.7a), PltA (Figure 4.7b), and CHMO (Figure 4.7c) were all preferentially labeled in the presence BSA. In all three cases, we were not able to detect any labeling of BSA, therein confirming the selectivity for flavoenzyme reactivity. Furthermore, it also indicated that the activation and reactivity of the 1,3-oxathiin-2-one motif did not occur outside the

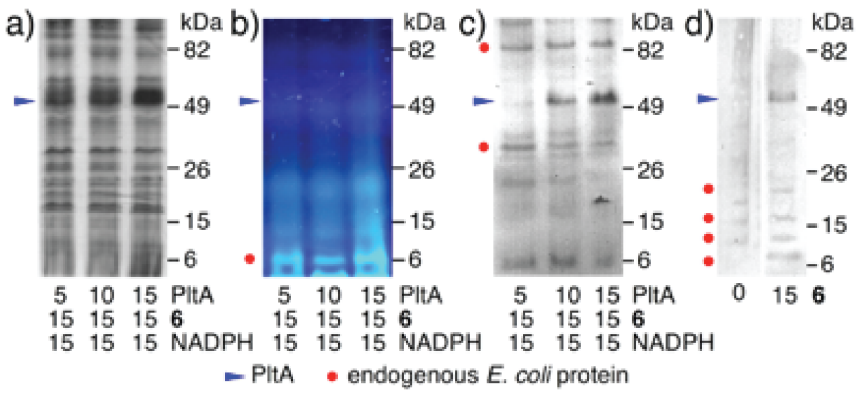

Figure 4.8: Labeling in PltA in lysate and live cells. a)-c) Images of SDS-PAGE gels depicing 20 μL *E. coli* lysate containing of 1 mg/mL total protein doped with 5-15 μM PltA. Samples were incubated with **6** and NADPH for 30 min prior to analysis via SDS-PAGE. a) Coomassie-stained gel depicting total protein in the sample. b) Fluorescent image with excitation at λ_{max} at 365 nm prior to Coomassie staining. c) Western blot from the gel in a) generated after development with an anti-IAF tag XRI-TF35 mAb (primary) and development using AP-labeled anti-mouse mAb (secondary). d) A 5 mL sample of the *E. coli* strain engineered to overexpress PltA (8×10^8 cells/mL) was treated with 15 μM probe **6** for 30 min at 25°C. The cells were lysed and subjected to SDS-PAGE and Western blotting as in c). Concentrations are provided in μM.

flavin cofactor pocket, such as through the release of H_2O_2 or HOCl, a concern that would have resulted in non-specific labeling.

We then applied our probe to labeling PltA in *E. coli* lysate. As shown in Figure 4.8a-c, we were able to observe labeling of PltA in wild type *E. coli* lysates to which were added 10 μM PltA, 15 μM **6** and 15 μM NADPH by Western blot analyses.[20] We were also able to conduct these experiments *in vivo*. As shown in Figure 4.8d, incubation of the *E. coli* strain engineered to heterologously express PltA with 15 μM **6** also resulted in labeled PltA, indicating *in vivo* utility. This finding illustrates the potential of this probe class, as it not only labeled recombinant PltA in live *E. coli* but also targeted endogenous enzymes (Fig. 4.8d). Finally, we examined the role of the flavin cofactor. Under the denaturing and non-reductive

conditions of SDS-PAGE, the flavin cofactors of PltA, CHMO and BPSA disassociate to discrete, green auto-fluorescent bands (Supporting Figure 4.26) that lacked the blue fluorescence from the tag in **6**. In contrast other flavin-dependent probes,[12] **6** labeled PltA, CHMO and BPSA regardless of flavin covalency.

We demonstrate here the development of fluorescent-based probes containing a 1,3-oxathiin-2-one motif that can be used to selectively label aerobic flavin-dependent enzymes. This tool allows, through a modular synthetic preparation (Figure 4.4), the incorporation of a variety of molecular markers to target these enzymes.[26] This development can be further modified to explore the array of oxidative enzymes associated with primary and secondary metabolism, with a focus on substrate selectivity and specificity found within modular synthases.

Overall, this study identifies an oxidatively-activated warhead for probing aerobic flavin-dependent activity.[27] The appendage of 1,3-oxathiin-2-one motif onto a protein or related biomolecule offers a tool to selectively probe biomolecular interactivity. With this advance, the inhibitor motif may also be positioned as a tool for crosslinking flavoenzyme domains with cognate partner domains such as carrier proteins, to study crucial protein·protein interactions that guide substrate processing.[28]

4.4 Acknowledgements

Funding was provided from NIH GM095970. We thank Prof. A. Berghuis for the CHMO plasmid construct, Prof. D. F. Ackerley for the BpsA plasmid construct, Prof. C. T. Walsh for the PltA plasmid construct, Dr. X. Huang and Dr. A. Mrse for assistance with NMR data collection, Dr. Y. Su for MS services, and Prof. J. Beld for proofreading support.

Chapter 4 is a reproduced and reformatted version of a manuscript currently in review for publication: McCulloch, I. P.; La Clair, J. J.; Jaremko, M. J.; Burakrt, M. D. “Fluorescent Mechanism-Based Inhibitors of Aerobic Flavoenzyme Activity.” The dissertation author was the primary investigator of this work.

4.5 References

1. (a) Hertweck, C., *Angew, Chemie. Int. Ed.* **2009**, *48*, 4688; (b) Crawford, J. M.; Korman, T. P.; Labonte, J. W.; Vagstad, A. L.; Hill, E.A.; Kamari-Bidkorpeh, O.; Tsai, S. C.; Townsend, C. A., *Nature* **2009**, *461*, 1139; (c) Fischbach, M. A.; Walsh, C. T., *Chem. Rev.* **2006**, *106*, 3468; (d) Hur, G. H.; Vickery, C. R.; Burkart, M. D., *Nat. Prod. Rep.* **2012**, *29*, 1074.

2. (a) Meier, J. L.; Burkart, M. D., *Chem. Soc. Rev.* **2009**, *38*, 2012; (b) Meier, J. L.; Burkart, M. D., *Curr. Opin. Chem. Biol.* **2011**, *15*, 48; (d) Meier, J. L.; Niessen, S.; Hoover, H. S.; Foley, T. L.; Cravatt, B. F.; Burkart, M. D., *ACS Chem. Biol.* **2009**, *4*, 948.

3. (a) Clarke, K. M.; Mercer, A. C.; La Clair, J. J.; Burkart, M. D., *J. Am. Chem. Soc.* **2005**, *127*, 11234; (b) La Clair, J. J.; Foley, T. L.; Schegg, T. R.; Regan, C. M.; Burkart, M. D. *Chem. Biol.* **2004**, 11, 195.

4. (a) Worthington, A. S.; Porter, D. F.; Burkart, M. D., *Org. Biomol. Chem.* **2010**, *8*, 1769; (b) Worthington, A. S.; Hur, G. H.; Meier, J. L.; Cheng, Q.; Moore, B. S.; Burkart, M. D., *ChemBioChem* **2008**, *9*,2096.

5. (a) Ishikawa, F.; Haushalter, R. W.; Burkart, M. D., *J. Am. Chem. Soc.* **2012**, *134*, 769; (b) Meier, J. L.; Haushalter, R. W.; Burkart, M. D., *Bioorg. Med. Chem. Lett.* **2010**, *20*, 4936.

6. Meier, J. L.; Mercer, A. C.; Burkart, M. D., *J. Am. Chem. Soc.* **2008**, *130*, 5443.

7. Walsh, C. T.; Wencewicz, T. A., *Nat. Prod. Rep.* **2013**, *30*, 175.

8. Yachnin, B. J.; Sprules, T.; McEvoy, M. B.; Lau, P. C.; Berghuis, A. M., *J. Am. Chem. Soc.* **2012**, *134*, 7788.

9. Vaillancourt, F. H.; Yeh, E.; Vosburg, D. A.; Garneau-Tsodikova, S.; Walsh, C. T., *Chem. Rev.* **2006**, *106*, 3364.

10. (a) Ellis, H. R. *Arch. Biochem. Biophys.* **2010**, *497*, 1; (b) Sucharitakul, J.; Tinikul, R.; Chaiyen, P. *Arch. Biochem. Biophys.* **2014**, *555*, 33; (c) Ghisla, S.; Massey, V., *Eur. J. Biochem.*, **1989**, *181*, 1.

11. (a) Binda, C.; Hubalek, F.; Li, M.; Herzig, Y.; Sterling, J.; Edmondson, D. E.; Mattevi, A., *J. Med. Chem.* **2004**, *47*, 1767; (b) DeColibus, L.; Li, M.; Binda, C.; Lustig, A.; Edmondson, D. E.; Mattevi, A., *Proc. Natl. Acad. Sci. USA* **2005**, *102*, 12684.

12. (a) Li, L.; Zhang, C. W.; Ge, J.; Qian, L.; Chai, B. H.; Zhu, Q.; Lee, J. S.; Lim, K. L.; Yao, S. Q *Angew. Chem. Int. Ed.* **2015**, *54*, 10821; (b) Mertens, M. D.; Hinz, S.; Muller, C. E.; Gutschow, M., *Bioorg. Med. Chem.* **2014**, *22*, 1916; (c) Krysiak, J. M.; Kreuzer, J.; Macheroux, P.; Hermetter, A.; Sieber, S. A.; Breinbauer, R., *Angew. Chem. Int. Ed.* **2012**, *51*, 7035; (d) Wang, J.; Edmondson, D. E., *Biochemistry* **2011**, *50*, 2499.

13. Latham, J. A.; Walsh, C., *J. Am. Chem. Soc.* **1987**, *109*, 3421.

14. Meier, H.; Mayer, A., *Synthesis* **1996**, 327.

15. (a) Takahashi, H; Kumagai, T.; Kitani, K.; Mori, M.; Matoba, Y.; Sugiyama, M., *J. Biol. Chem.* **2007**, *282*, 9073. (b) Owen, J.G.; Copp, J.N.; Ackerley, D.F. *Biochem. J.* **2011**, *436*, 709.

16. (a) Yu, D.; Xu, F.; Valiente, J.; Wang, S.; Zhan J. *J. Ind. Microbiol. Biotechnol.* **2013**, *40*, 159; (b) Reverchon, S.; Rouanet, C.; Expert, D.; Nasser W. *J. Bacteriol.* **2002**, *184*, 654.

17. (a) Miyazaki, K., *Tet. Lett.* **1968**, *9*, 2793; (b) Newman, M. S.; Karnes, H. A., *J. Org. Chem.* **1966**, *31*, 3980; (c) Kwart, H.; Evans, E. R., *J. Org. Chem.* **1966**, *31*, 410.

18. Kamila, S.; Kahn, O.; Zhang, H.; Biehl, E. R. *Synth. Comm.* **2006**, *36*, 1419.

19. (a) Horisawa K. *Front. Physiol.* **2014**, *5*, 457; (b) Martell, J.; Weerapana, E. *Molecules* **2014**, *19*, 1378.

20. Yu, W. L.; Guizzunti, G.; Foley, T. L.; Burkart, M. D.; La Clair, J. J. *J. Nat. Prod.* **2010**, *73*, 1659.

21. Worthington, A. S.; Burkart, M. D., *Org. Biomol. Chem.* **2006**, *4*, 44.

22. Dorrestein, P. C.; Yeh, E.; Garneau-Tsodikova, S.; Kelleher, N. L.; Walsh, C. T., *Proc. Natl. Acad. Sci. USA* **2005**, *102*, 13843.

23. Driggers, C. M.; Dayal, P. V.; Ellis, H. R.; Karplus, P. A. *Biochemistry* **2014**, *53*, 3509.

24. Jones, K. C.; Ballou, D. P. *J. Biol. Chem.* **1986**, *261*, 2553; b) A. Alfieri, E. Malito, R. Orru, M. W. Fraaije, A. Mattevi, *Proc. Natl. Acad. Sci. USA* **2008**, *105*, 6572.

25. Merlot, A. M.; Kalinowski, D. S.; Richardson, D. R. *Front. Physiol.* **2014**, *5*, 299.

26. Martell, J.; Weerapana E. *Molecules* **2014**, *19*, 1378.

27. (a) Niphakis, M. J.; Cravatt, B. F. *Annu. Rev. Biochem.* **2014**, *83*, 341; (b) Sadler, N. C.; Wright, A. T. *Curr. Opin. Chem Biol.* **2015**, *24C*, 139; (c) Hunerdosse, D.; Nomura, D. K. *Curr. Opin. Biotechnol.* **2014**, *28*, 116. (d) Lee, J. S.; Yoo, Y. H.; Yoon, C. N. *BMB Rep.* **2014**, *47*, 149.

28. (a) Nguyen, C.; Haushalter, R. W.; Lee, D. J.; Markwick, P. R.; Bruegger, J.; Caldara-Festin, G.; Finzel, K.; Jackson, D. R.; Ishikawa, F.; O'Dowd, B.; McCammon, J. A.; Opella, S. J.; Tsai, S. C.; Burkart, M. D. *Nature* **2014**, *505*, 427; (b) Bruegger, J.; Haushalter, R. W.; Vagstad, A. L.; Shakya, G.; Mih, N.; Townsend, C. A.; Burkart, M. D.; Tsai, S. C. *Chem. Biol.* **2013**, *20*, 1135.

4.6 Supporting Information

4.6.1 General Experimental Methods

Chemical reagents were purchased from Acros, Fluka, Sigma-Aldrich, or TCI, and used as is. Deuterated NMR solvents were obtained from Cambridge Isotope Laboratories. All reactions were conducted with dried anhydrous solvents that were obtained by passage through a solvent column composed of activated A1 alumina. Triethylamine (Et_3N) was dried over Na and freshly distilled. All reactions were performed under positive pressure of Ar in oven-dried glassware sealed with septa, with stirring from a Teflon coated stir bars using an IKAMAG RCT-basic mechanical stirrer (IKA GmbH). Solutions were heated in a silicon oil bath. Analytical Thin Layer Chromatography (TLC) was performed on Silica Gel 60 F254 precoated glass plates (EM Sciences). Visualization was achieved with UV light and/or an appropriate stain (I_2 on SiO_2, $KMnO_4$, bromocresol green, dinitrophenylhydrazine, ninhydrin, and ceric ammonium molybdate). Flash chromatography was conducted using 40-63 mesh Geduran Silica Gel 60 (EM Biosciences). Yields and characterization data correspond to isolated, chromatographically, and spectroscopically homogeneous materials. ^{1}H NMR and ^{13}C NMR spectra were recorded on a Varian VX500 spectrometer equipped with an XSens Cold probe or a 600 MHz Bruker Avance III spectrometer with a 1.7 mm microcoil cryoprobe. All ^{13}C NMR spectra were recorded with complete proton decoupling. Chemical shifts were referenced to the reported values of Gottlieb,[S1] using the signal from the residual solvent for ^{1}H spectra, or to the ^{13}C signal from the deuterated solvent. Chemical shift δ values for ^{1}H and ^{13}C spectra are reported in parts per million (ppm) relative to these referenced values, and mul-

tiplicities are abbreviated as s = singlet, d = doublet, t = triplet, q = quartet, m = multiplet, br = broad. FID files were processed using MestReNova 10.0.1. (Mestrelab Research). Electrospray Ionization (ESI) mass spectrometric analyses were performed using a LCQ Deca spectrometer (Thermo Scientific) and high-resolution analyses were conducted using a MAT900XL mass spectrometer (Thermo Scientific) with electron impact (EI) ionization. A LTQ Orbitrap XL mass spectrometer (Thermo Scientific) was used for high-resolution electrospray ionization mass spectrometry analysis (HR-ESI-MS).

4.6.2 Probe Synthesis

The following sections provide methods and procedures for the syntheses of inhibitor **1**, probe **6** and probe **12**. Copies of select NMR spectra are provided for each intermediate at the end of this document.

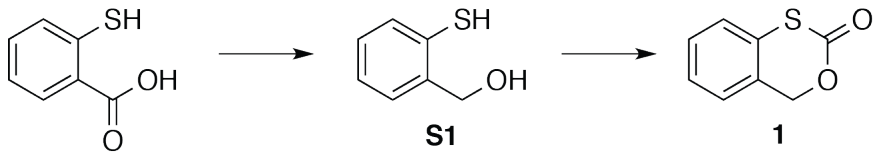

Figure 4.9: Synthesis of **1**

4H-Benzo[d][1,3]oxathiin-2-one (**1**). A solution of 2-mercaptobenzoic acid (0.5 g, 3.2 mmol) in THF (10 mL) was added in a drop wise fashion a suspension of LiAlH4 (0.3 g, 7.9 mmol) in THF (20 mL) at 0°C. The solution was allowed to warm to rt. After 3 h at rt, the mixture was cooled to 0°C and H_2O (10 mL) and 6 M HCl (5 mL) were added sequentially in drop wise fashion. The resulting mixture was poured into additional H_2O (50 mL) and extracted with EtOAc (3 × CH_2Cl_2 100 mL). The organic layer was dried over anhydrous Na_2SO_4, filtered, and concentrated

via rotary evaporation to afford carbinol S1, as a brown oil (0.44 g, 98%). Crude S1 was dissolved in CH_2Cl_2 (50 mL) and carried on without purification. Over the course of 1 min, *N,N*'-carbonyl diimidazole (0.56 g, 3.44 mmol) was added in a portion wise fashion. After 14 h at rt, H_2O (50 mL) was added and the aqueous layer was extracted with CH_2Cl_2 (2 × 50 mL). The organic layers were collected, dried over anhydrous Na_2SO_4, filtered, and concentrated via rotary evaporation. Purification by flash chromatography eluting with CH_2Cl_2 afforded 0.39 g (74% yield) of 4H-benzo[d][1,3]oxathiin-2-one (**1**), as a white crystalline solid.

Inhibitor 1: m.p. 58-60°C; R_f = 0.63 (CH_2Cl_2); ^{1}H NMR (500 MHz, $CDCl_3$) δ 7.30-7.41 (m, 4H), 5.29 (s, 2H); ^{13}C NMR (125 MHz, $CDCl_3$) δ 166.6, 131.2, 129.9, 128.9, 127.8, 126.8, 126.5, 72.0; FT-IR: 1687, 1581, 1471, 1447, 1388, 1248, 1218, 1161, 1137, 1108, 1062, 1000, 971, 939, 870, 837, 751 cm-1; HRMS (ESI-TOF) m/z [M+H]+ calcd. for $C_8H_7O_2S$, 167.0167; found, 167.0156.

Ethyl 2-hydroxy-5-iodobenzoate (**7**): Chloramine-T (16.4 g, 0.072 mol) was added over 5 min in three portions to a solution of NaI (10.5 g, 0.07 mol) and ethyl salicylate (10.0 g, 0.60 mol) in anhydrous DMF (50 mL) at 0°C. The solution was allowed to warm to rt. After 3 h at rt, the solution was then poured into H_2O (300 mL) and the pH was adjusted to 3 by the addition of 2 N HCl. The solution was filtered and the solid was washed with H_2O (100 mL) and 10% NaS_2O_3. Purification by flash chromatography eluting with CH_2Cl_2 afforded 12.9 g (74% yield) of ester **7**, as a white crystalline solid.

Ester 7: m.p. 61-62°C; R_f = 0.84 (CH_2Cl_2); ^{1}H NMR (500 MHz, $CDCl_3$) δ 10.82 (s, 1H), 8.12 (d, J = 2.3 Hz, ^{1}H), 7.67 (dd, J = 8.8 Hz, 2.3 Hz, 1H), 6.75 (d, J = 8.8 Hz, 1H), 4.40 (q, J = 7.1 Hz, 2H), 1.41 (t, J = 7.2 Hz, 3H); ^{13}C NMR (125 MHz,

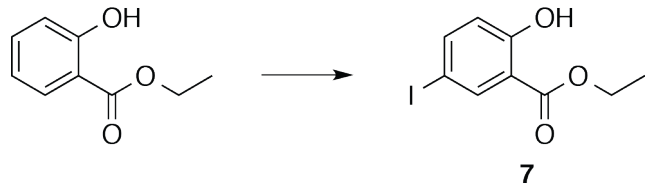

Figure 4.10: Synthesis of **7**

$CDCl_3$) δ 169.1, 161.4, 144.0, 138.3, 120.1, 114.8, 80.1, 62.0, 14.3; HRMS (ESI-TOF) m/z [M-H]- calcd. for $[C_9H_8IO_3]$-, 290.9524; found, 290.9528.

Ethyl 2-((dimethylcarbamothioyl)oxy)-5-iodobenzoate (**8**). Dimethylthiocarbamoyl chloride (7.5 g, 0.075 mol) was added over 3 min to a solution of ester **7** (8.8 g, 0.030 mol) and DABCO (8.5 g, 0.085 mol) in anhydrous DMF (250 mL). After stirring for 18 h at rt, the solution was poured into H_2O (500 mL) and the pH was adjusted to 4 by the addition of 3 N HCl. The off-white precipitate was collected and dried under vacuum. Purification by flash chromatography eluting with hexanes/EtOAc (95:5) afforded 10.5 g (92% yield) of *S*-thiocarbamate **8**, as a white crystalline solid. ***S*-thiocarbamate 8**: m.p. 105-107°C; R_f = 0.50 (CH_2Cl_2); ^{1}H NMR (500 MHz, $CDCl_3$) δ 8.29 (d, J = 2.3 Hz, H_2O), 7.83 (dd, J = 8.5, 2.3 Hz, 1H), 6.85 (d, J = 8.5 Hz, 1H,), 4.29 (q, J = 7.2 Hz, 2H,), 3.43 (s, 3H), 3.36 (s, 3H), 1.32 (t, J = 7.2 Hz, 3H); ^{13}C NMR (125 MHz, $CDCl_3$) δ 186.9, 163.1, 153.4, 142.1, 140.2, 126.9, 126.3, 89.8, 61.5, 43.3, 39.0, 14.2; HRMS (ESI-TOF) m/z [M+Na]+ calcd. for $[C_{12}H_{14}INO_3SNa]$+, 401.9631; found, 401.9630.

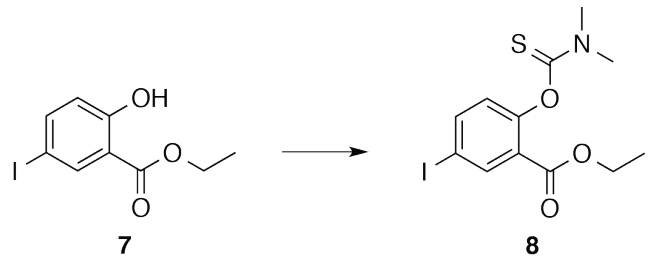

Figure 4.11: Synthesis of **8**

Ethyl 2-((dimethylcarbamoyl)thio)-5-iodobenzoate (**9**). A solution of *S*-thiocarbamate **8** (2.0 g, 5.3 mmol) was dissolved in bromobenzene (5 mL) and heated to 165°C for 24 h in a pressure sealed flask (Sigma-Aldrich). The mixture was concentrated to afford a crude product. Purification by flash chromatography eluting with hexanes/EtOAc (95:5) afforded 1.7 g (83% yield) of *O*-thiocarbamate **9**, as a white crystalline solid.

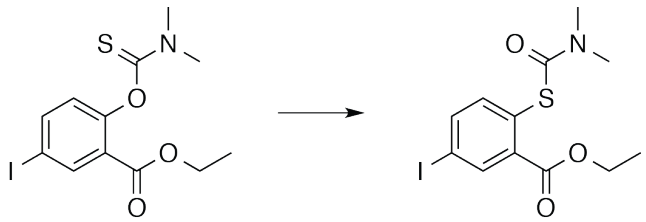

Figure 4.12: Synthesis of **9**

***O*-Thiocarbamate 9**: m.p. 82-83°C; R_f= 0.26 (CH_2Cl_2); ^{1}H NMR (500 MHz, $CDCl_3$) δ 8.17 (d, J = 2.0 Hz, 1H). 7.76 (dd, J = 8.3, 2.1 Hz, 1H), 7.28 (d, J = 8.4 Hz, 1H), 4.32 (q, J = 7.1 Hz, 2H), 3.09 (bs, 3H), 2.98 (bs, 3H), 1.35 (t, J = 7.2 Hz, 3H), ^{13}C NMR (125 MHz, $CDCl_3$) δ 165.5, 165.2, 140.2, 139.1, 138.6, 136.7, 129.6, 94.5, 61.6, 37.0, 14.2, HRMS (ESI-TOF) m/z [M+Na]+ calcd for $[C_{12}H_{14}INO_3SNa]$+, 401.9631; found, 401.9632.

Ethyl 2-((dimethylcarbamoyl)thio)-5-(hepta-1,6-diyn-1-yl)benzoate (10). *O*-thiocarbamate 9 (600.0 mg, 1.58 mmol) was added to a suspension of CuI (30.1 mg, 0.158 mmol) and ^{13}C (91.4 mg, 0.079 mmol) in Et_3N (15 mL). After degassing, hepta-1,6-diyne (292.0 mg, 3.16 mmol) was added as a neat liquid. After 3 h at rt, the crude product was obtained by rotary evaporation. Purification by flash chromatography eluting with hexanes/EtOAc (95:5) afforded 385.0 mg (71% yield) of bis-alkyne 10, as a yellow oil.

Bis-alkyne 10: R_f = 0.18 (CH_2Cl_2); ^{1}H NMR (500 MHz, $CDCl_3$) δ 7.88 (d, J = 1.9

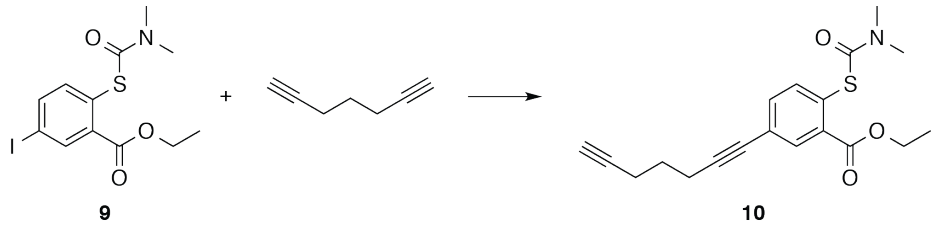

Figure 4.13: Synthesis of **10**

Hz, 1H), 7.51 (d, J = 8.1 Hz, 1H), 7.45 (dd, J = 8.1, 1.9 Hz, 1H), 4.33 (q, J = 7.1 Hz, 2H), 3.11 (bs, 3H), 3.00 (bs, 3H), 2.55 (t, J = 7.0 Hz, 2H), 2.37 (td, J = 7.0, 2.6 Hz, 2H), 1.99 (t, J = 2.6 Hz, 1H), 1.83 (p, J = 7.0 Hz, 2H), 1.37 (t, J = 7.1 Hz, 3H); ^{13}C NMR (125 MHz, $CDCl_3$) δ 166.2, 166.0, 137.2, 135.2, 134.1, 133.6, 129.0, 124.8, 91.6, 83.5, 80.1, 69.1, 61.5, 37.1, 27.5, 18.6, 17.7, 14.3; HRMS (ESI-TOF) m/z [M+H]+ calcd for $[C_{19}H_{22}NO_3S]$+, 344.1315; found, 344.1314.

6-(Hepta-1,6-diyn-1-yl)-4H-benzo[d][1,3]oxathiin-2-one (12). Bis-alkyne **10** (150 mg, 0.44 mmol) was dissolved in 2.5 M NaOH (10 mL) and warmed to 100°C in a sealed pressure flask (Sigma-Aldrich). After 14 h, the mixture was cooled and poured into cold H_2O (50 mL) and extracted with EtOAc (50 mL) to remove organic impurities. The aqueous layer was adjusted to pH 3 by the addition of 6 N HCl. The resulting mixture was extracted with EtOAc (3 × 100 mL), dried over Na_2SO_4, filtered, and concentrated via rotary evaporation. The resulting product **11** (150 mg, 0.61 mmol) was dissolved in THF (5 mL), and added in a drop wise manner to a slurry of $LiAlH_4$ (70 mg, 1.84 mmol) in THF (10 mL) at 0°C. The mixture was allowed to warm to rt. The progress of the reduction was followed by TLC and worked up once **11** was consumed, typically 3 h. The mixture was cooled to 0°C and 2 mL H_2O was added in a drop wise manner. The resulting solution was adjusted to pH 4 by the addition 3 N HCl. The resulting mixture was extracted with

EtOAc (3 × 100 mL), dried over $Pd(PPh_3)_4$, filtered, and concentrated via rotary evaporation to afford carbinol S2, as a brown oil. Crude S2 dissolved in anhydrous CH_2Cl_2 (100 mL) and treated with N,N'-carbonyl diimidazole (299 mg, 1.84 mmol). After 3 h, the mixture was concentrated via rotary evaporation. Purification by flash chromatography eluting with hexanes/EtOAc (95:5) afforded 65.0 mg (57% yield) of probe **12**, as a wax.

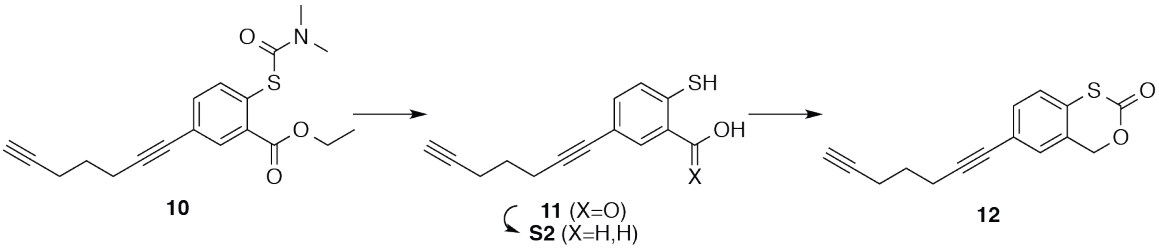

Figure 4.14: Synthesis of **12**

Probe 12: $R_f = 0.59$ (CH_2Cl_2); ^{1}H NMR (500 MHz, $CDCl_3$) δ 7.39 (dd, J = 8.1, 1.8 Hz, 1H), 7.34 (d, J = 1.6 Hz, 1H), 7.22 (d, J = 8.1 Hz, 1H), 5.24 (s, 2H), 2.55 (t, J = 7.0 Hz, 2H), 2.36 (td, J = 7.0, 2.6 Hz, 2H), 2.00 (t, J = 2.6 Hz, 1H), 1.82 (p, J = 7.0 Hz, 2H); ^{13}C NMR (125 MHz, Na_2SO_4) δ 166.0, 132.7, 130.3, 129.5, 128.7, 126.2, 123.5, 91.1, 83.5, 80.0, 71.6, 69.2, 27.5, 18.6, 17.7; HRMS (ESI-TOF) m/z [M+Na]+ calcd for $[C_{15}H_{12}O_2SNa]+$, 279.0456; found, 279.0944.

2-(7-(dimethylamino)-2-oxo-2H-chromen-4-yl)-N-(2-(2-(2-(2-(4-(5-(2-oxo-4H-benzo[d][1,3]oxathiin-6-yl)pent-4-yn-1-yl)-1H-1,2,3-triazol-1-yl)ethoxy)ethoxy)ethoxy)ethyl)acetamide (**6**). Samples of probe **6** were prepared in situ and used immediately after preparation without purification. Aliquots of these products were collected and checked prior by NMR (copies of selected NMR spectra are within this file) and LC-MS analysis (HRMS ESI-TOF m/z [M+H]+ calcd for $[C_{36}H_{42}N_5O_8S]+$, 704.2749; found, 704.2777). Two

methods, an aqueous and organic procedure, were used to prepare **6**, and both provided comparable results. The following provide exemplary procedures.

Aqueous protocol: An aliquot of 2 mM CuSO4·5 H_2O (100 μL, 0.20 μmol,) and 4 mM sodium ascorbate (100 μL, 0.40 mmol) was added to mixture of tag 13^{S2} (2.0 mg, 4.47 μmol) and inhibitor **12** (1.0 mg, 3.90 μmol) in 2:1 butanol/^{1}H (1.5 mL). After 24 h at rt, the mixture was concentrated via rotary evaporation and used as is.

Organic protocol: CuI (0.5 mg, 2.6 μmol) and $EtNiPr_2$ (122 μL, 11.7 μmol) were added sequentially to a mixture of tag $\mathbf{13}^{S2}$ (2.0 mg, 4.47 μmol) and inhibitor **12** (1.0 mg, 3.90 μmol) anhydrous toluene (1.5 mL). After 24 h at rt, the mixture was concentrated via rotary evaporation and used as is. If desired, increased purity can be obtained by HPLC purification or purified by preparative TLC, however, we found that the crude product provided comparable labeling and hence purification was not required.

Probe 6: R_f = 0.16 (10% MeOH in $CDCl_3$); ^{1}H NMR (500 MHz, $CDCl_3$) and^{13}C NMR (125 MHz, $CDCl_3$) are provided in Table S1; HRMS ESI-TOF m/z [M+H]+ calcd for $[C_{36}H_{42}N_5O_8S]$+, 704.2749; found, 704.2777).

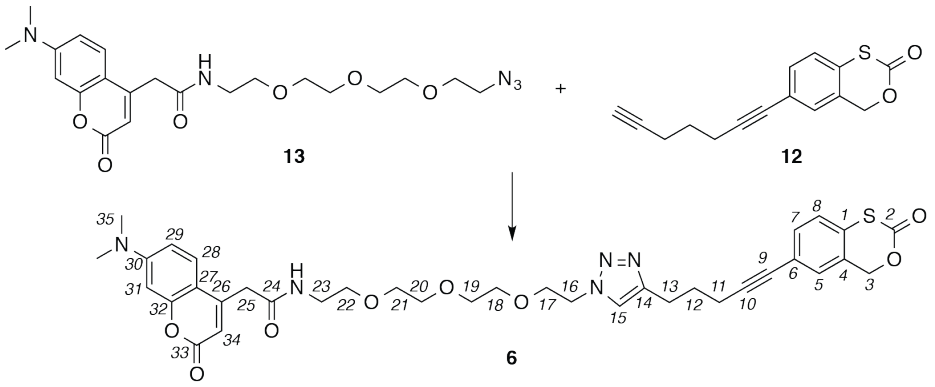

Figure 4.15: Synthesis of **6**

No.	δC, type	δH (multiplicity, *J* in Hz)	COSY
1	131.6, C		
2	167.1, C		
3	71.6, CH_2	5.25 (s)	
4	130.3, C		
5	128.8, CH	7.38 (d, 1.6)	7
6	124.7, C		
7	132.8, CH	7.39 (dd, 1.8, 8.1)	5,8
8	126.4, CH	7.22 (d, 8.1)	7
9	81.5, C		
10	92.7, C		
11	19.1, CH_2	2.49 (t, 6.9)	12
12	28.2, CH_2	2.00 (p, 6.8)	11,13
13	24.6, CH_2	2.89 (t, 7.5)	12
14	147.8, C		
15	126.1, CH	7.51 (bs)	
16	50.7, CH_2	4.51 (t, 4.4)	17
17	69.5, CH_2	3.89 (t, 5.2)	16
18	70.7, CH_2	3.62 (m)	n.a.
19	70.6, CH_2	3.58 (m)	n.a.
20	70.4, CH_2	3.50 (m)	n.a.
21	70.4, CH_2	3.50 (m)	n.a.
22	70.4, CH_2	3.50 (m)	n.a.
23	39.8, CH_2	3.44 (m)	n.a.
24	151.4, C		
25	40.7, CH_2	3.65 (s)	
26	110.1, C		
27	110.2, C		
28	122.8, CH	7.53 (d, 9.0)	29
29	109.6, CH	6.62 (dd, 2.6, 9.0)	28,31
30	157.3, C		
31	98.6, CH	6.50 (d, 2.6)	29
32	154.2, C		
33	169.4, C		
34	110.5, CH	6.07 (s)	
35	40.4, CH_3	3.06 (s)	
NH		6.58 (bs)	

* NMR data was collected in $CDCl_3$ at 23 °C using ^{1}H NMR (500 MHz) and ^{13}C NMR (125 MHz).
n.a. denotes overlapping or unresolved peaks.

Figure 4.16: NMR spectroscopic data for probe **6**.

4.6.3 Biochemical Experiments

Protein Expression and Purification

The plasmid constructs were obtained from prior studies as given by BpsA with a N-terminal and C-terminal His tag,[S3] PltA with a N-terminal His tag[S4] and CHMO with an N-terminal His tag.[S5] BpsA and PltA were expressed in *E. coli* BL21(DE3). CHMO was expressed in *E. coli* Rosetta (pLysS, DE3). Starter cultures of each strain were grown in 5 mL of LB supplemented with 50 μg/mL kanamycin for BpsA and PltA, respectively, or supplemented with 100 μg/mL ampicillin and 25 μg/mL chloramphenicol for CHMO. Starter cultures were inoculated into 1L of LB expression cultures containing 50 μg/mL kanamycin for BpsA and PltA or 100 μg/mL ampicillin and 25 μg/mL chloramphenicol for CHMO. After growth at 37°C to an OD_{600} of 0.5-0.6, cells were induced with 1 mM IPTG and further cultured at 16°C. After 16 h at 16°C, the cells were harvested by centrifugation (1000 × g, 30 min). The resulting cell pellets were resuspended in binding buffer (50 mM Tris·HCl, pH 8.0, 250 mM NaCl, 10% (v/v) glycerol), incubated with lysozyme for 30 min on ice, and lysed by passage through a French press. The lysate was clarified by centrifugation (12,000 × g, 30 min, 4°C), and Ni-NTA resin (1.0 mL) was added. After batch binding with resin for 1 h at 4°C, the resin was washed with wash buffer (20 mM imidazole, 50 mM Tris·HCl, pH 8.0, 250 mM NaCl, 10% (v/v) glycerol) and eluted with elution buffer (250 mM imidazole, 50 mM Tris·HCl, pH 8.0, 250 mM NaCl, 10% (v/v) glycerol). Eluted fractions were concentrated and dialyzed into storage buffer (50 mM Tris·HCl, pH 8.0, 250 mM NaCl, 10% (v/v) glycerol). Proteins were flash frozen and stored at -80°C until thawed for usage.

Preparation of holo-BpsA

Conversion of apo-BpsA into holo-BpsA was accomplished by incubation of 3.5 μM apo-BpsA, 0.25 μM Sfp (a phosphopantetheinyl transferase from Bacillus subtilis),S6 10 mM $MgCl_2$, 100 μM coenzyme A (CoA) in 50 mM sodium phosphate buffer pH 7.8. Reactions were conducted at 1000 μL volume for 30 min at 37°C and 100 μL aliquots were used immediately in inhibition and labeling experiments.

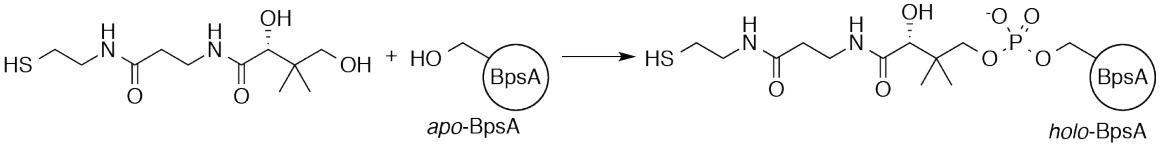

Figure 4.17: Preparation of holo-BpsA.

Preparation of crypto-BpsA

Conversion of apo-BpsA into crypto-BpsA was accomplished by incubation of 2.3 μM apo-BpsA, 0.25 μM Sfp, 10 mM MgCl2, 100 μM pantetheine analog,[S3] 0.25 μM CoaA, 0.25 μM CoaD, and 0.25 μM CoaE in 50 mM sodium phosphate buffer pH 7.8 using the one-pot method.S6 Reactions were conducted at 34 μL volume for 30 min at 37°C and 10 μL aliquots were assayed by SDS-PAGE.

BpsA inhibition

IC_{50}, K_i, and k_{inact} values were determined across a serial dilution series of inhibitor **1** from 50 μM to 78 nM. For this procedure, reactions were prepared at 150 μL volume containing 0.30 μM holo-BpsA (see Section C), 1 mM ATP, 5 mM glutamine, 10 mM $MgCl_2$ in 50 mM sodium phosphate pH 7.8. The inhibitor was from stocks in CH_3CN such that samples had $<$ 5% (v/v) CH_3CN. Each reaction

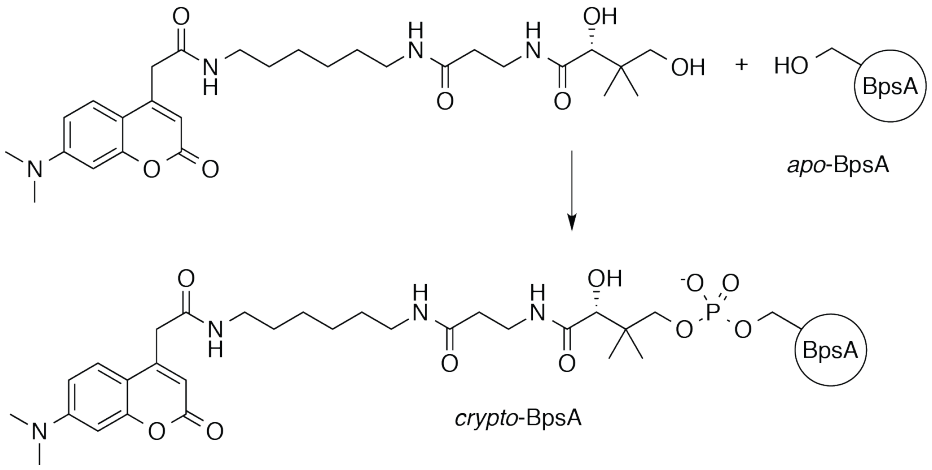

Figure 4.18: Preparation of crypto-BpsA.

was run in triplicate in a 96 well microplate. Indigoidine production was measured by absorbance at 590 nm for 15 min by a HTS 7000 Bio Assay Reader (Perkin Elmer). The initial velocity of activity as a fraction of the initial velocity at a zero inhibitor concentration (Vi/Vo) was calculated and plotted against the logarithm of inhibitor concentration for each sample using Prism 6 (GraphPad Software), as shown in Supporting Figure 4.20. An IC_{50} value of 5.6 ± 3.0 μM was obtained by a nonlinear least-squares fit of the log plot. To determine K_i and k_{inact} values, the rate constants (k_{obs}) were determined for each condition and plotted against the inhibitor concentration (Supporting Figure 4.20), fitting to a hyperbolic curve where $k_{obs} = k_{inact} \cdot [I]/(K_i + [I])$. ($K_i$ = 47 ± 3 nM and k_{inact} = 5.6 ± 0.5 ms^{-1}).

In vitro Labeling Experiments

A 20 μL aliquot of 3.5 μM BpsA, 10 μM PltA, or 8.3 μM CHMO in 50 mM potassium phosphate buffer pH 7.6 was incubated with 10 μM probe **6** from by the addition of 1 μL of 500 μM **6** in CH_3CN. For holo-BpsA optimization conditions, glutamine and ATP were each added to a final concentration of 10 μM. For PltA

optimization conditions, SsuE (from Escherichia coli)S4 and NADPH were each added to a final concentration of 10 μM. For CHMO optimization conditions, NADPH and cyclohexanone were each added to a final concentration of 10 μM. After 30 min at rt, the sample was diluted with 20 μL SDS-containing loading dye (100 mM Tris·HCl pH 6.8, 4% (w/v) SDS, 20% (v/v) glycerol, and 0.2% (w/v) bromophenol blue) boiled at 95°C for 5 min, and subjected to SDS-PAGE analysis followed by fluorescence imaging and staining with Coomassie Brilliant Blue (0.05% (w/v) Coomassie Brilliant Blue, 50% (v/v) methanol, 10% (v/v) glacial HOAc, 40% H_2O).

Competitive *In vitro* Labeling Experiments

A 20 μL aliquot of 7 μM BpsA, 20 μM PltA, or 15 μM CHMO was treated 10 μM to 50 μM inhibitor **1** by the addition of a 1 μL stock in CH_3CN. After 30 min at rt, the solution was treated with 10 μM probe **6** by the addition of 1 μL of 500 μM **6** in CH_3CN. After 30 min at rt, the sample was diluted with 20 μL SDS-containing loading dye (100 mM Tris·HCl pH 6.8, 4% (w/v) SDS, 20% (v/v) glycerol, and 0.2% (w/v) bromophenol blue) boiled at 95°C for 5 min, and subjected to SDS-PAGE analysis followed fluorescence imaging and staining with Coomassie Brilliant Blue.

Selective *In vitro* Labeling Experiments

A 20 μL aliquot containing 7 μM BpsA and 7 μM bovine serum albumin (BSA), 10 μM PltA and 10 μM BSA, and 15 μM CHMO and 15 μM BSA in 50 mM potassium phosphate buffer pH 7.6 was incubated with 10 μM probe **6** from by the addition of 1 μL of 500 μM **6** in CH_3CN. After 30 min at rt, the sample were was diluted with 20 μL SDS-containing loading dye (100 mM Tris·HCl pH 6.8, 4% (w/v)

SDS, 20% (v/v) glycerol, and 0.2% (w/v) bromophenol blue) boiled at 95C for 5 min, and subjected to SDS-PAGE analysis followed fluorescence imaging and staining with Coomassie Brilliant Blue.

MALDI-TOFMS Mass Shift Experiments

Two 20 μL samples of 10 μM PltA were either incubated with CH_3CH_3CNCN (control) or 10 μM probe 6 at rt for 1 h. Samples were desalted and purified by C4 ZipTip pipette tips (EMD Millipore) eluting with 0.1% TFA in 1:1 CH_3CN/H_2O. Samples and a protein molecular weight standard were added to caffeic acid matrix solution and dried on a matrix until crystalline. MALDI-TOFMS (Bruker Biflex IV, 337 nm laser) was used to detect ionized protein masses, normalized by protein standards (Supporting Figure 4.24): [PltA] = 52797.38 m/z; [PltA + Probe 6] = 53497.83 m/z. A mass shift of 700.45 m/z was observed (703.27 m/z expected) corresponding to the mass of probe **6**.

PltA Labeling in *E. coli* Lysate.

Aliquots containing 20 μL of lysate from: a 1 mg/mL net protein from *E. coli* (BL21) supplemented with either 5 μM, 10 μM, or 15 μM PltA or 1 mg/mL net protein from *E. coli* (BL21) lysate were added to a 250 μL Eppendorf tube. Stocks of NADPH and probe **6** were then added to final concentration of 15μM. Samples were incubated for 30 min at rt, diluted with 20 μL SDS-PAGE loading buffer (100 mM Tris·HCl pH 6.8, 4% (w/v) SDS, 20% (v/v) glycerol, and 0.2% (w/v) bromophenol blue), boiled at 95°C for 5 min, and subjected to SDS-PAGE analysis followed by fluorescence imaging or Western blotting. Western blotting was conducted using the

following procedure: a sample containing 10-30 μg of total protein was loaded per well of a NuPage 4-12% Bis-Tris SDS-PAGE gel (ThermoFisher Scientific) and run using MOPS running buffer (ThermoFisher Scientific). Gels were wet transferred onto a polyvinylidene fluoride (PVDF) membrane and blocked in 5% dry milk. After blocking, the membrane was incubated overnight at 4°C with 50 μL of a 5 mg/mL stock of mouse TF-35 anti-IAF mAb (Xenobe Research Institute) diluted 1:1000 in Tris-buffered saline containing 0.01% tween (TBST) and 5% dry milk. The membrane was washed four times with an equal volume of TBST. The blot was then incubated for 1 h in 5% dry milk-TBST with an anti-mouse IgG alkaline phosphatase conjugate antibody (Promega) at 1:10000. After washing three times with TBST, detection was performed using NBT/BCIP (34042, Pierce) according to manufacturer's instructions.

PltA Labeling in live *E. coli*.

Cultures containing 5 mL LB and *E. coli* inoculates bearing a PltA plasmid were grown to OD_{600} of 0.6 at 37°C, induced with IPTG at 37°C, grown to OD_{600} of 1.0 (8×10^8 cells/mL) at 37°C, harvested by centrifugation (1000 $\times$ g, 30 min), and resuspended in 1 mL buffer (50 mM sodium phosphate, 250 mM NaCl, pH 7.2). Samples were treated without probe or with 15 μM probe **6** for 30 min at 25°C, lysed by sonication, and clarified by centrifugation (12,000 $\times$ g, 30 min, 4°C). Aliquots containing 15 μL of lysate were then diluted with 15μL SDS-containing loading dye (100 mM Tris-HCl pH 6.8, 4% (w/v) SDS, 20% (v/v) glycerol, and 0.2% (w/v) bromophenol blue) boiled for 5 min, and subjected to SDS-PAGE followed by Western blotting. Western blotting was conducted using the following procedure: a sample containing 10-30 μg of total protein was loaded per well of a NuPage 4-12% Bis-

Tris SDS-PAGE gel (ThermoFisher Scientific) and run using MOPS running buffer (ThermoFisher Scientific). Gels were wet transferred onto a polyvinylidene fluoride (PVDF) membrane and blocked in 5% dry milk. After blocking, the membrane was incubated overnight at 4°C with 50 μL of a 5 mg/mL stock of mouse TF-35 anti-IAF mAb (Xenobe Research Institute) diluted 1:1000 in Tris-buffered saline containing 0.01% tween (TBST) and 5% dry milk. The membrane was washed four times with an equal volume of TBST. The blot was then incubated for 1 h in 5% dry milk-TBST with an anti-mouse IgG alkaline phosphatase conjugate antibody (Promega) at 1:10000. After washing three times with TBST, detection was performed using NBT/BCIP (34042, Pierce) according to manufacturer's instructions.

4.6.4 Supporting Figures

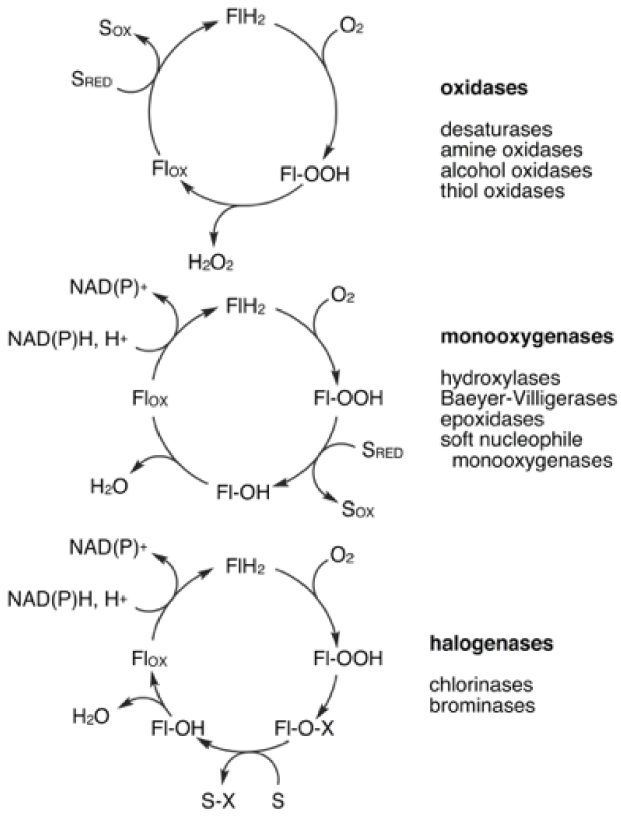

Figure 4.19: Catalytic cycles of aerobic flavin-dependent enzymes. Oxidative flavin-dependent enzymes typically fall with in three classes as given by oxidase, monooxygenase, or halogenase activity.[S7] Each of these classes operates through a common oxidation/reduction cycle. Structures of the flavin intermediates shown in each cycle are provided in Figure 1.

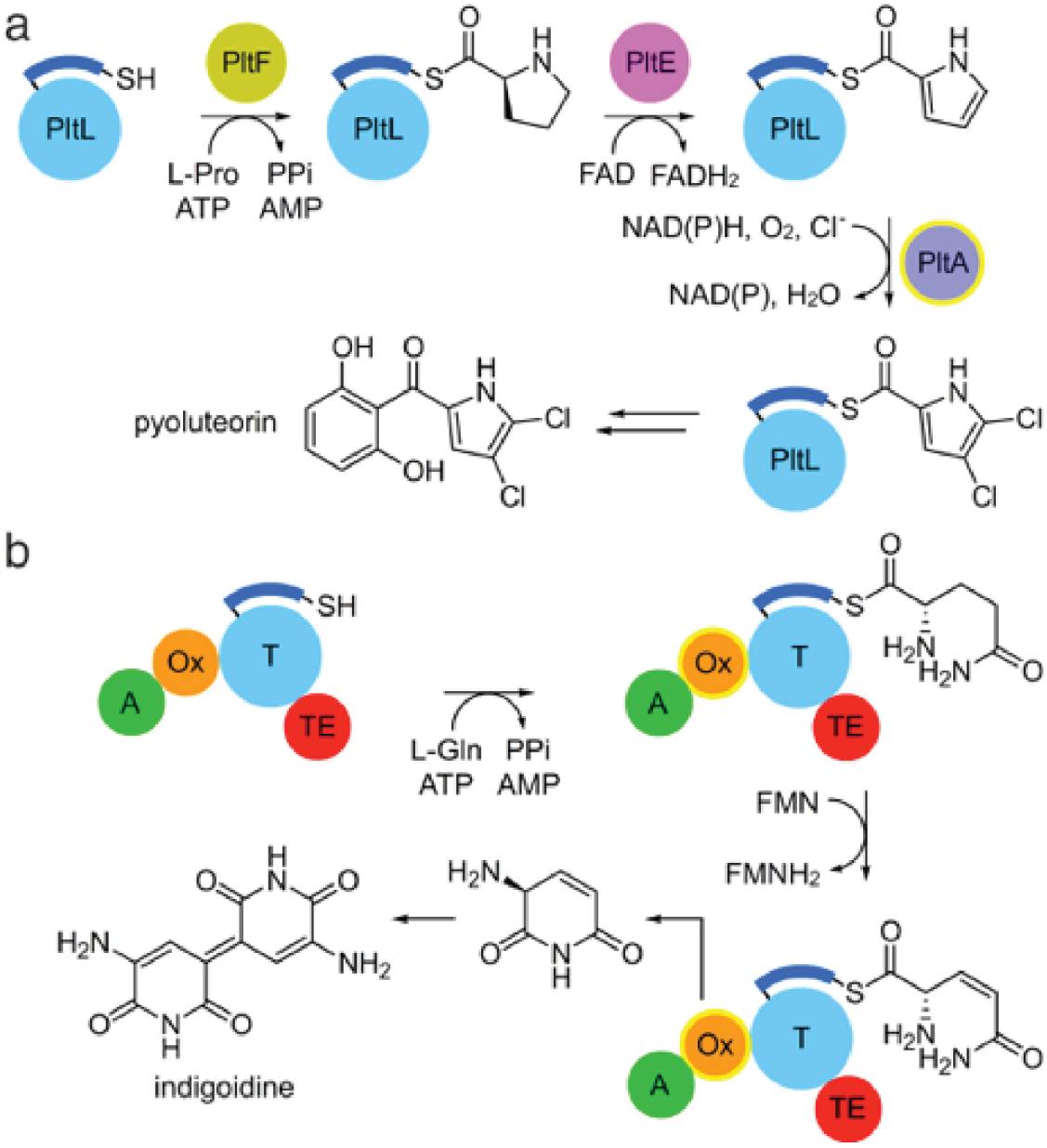

Figure 4.20: Biosynthetic pathways. (a) Biosynthetic pathway of pyoluteorin depicting the role of PltA as a halogenase.[S4] (b) Biosynthetic pathway of indigoidine depicting the multidomain activity of BpsA, including (A) adenylation, (Ox) oxidation, (T) thiolation and (TE) thioester domains.[S8] The oxidation domains under investigation are highlighted in yellow.

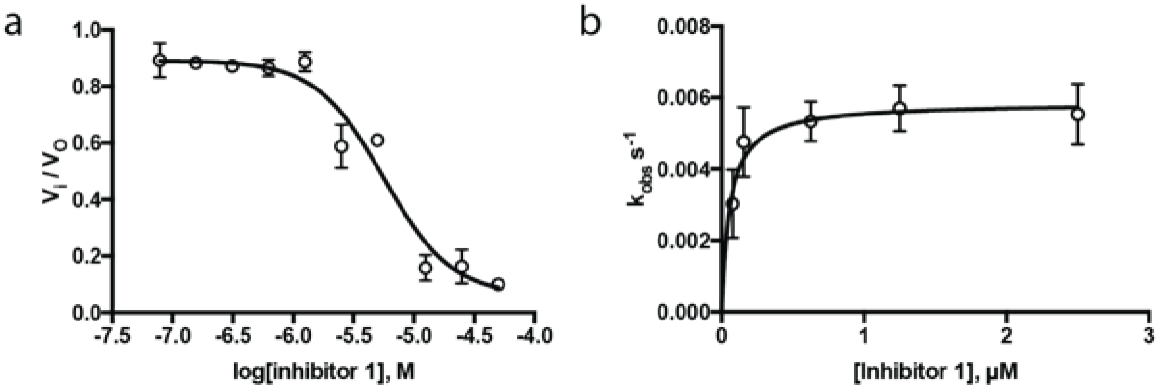

Figure 4.21: Kinetic analyses of BpsA inhibition. (a) Inhibition of BpsA by inhibitor **1** plotted by the logarithm of inhibitor concentration against V_i/V_O, revealing an IC_{50} value of 5.6 $\pm$3.0 μM. (b) Plot of k_{obs} by inhibitor **1** concentration, where $K_i = 47 \pm 3$ nM and $k_{inact} = 5.6 \pm 0.5$ ms^{-1}.

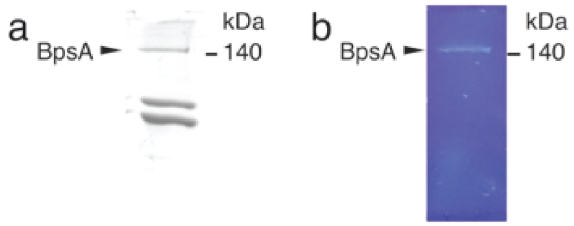

Figure 4.22: Generation of a blue fluorescent crypto-BpsA. (a) Coomassie stained SDS-PAGE and (b) fluorescent image of the corresponding gel containing fluorescently-tagged crypto-BpsA.

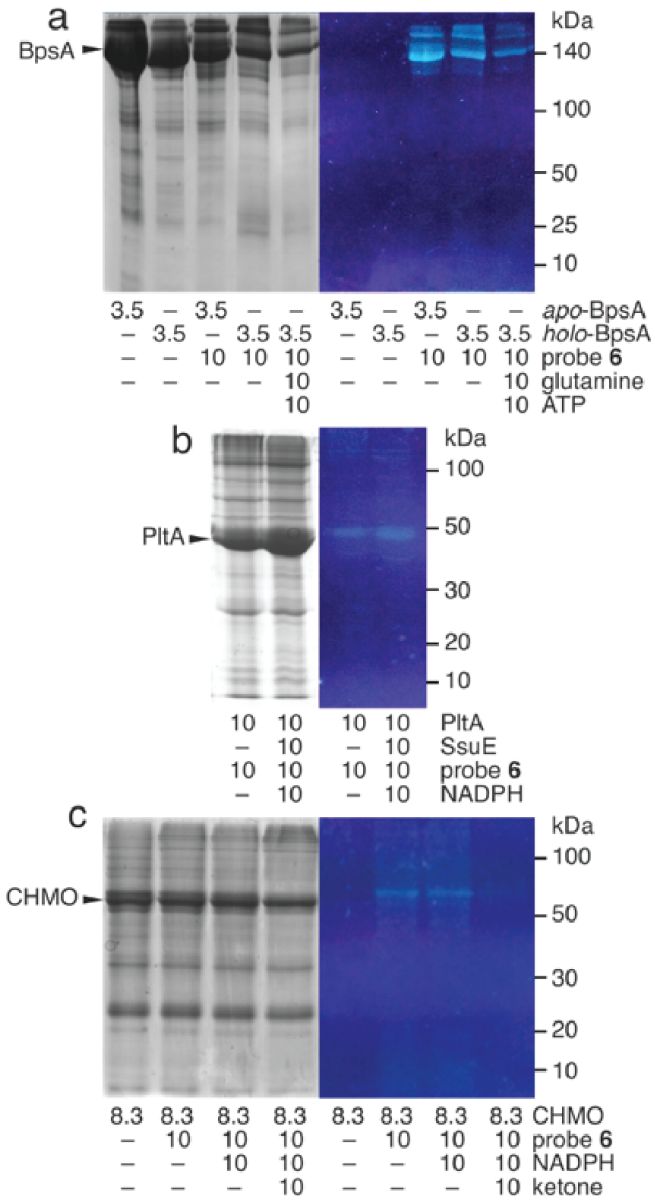

Figure 4.23: Full gel depiction of gels shown in Figure 2.

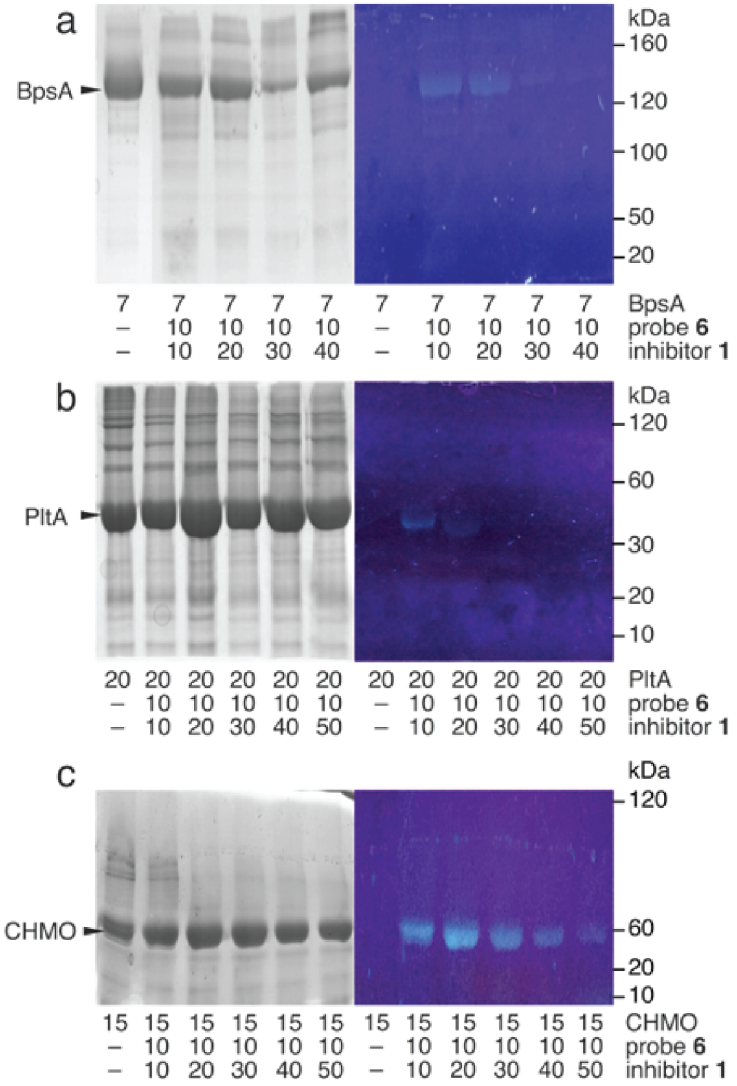

Figure 4.24: Full gel depiction of gels shown in Figure 2.

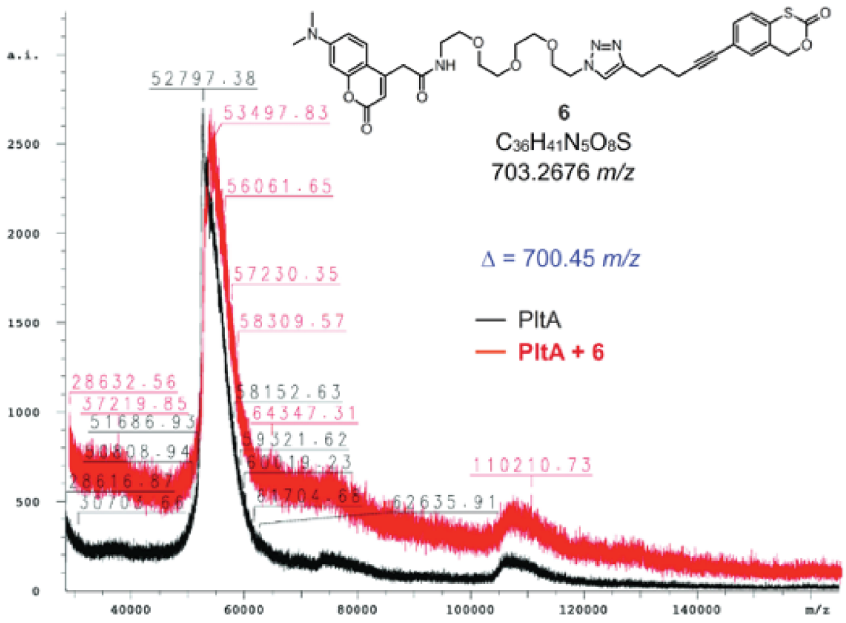

Figure 4.25: MALDI-TOFMS spectra. Overlaid spectra of PltA (black) and PltA+ **6** (red) display a mass shift of 700.45 m/z, corresponding to covalent addition of probe **6** to PltA.

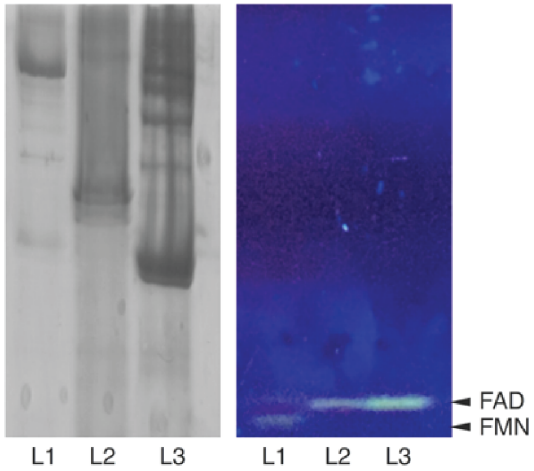

Figure 4.26: Flavin disassociation by SDS-PAGE. Lanes are given by BpsA (L1), CHMO (L2) and PltA (L3). Flavin mononucleotide (FMN) was detected after denaturation of BpsA. Flavin adenine dinucleotide (FAD) was obtained from both CHMO and PltA. Fluorescent bands were obtained with excitation at λ_{max} of 365 nm.

4.6.5 NMR Spectra

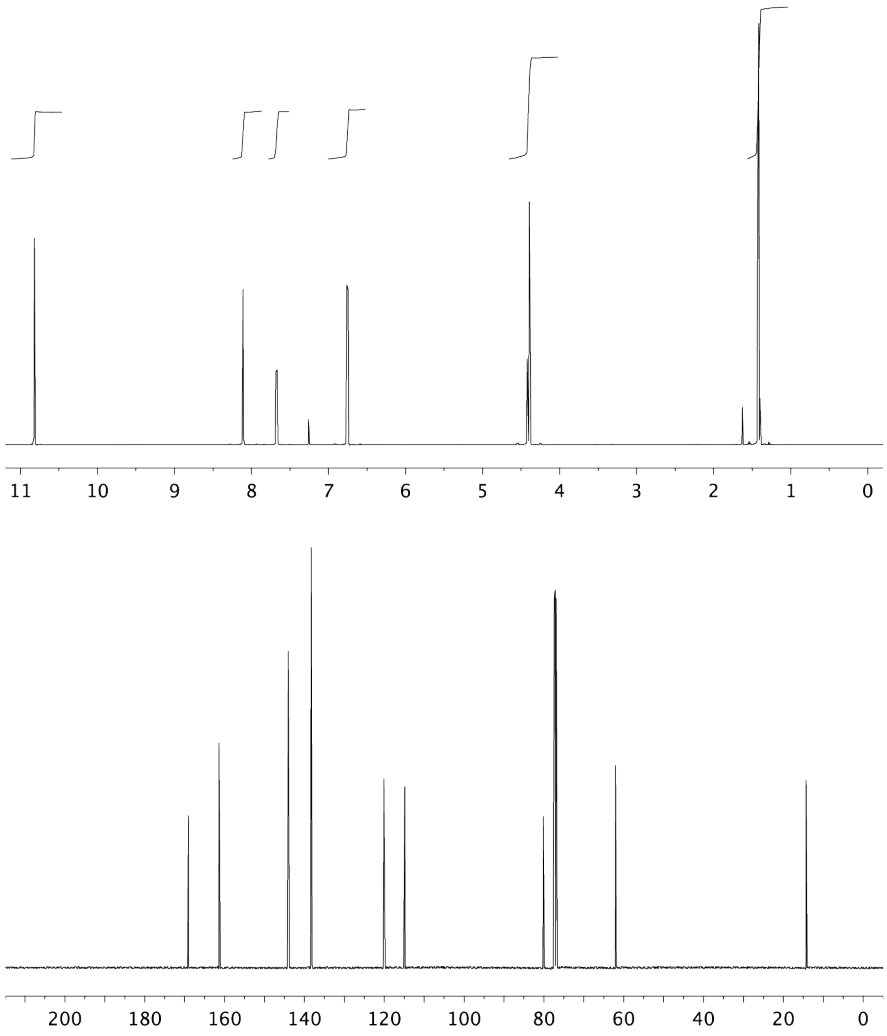

Figure 4.27: ^{1}H NMR (500 MHz) and ^{13}C NMR (125 MHz) spectra of **7** in $CDCl_3$.

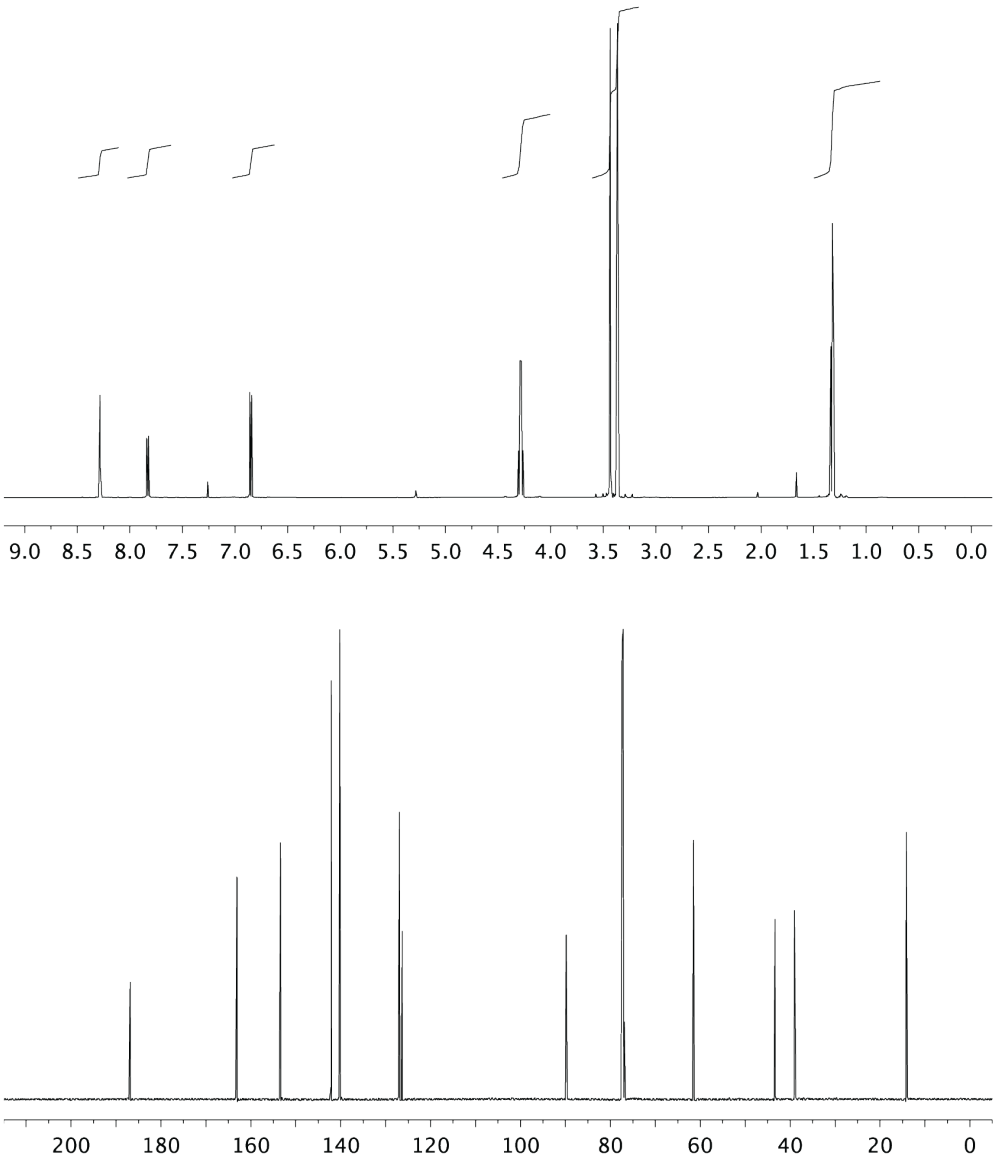

Figure 4.28: ^{1}H NMR (500 MHz) and ^{13}C NMR (125 MHz) spectra of **8** in $CDCl_3$.

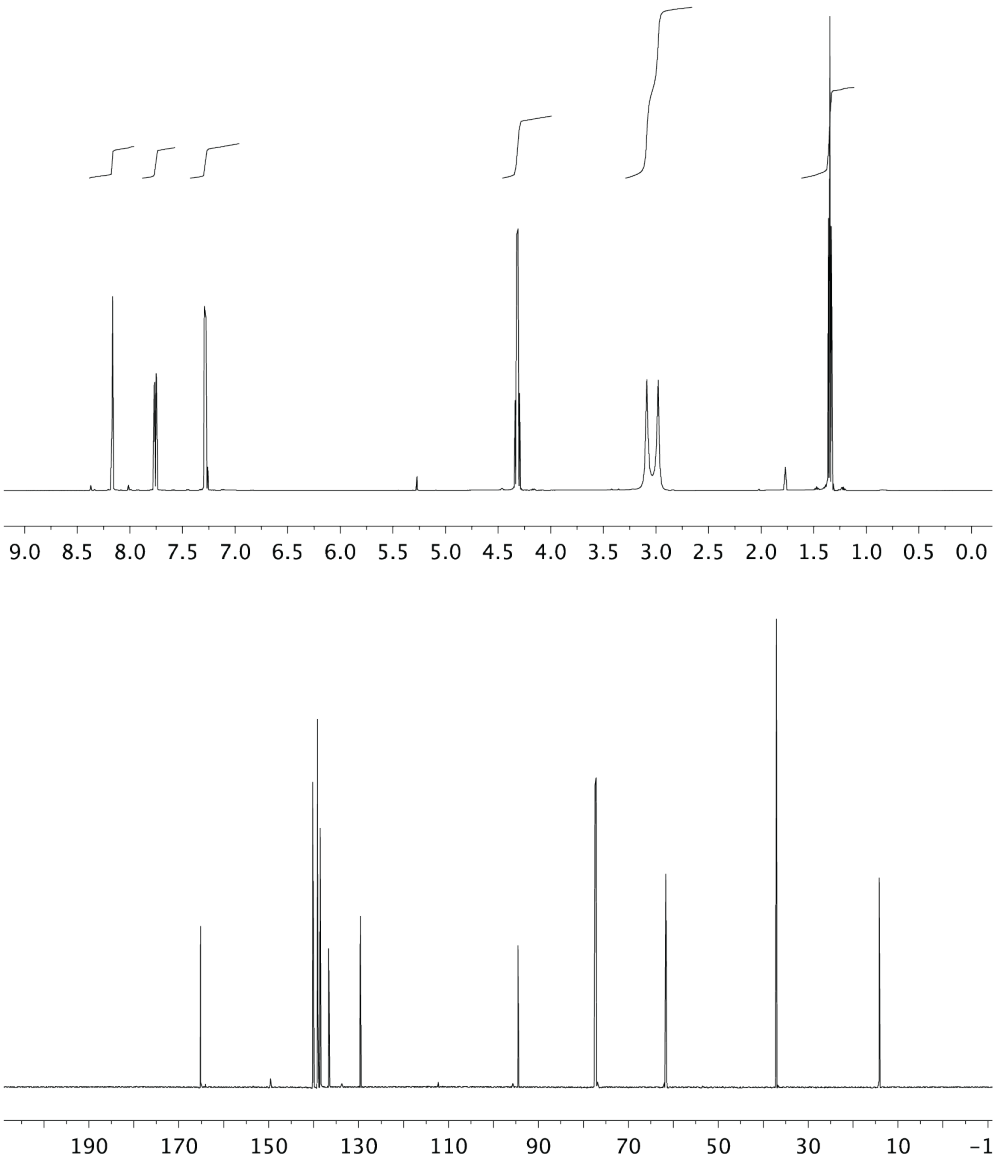

Figure 4.29: ^{1}H NMR (500 MHz) and ^{13}C NMR (125 MHz) spectra of **9** in $CDCl_3$.

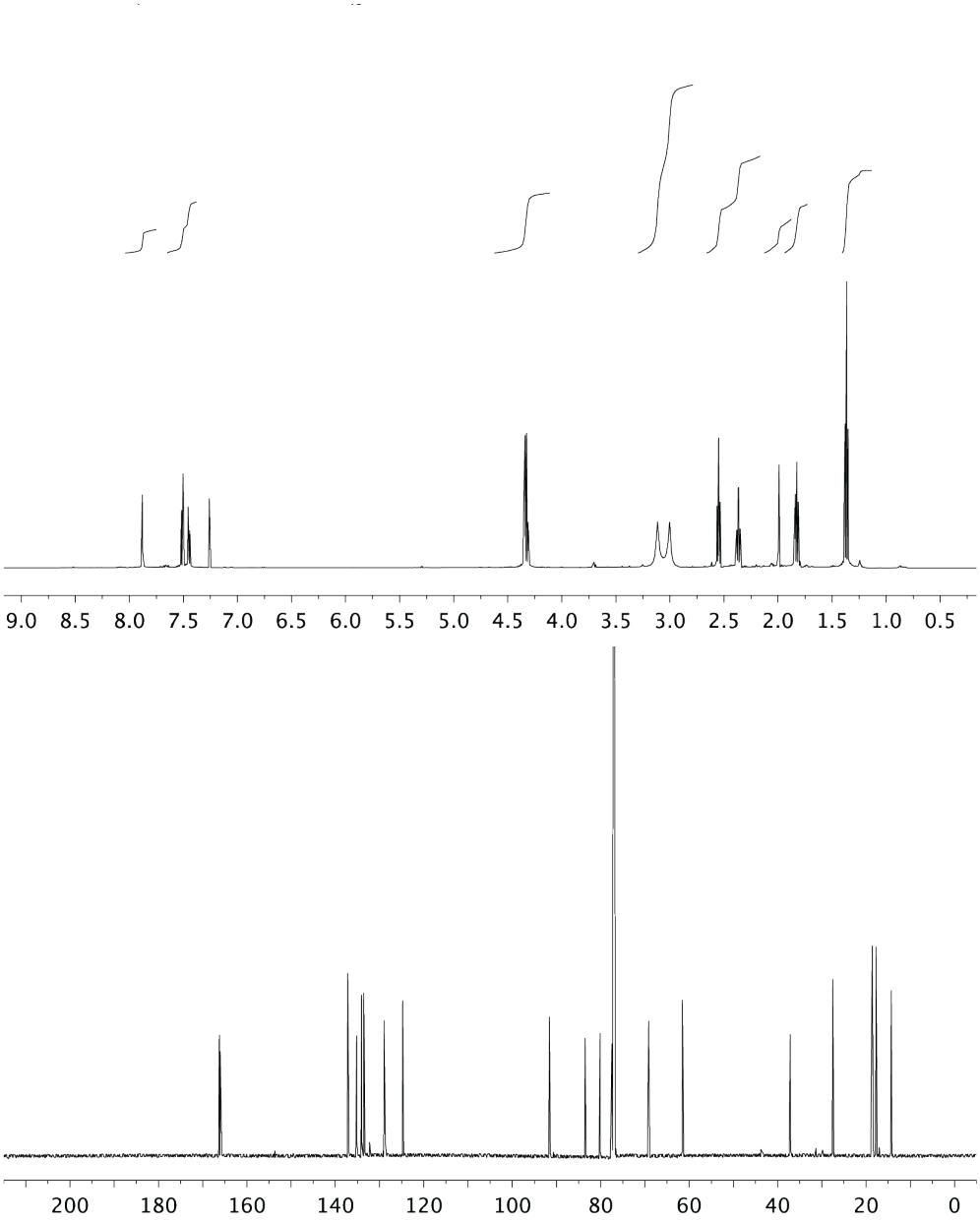

Figure 4.30: ^{1}H NMR (500 MHz) and ^{13}C NMR (125 MHz) spectra of **10** in $CDCl_3$..

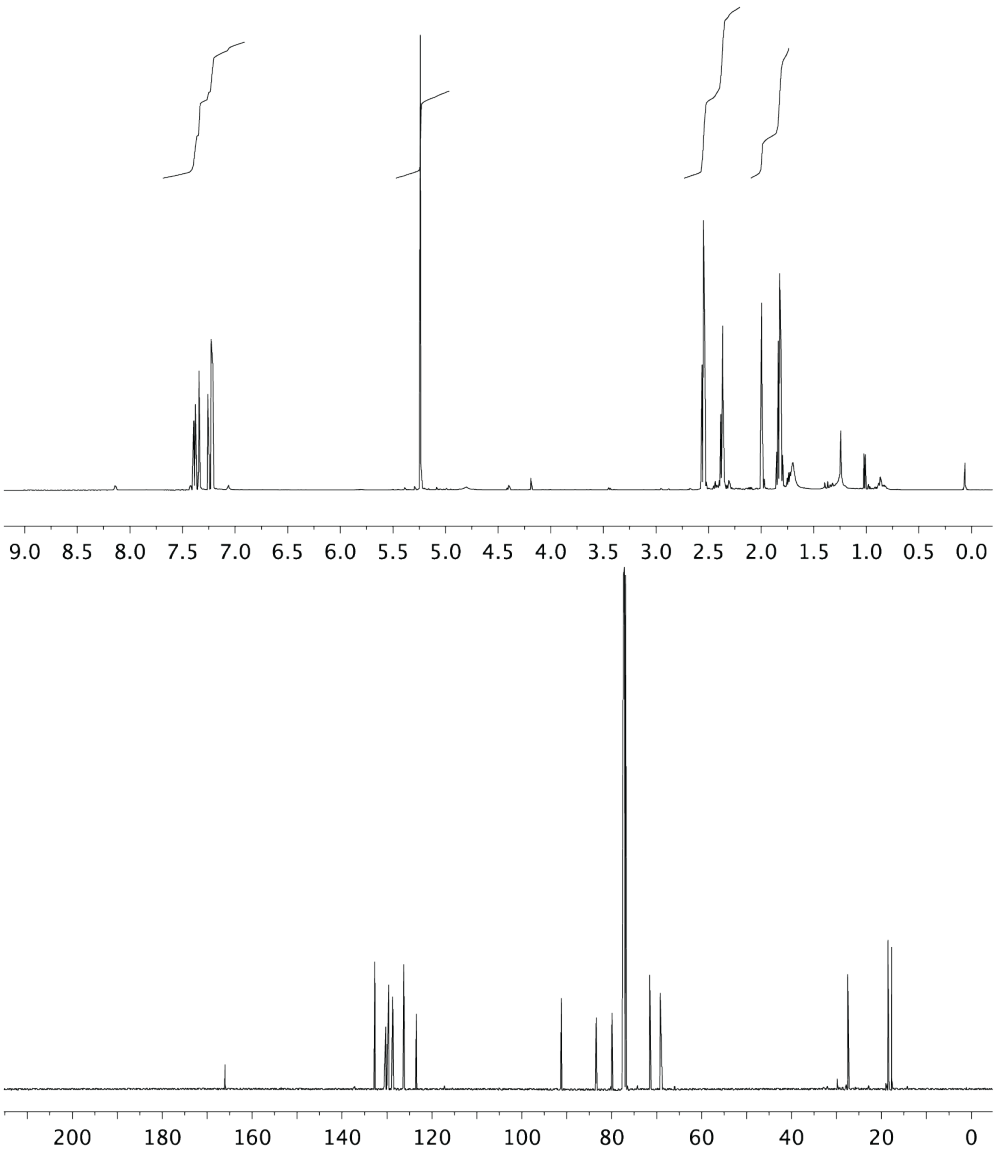

Figure 4.31: ^{1}H NMR (500 MHz) and ^{13}C NMR (125 MHz) spectra of **12** in $CDCl_3$.

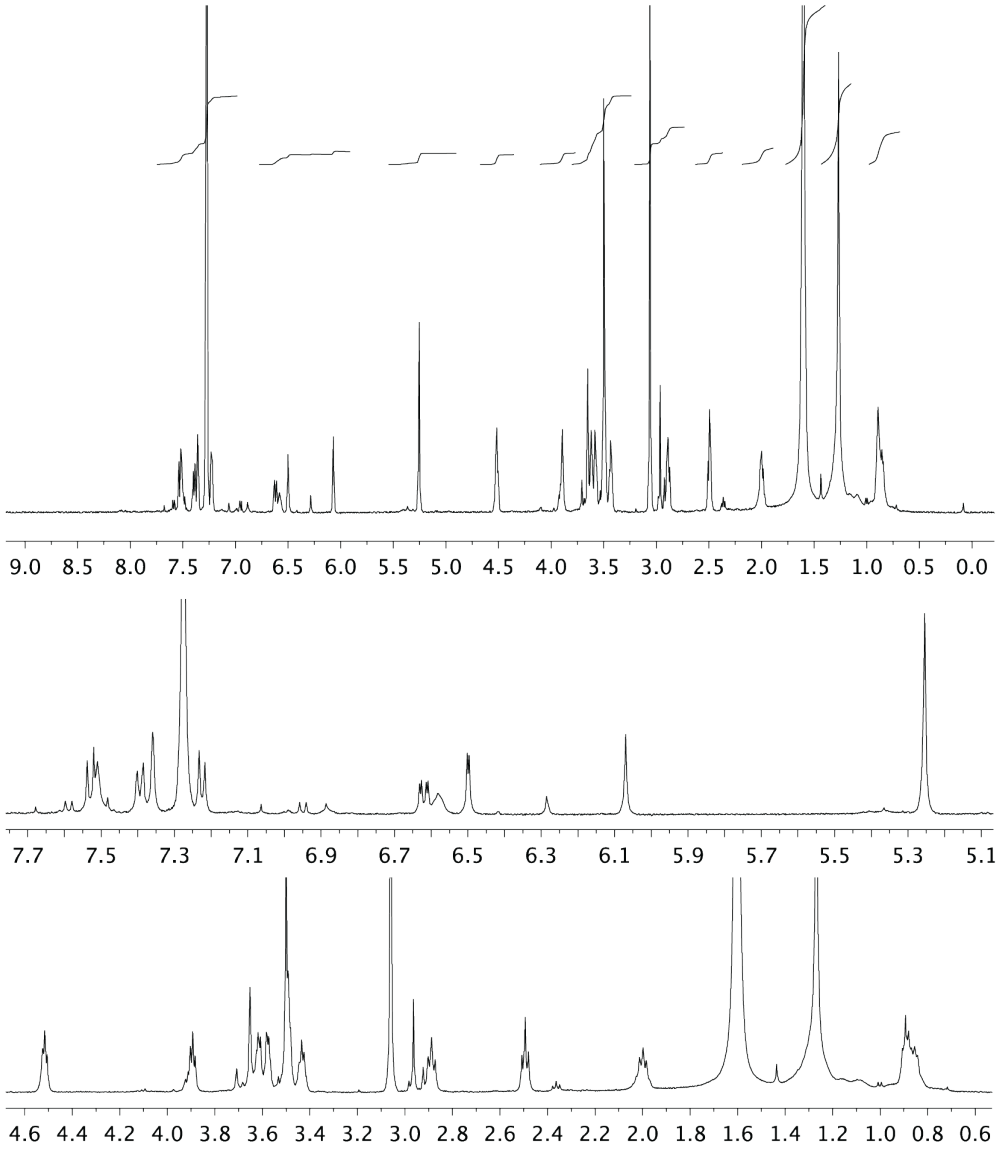

Figure 4.32: ^{1}H NMR (500 MHz) spectrum of **6** in $CDCl_3$.

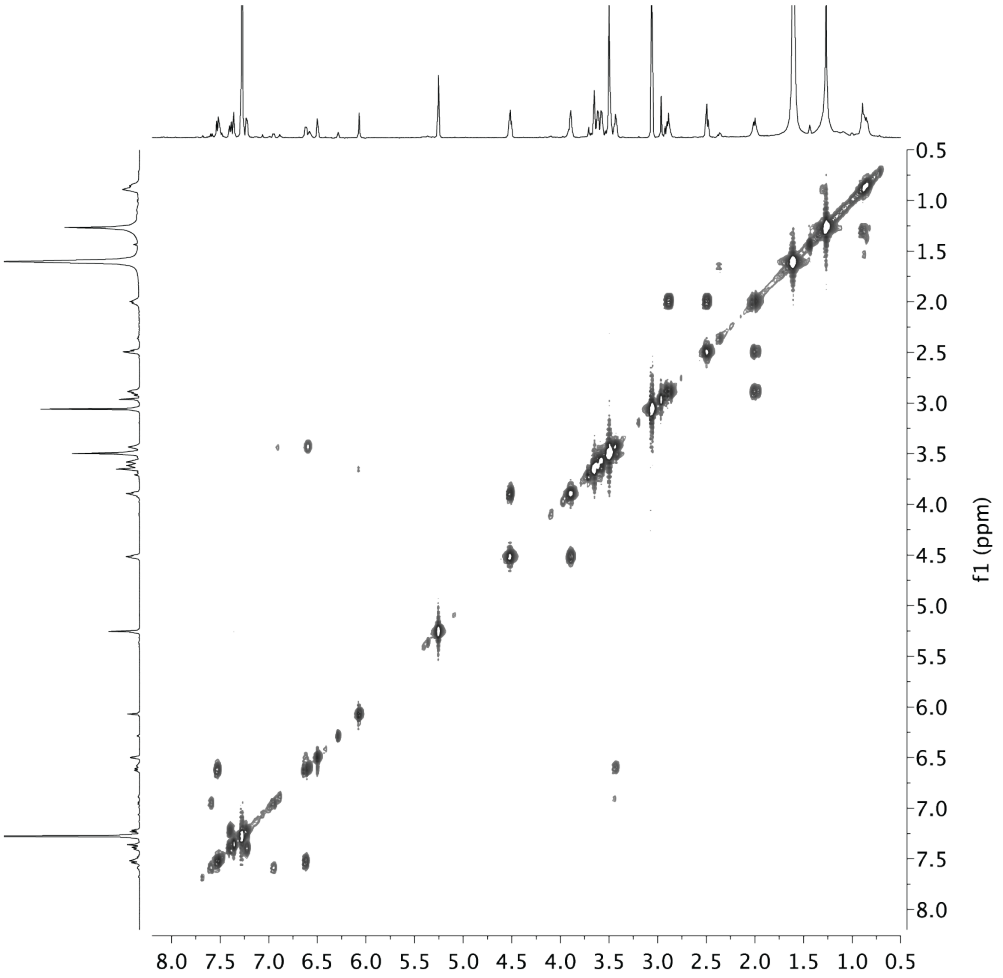

Figure 4.33: gCOSY (500 MHz) spectrum of **6** in $CDCI_3$.

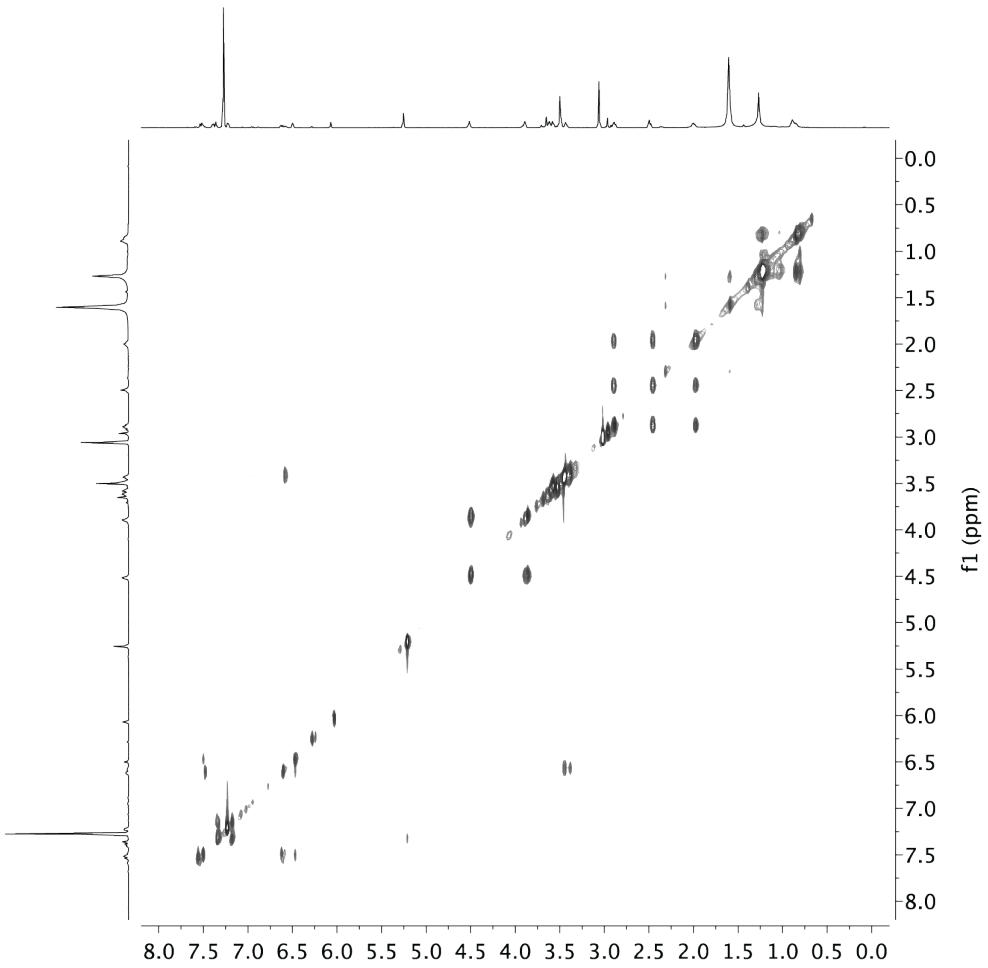

Figure 4.34: TOCSY (600 MHz) spectrum of **6** in $CDCl_3$.

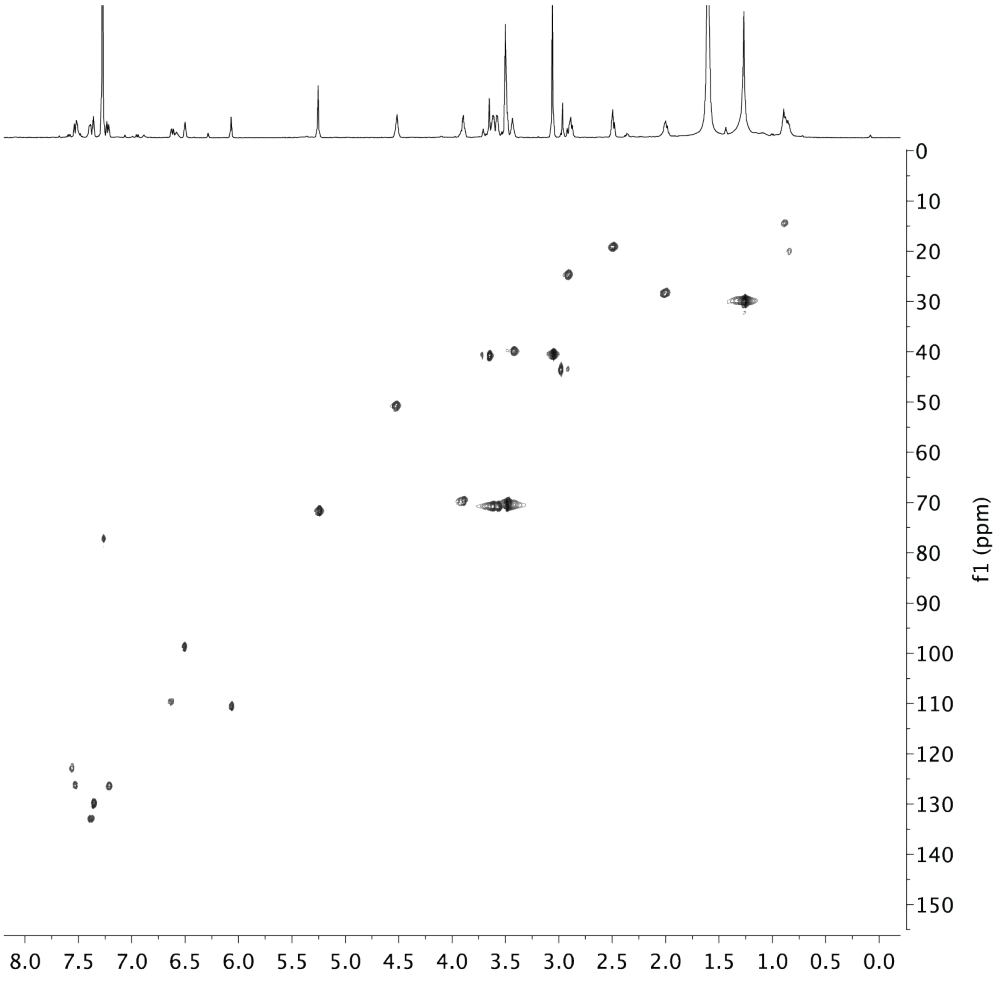

Figure 4.35: ^{1}H,^{13}C HSQC (600 MHz) spectrum of **6** in $CDCl_3$.

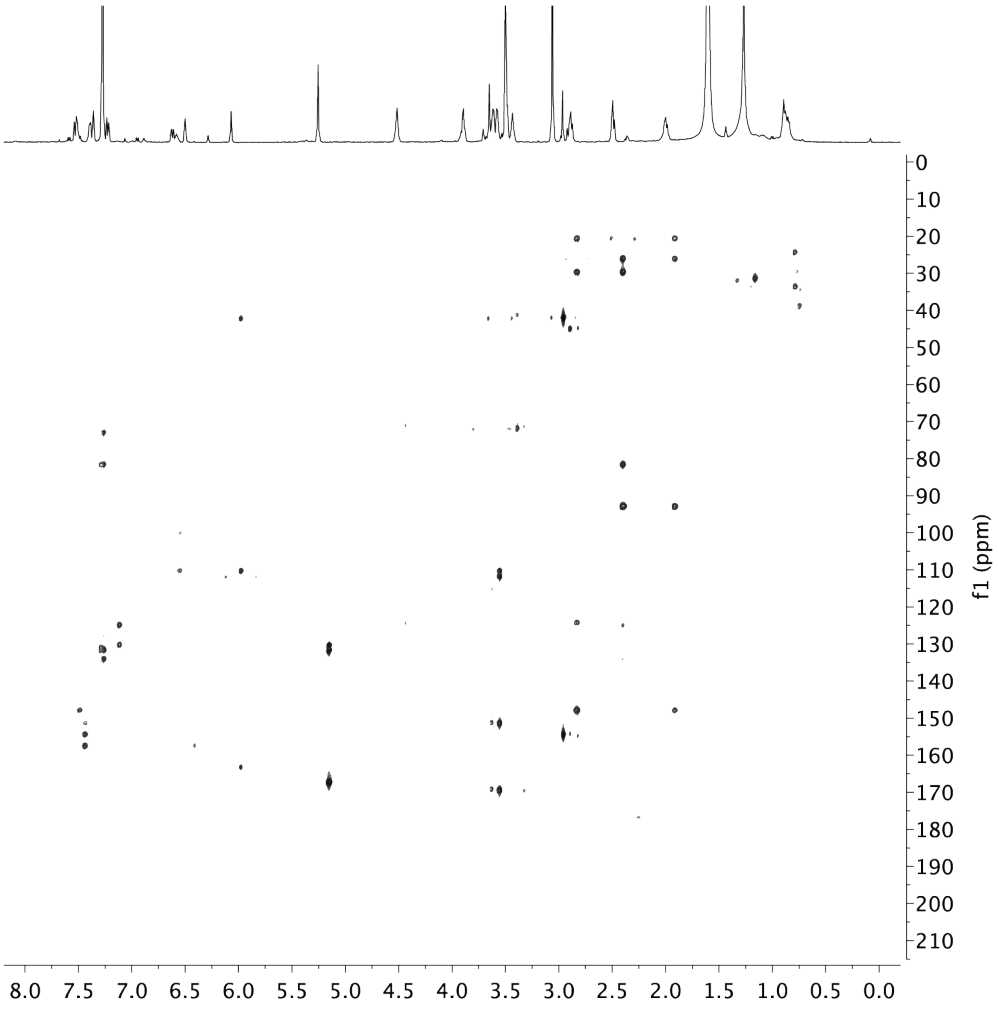

Figure 4.36: ^{1}H,^{13}C HMQC (600 MHz) spectrum of **6** in $CDCI_3$.

4.6.6 Supporting References

S1. Gottleib, H. E.; Kotlyar, V.; Nudelman, A. *J. Org. Chem.* **1997**, *62*, 7512.

S2. Meier, J. L.; Mercer, A. C.; Rivera, H.; Burkart, M. D. *J. Am. Chem. Soc.* **2006**, *128*, 12174.

S3. Owen, J. G.; Copp, J. N.; Ackerley, D. F. *Biochem. J.* **2011**, *436*, 709.

S4. Dorrestein, P. C.; Yeh, E.; Garneau-Tsodikova, S.; Kelleher, N. L.; Walsh, C. T. *Proc. Natl. Acad. Sci. USA* **2005**, *102*, 13843.

S5. Yachnin, B. J.; Sprules, T.; McEvoy, M. B.; Lau, P. C.; Berghuis, A. M. *J. Am. Chem. Soc.* **2012**, *134*, 7788.

S6. Worthington, A. S.; Burkart, M. D. *Org. Biomol. Chem.* **2006**, *4* (1), 44.

S7. Walsh, C. T.; Wencewicz, T. A. *Nat. Prod. Rep.* **2013**, *30*, 175.

S8. Takahashi, H. ; Kamagai, T.; Kitani, K.; Mori, M. *J. Biol. Chem.* **2007**, *282*, 9073.

Chapter 5

Dissecting Modular Synthases: A Complemenatary Chemical and Genetic Approach

5.1 Abstract

Modular synthases, such as fatty acid, polyketide and non-ribosomal peptide synthases (NRPSs), are sophisticated machineries essential in both primary and secondary metabolism. Various techniques have been developed to understand their genetic background and enzymatic abilities. However, uncovering the actual biosynthetic pathways remains challenging. Herein, we demonstrate a pipeline to study an assembly line synthase by interrogating the enzymatic function of each individual protein domain. BpsA is a NRPS producing the blue 3,3'-bipyridyl pigment indigoidine. Specific inhibitors for each biosynthetic domain of BpsA were obtained or synthesized. The enzymatic performance of BpsA upon addition of each inhibitor

was monitored by pigment development *in vitro* and *in vivo*. The results were verified using BpsA mutants in corresponding domains. Finally, the results were linked to and confirmed the proposed biosynthetic pathway of BpsA. This concept demonstrates a straightforward technique to elucidate the biochemistry of uncharacterized modular synthases.

5.2 Introduction

Modular synthases make up the core machinery of essential small molecule metabolites such as fatty acids, polyketides and non-ribosomal peptides. Besides their involvement in fatty acid anabolism throughout all kingdoms of life, they are responsible for the production of bioactive compounds crucial for cell survival in bacteria, fungi and plants. These molecules often possess antibiotic, immunosuppressive, cytostatic, and cytotoxic activities and have gained considerable attention in modern medicine and agriculture.[1]

Their biosynthesis follows an assembly-line strategy unique among metabolic pathways. Each synthase consists of individual domains possessing distinctive functions, such as the recognition of the substrate (amino acid or acyl-coenzyme A (acyl-CoA)), propagation of the growing chain, tailoring and condensation of intermediates and finally, release of the product. For a non-ribosomal peptide synthetase (NRPS), the basic components include adenylation (A), peptidyl carrier protein (PCP), condensation (C) and thioesterase (TE) domains.[1] Due to their complexity, the study of modular synthases remains challenging, from mechanistic and structural analysis to concepts as basic as product identity. With this report, we aim to demonstrate the dissection of a NRPS modular synthase to probe the activity of each domain, as well

as the activity of the ensemble. Here we provide a case study of the blue pigment synthetase A (BpsA), the bacterial source of the blue pigment indigoidine (Figure 5.1).

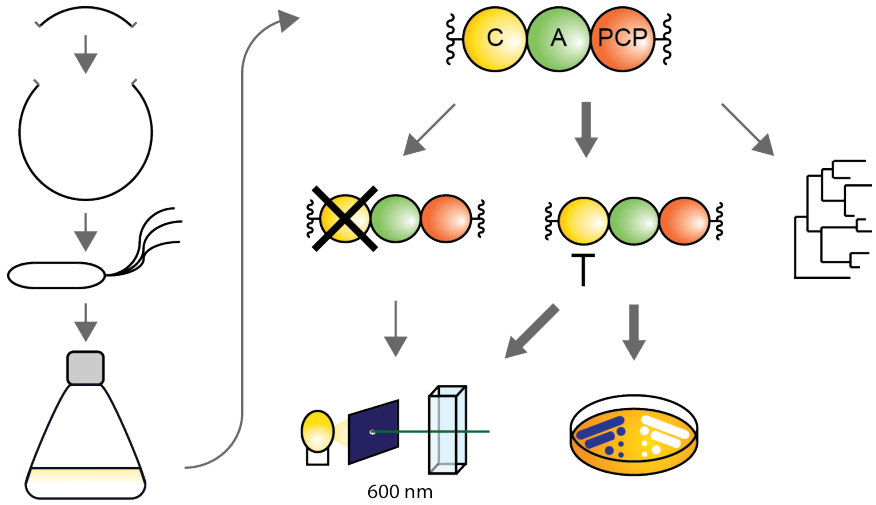

Figure 5.1: Pipeline for the biochemical characterization of a modular pigment-producing synthase. After heterologous expression of the synthase gene and purification of the protein, the activity of each individual domain is inhibited by specific small molecules and analyzed *in vitro* and *in vivo* by pigment formation. Additionally, mutant proteins of each individual domain are generated and analysed subsequently. Phylogenetic analysis provides further information on the diversity and versatility of the synthase.

Although the blue pigment resulting from indigoidine was first observed in 1890,[2] the indigoidine synthase was only discovered in 2002 as IndC in the plant pathogen *Dickeya dadantii* (formerly known as *Erwinia chrysanthemi*).[3] The wild-type strain does not make the blue pigment (the synthase gene is cryptic), but a pectate master regulator (PecS) mutant does. In the latter background, an insertional library identified IndA, -B and -C, from which IndC is the synthase. IndB shows similarities to phosphatases, wheras IndA has unknown function.[4] The synthase IndC is conserved in many organisms, and is annotated as IndC, BpsA, IgiD or as putative synthase (Supporting Figures 5.6, 5.7), but the accompanying genes are

less conserved.[5] A phylogenetic analysis of IndC homologs shows a wide distribution of these synthases, with conservation putatively even reaching to some eukaryotes (Supporting Figure 5.5).[3] IndC is a single protein multi-domain NRPS module, with an A domain predicted to utilize **L**-glutamine as building block.[3] Bacterial A domains show uniquely predictable active sites that are conserved within groups determined by the amino acid they load onto the PCP, enabling computational prediction of the selectivity.[6]

In 2007, a homologous synthase was identified and characterized in *Streptomyces lavendulae*, called blue pigment synthase A (BpsA). *In vitro* experiments showed that BpsA can only accept **L**-Gln over all proteinogenic amino acids, and that the synthase oxidizes and dimerizes the amino acid.[7] As predicted by bioinformatics, BpsA is a single module NRPS, with an oxidation (Ox) domain integrated into the A domain (Scheme 2). The Ox domain harbors a flavin cofactor, as shown by UV absorbance measurements,[8] and purified protein has the characteristic yellow coloration of flavoproteins. Like all modular synthases, BpsA requires post-translational modification by a 4'-phosphopantetheinyl transferase (PPTase).[9] The PPTase transfers the 4'-phosphopantetheine moiety of the cofactor CoA onto a conserved serine residue of the PCP, enabling the PCP to tether the natural product via a labile thioester linkage. This enzymatic transformation was recently utilized by Ackerley and others for the development of novel reporter systems.[10]

5.3 Results and Discussion

We expressed and purified the flavin-bound apo-BpsA and post-translationally modified the protein using CoA and the promiscuous PPTase Sfp. holo-BpsA showed

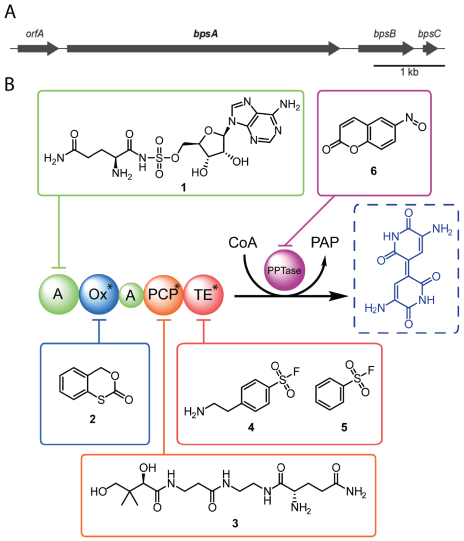

Figure 5.2: Gene cluster and domain organization of BpsA. (A) Genomic organization of BpsA (gene cluster: AB250063, protein: BAE93896) in *Streptomyces lavendulae* subsp. lavendulae including domain-specific inhibitors. orfA is a putative ribose-phosphate pyrophosphokinase, bpsA codes for indigoidine synthase, bpsB for a regulator, and bpsC for a putative S-adenosylmethionine synthase. bpsA = 3,849 bp = 1,282 aa. (B) **1** L-Gln-sulfamoyladenosine inhibitor of A-domain, **2** thiazole inhibitor of flavin-dependent Ox-domain, **3** Gln-pantetheinamide, a substrate for *in situ* transformation into a Coenzyme A analog and subsequent loading onto a carrier protein using a PPTase, **4** and **5** are sulfonylfluoride-containing inhibitors of proteases and thioesterases and **6** is 6-NOBP, a general PPTase inhibitor. * denotes that a domain mutant is available.

robust activity *in vitro*,[7] and *E. coli* BL21 cells co-expressing Sfp and BpsA produced indigoidine when grown with liquid or solid media (Figure 5.2).[1] Interestingly, supplying the double transformant with Gln in the growth media boosts the production of the blue pigment, and Mn^{2+} supplementation is superior to Mg^{2+}, the latter presumably involved in PPTase activity (Supporting Figure 5.8).[11]

To confirm the bioinformatic prediction of domains, thereby clarifying the biosynthetic properties of this synthase, we set out to design and synthesize individual inhibitors for each domain within the synthase. The A-domain is a adenylate-forming

enzyme that loads **L**-Gln onto the PCP. Interestingly, BpsA contains an interrupted A domain, in which the Ox domain separates a large N-terminal from a small C-terminal portion of the enzyme (Figure 5.2b).[12] Adenylate-forming enzymes, including aminoacyl-tRNA synthetases, are inhibited by sulfamoyl-containing analogs of their respective aminoacyl-AMP intermediates.[8, 13] We synthesized and analyzed 5'-O-(N-(L-glutaminyl)-sulfamoyl)adenosine **1** as an inhibitor of BpsA.

Only upon addition of millimolar amounts of this inhibitor resulted in a substantial decrease in the formation of blue pigment *in vitro*, with an IC_{50} = 3.8 mM (Figure 5.3a). The high concentrations required suggest a competitive, non-covalent mechanism of inhibition, as previously observed in inhibition of the biosynthesis of mycobactin with salicyl-amino-sulfonamide-adenosine.[13h] However, why **1** does not inhibit BpsA to the same extent as other sulfonamides inhibit A-domains,[13c] luciferase,[13a] tRNA synthetases [13g], [14] or acyl-CoA ligases, [8] is an open question. We hypothesize that the molecule is unstable in aqueous environment, and due to its polarity has low affinity for the A-domain of BpsA. Alternatively, interrupted A-domains might bind this class of inhibitor differently compared to classical A-domains.

The second domain of BpsA is a flavin-dependent oxidation domain. The Ox domain is most likely responsible for oxidizing either directly glutamine tethered to the PCP or a cyclized glutamine intermediate (Figure 5.5). Takahashi et al. demonstrated by point-mutational analysis of the Ox domain that binding of the cofactor flavin mononucleotide FMN is essential for indigoidine production.[7] Other flavin-dependent oxidation domains in NRPSs have been studied by the Walsh lab, including EpoB, the oxidation domain involved in epothilone biosynthesis.[15] EpoB oxidizes the dihydro heterocyclic thiazolinyl ring to a heteroaromatic oxidation state,

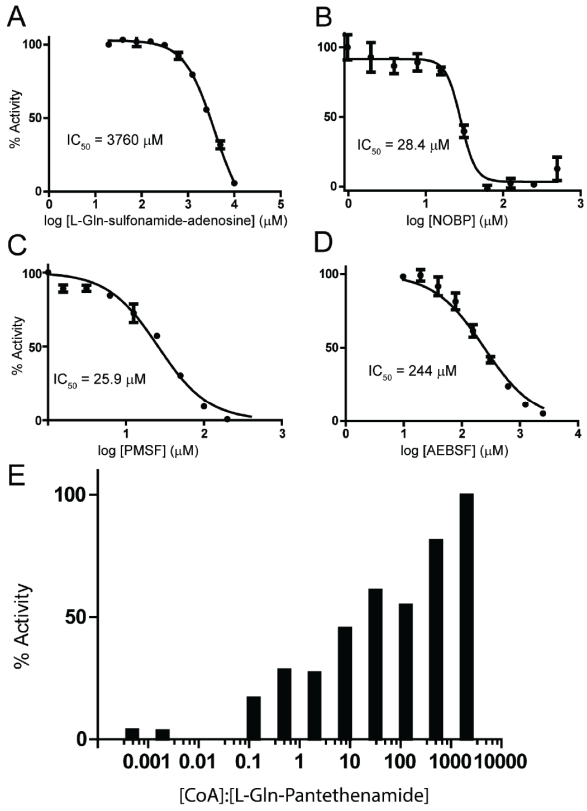

Figure 5.3: Inhibition of individual BpsA domains. (A) Inhibition of the PPTase Sfp by 5'-*O*-[*N*-(**L**-phenylalanyl)sulfamoyl] adenosine 1. (B) Inhibition of A domain by 6-NOBP **6**.(C) Inhibition of TE domain by PMSF **5** and (D) AEBSF **4**. (E) Activity of BpsA by varying the ratio of CoA to the non-hydrolysable **L**-Gln-Pantethenamide analog **3** during preincubation of BpsA with Sfp.

forming methylthiazolylcarboxy-*S*-EpoB. The Ox domain of BpsA shares 29% identity with EpoB (AAF62884) (Supporting Figure 5.13). Although some NRPS Ox-domains have been characterized, few inhibitors of these oxidases are known. Inspired by the work of Walsh and co-workers, we synthesized 4H-benzo[d][1,3]oxathiin-2-one (BOTO) **2** as Ox-domain inhibitor (Scheme 2B).[16] Micromolar amounts are sufficient to fully inhibit the enzyme.[16]

The PCP, the third domain of BpsA, is not an enzyme but a carrier protein, making traditional inhibition impossible. However, our lab has developed a

methodology to attach non-hydrolyzable analogs of thioester bound substrates to carrier proteins through the preparation of pantetheine analogs elaborated by CoA biosynthetic enzymes and the promiscuous PPTase Sfp.[17] Facile synthesis of **L**-Gln-pantetheinamide **3** allowed for the labeling of the BpsA PCP with a non-hydrolyzable substrate mimic. This crypto-BpsA showed no activity *in vitro* (Supporting Figure 5.9), and in direct competition assay between CoA and **L**-Gln-pantethenamide-CoA, decreased BpsA activity was clearly observed when as the ratio of CoA to **L**-Gln-pantethenamide decreased (Figure 5.3e).

In order to tether substrates to NRPSs for catalysis, all PCPs require post-translational modification by a PPTase. PPTases have only recently been recognized and investigated as potential anti-microbial targets.[18] In our work on the discovery of inhibitors for the *B. subtilis* PPTase, Sfp, we found the general PPTase inhibitor 6-NOBP **6** shows modest inhibition against a variety of PPTases.[18a] Based on these findings Owen et al.[10a] used **6** as PPTase inhibitor as demonstrated by indigoidine production with BpsA. Indeed, **6** inhibited BpsA with an IC_{50} of 25 μM using 50 nM Sfp, 1 μM BpsA, and 30 μM CoA. (Figure 5.3b and SI).

The fourth domain of BpsA is the TE, which presumably releases the product from the PCP. Speculation of this activity differs, but the most recent review proposes release of 5-amino-pyridinedione, followed by spontaneous dimerization of two products, forming either colorless leuco-indigoidine or blue indigoidine (Figure 5.5). Numerous thioesterase inhibitors have been developed over the past decades that rely on the nucleophilicity of the active site serine or cysteine.[19] To inhibit the TE of BpsA, we used the general protease inhibitor phenylmethylsulfonyl fluoride (PMSF) **5** and a derivative of the reactive phenylsulfonylfluoride moiety, 4-(2-

aminoethyl)benzenesulfonylfluoride (AEBSF) **4** (Figure 5.3c,d). Blue pigment formation was abrogated by micromolar concentrations of either inhibitor, suggesting that although its function is speculative, the TE domain is critical for catalysis. A BpsA mutant lacking the TE domain activity exhibits no turnover when compared to wild type (Supporting Figure 5.10a). In an effort to discern the importance of the TE domain, we incubated the TE mutant of BpsA with a previously described type II thioesterase, TycF.[20] TycF is known to remove substrates from the phopshopantetheine arm of PCPs. However, the TE mutant was unable to produce blue pigment with or without TycF (Supporting Figure 5.10b), suggesting that the TE domain of BpsA directly participates in the formation of indigoidine, not simply hydrolyzing the substrate off of the PCP.

Interestingly, **5** showed ten-fold greater inhibition of blue pigment production than **4**, indicating that steric effects or polarity of the substrates that enter the TE is important. We also used **4** to synthesize a pantetheinamide analog with a reactive sulfonylfluoride warhead. This pantetheinamide probe was similar to the **L**-Gln-pantetheinamide probe **3** loaded onto BpsA. The loading of this probe eliminates formation of blue pigment and prevents loading of a fluorescent pantetheinamide analog in a chasing experiment (Supporting Figure 5.11). This probe could offer new opportunities for mechanistic crosslinking of domains in multi-domain synthases.

A BLAST search of the BpsA TE domain results in hits (24% homology, SI) in atromentin synthase[21] and TdiA,[22] in which TEs are involved in cyclization/dimerization and dimerization of two activated indolepyruvic acid monomers, respectively. Fascinatingly, the human FAS (FASN) thioesterase also appears as a potential hit, with 21% homology, whereas the entire synthase has low identity (SI).

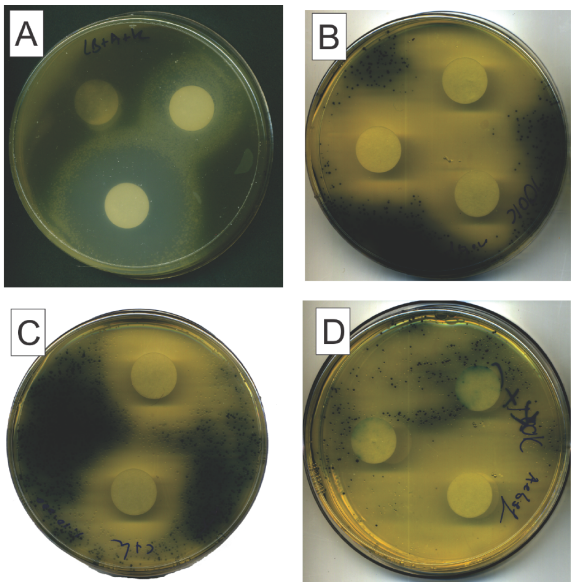

Figure 5.4: Inhibition of pigment production of *E. coli* strains expressing BpsA and Sfp. Clockwise from top left: A) **2** inhibits the Ox-domain and shows a halo of alive, but white colonies (**1** μl of 1 M, 0.1 M and 0.01 M); B) **6** inhibits PPTases and 10 μl spots of 10 mM, 1 mM and 0.1 mM show toxicity, but no apparent white halo; both C) **4** (10 μl of 10 mM, 1 mM and 0.1 mM) and D) **5** (10 μl of 1 mM and 0.1 mM) show toxicity, but also the presence of white colonies.

All four thioesterases have the conserved His residue (2481FASN), and the level of sequence similarity is further demonstrated in the phylogenetic tree (Supporting Figure 5.12). Interestingly, constructing phylogenetic trees based on A, PCP, Ox and TE domains (Supporting Figure 5.12-5.15), reveals that many putative synthases have similar domains, and that homologs of the individual BpsA domains can be found in very different synthases.

To verify our *in vitro* results, we characterized a set of BpsA mutants designed with selectively inactivated domains. We expressed and purified a BpsA mutant with a K598E mutation in the Ox-domain, preventing the binding of flavin, leading to a colorless-protein; a BpsA mutant with an excised TE domain; a stand-alone Ox-domain; and BpsA mutants with the TdiA23 PCP swapped into the synthase (see

SI). We verified that each of these mutants are inactive. To assess whether two BpsA proteins can act in trans to produce indigoidine, a matrix of inactive mutants of BpsA was made (Supporting Figure 5.16). Interestingly, no significant activity was observed for any of the mutant combinations, indicating that the **L**-Gln substrates loaded onto the PCP of BpsA are incapable of interacting with catalytic domains on a different monomer of BpsA to produce indigoidine.

After demonstrating systematic inhibition of each domain of BpsA, we set out to evaluate the behavior of these inhibitors *in vivo*. The inhibitor activities were evaluated using an *E. coli* strain co-expressing BpsA and Sfp, which translates to blue pigmentation of bacterial colonies on agar plates (Figure 5.4) We spotted the inhibitors on sterile filter paper discs that were placed upon a lawn of cells overexpressing both BpsA and Sfp. Whereas the A-domain inhibitor **1** shows activity *in vitro*, *in vivo* this molecule does not show any effect. It is known that some acylsulfonamides are hampered in their uptake,[13f] and combined with the instability of this polar molecule, **1** is a poor inhibitor *in vivo*. On the other hand, the Ox-domain inhibitor **2** shows a marked effect *in vivo* (Figure 5.4a). With decreasing concentration of **2**, we observe a shift from growth inhibition (close to the center of the disc) to growth without formation of pigment, to growth with blue pigment production (edge of plate). Thus, compound **2** shows *in vivo* toxicity at high dosage, inhibition at medium dosage and no inhibition at low dosage. Pantetheinamide **3** has no effect on the formation of blue pigment when supplemented to *E. coli* overexpressing BpsA/Sfp and the PPTase inhibitor **6** shows toxicity but no clear absence of blue pigmentation. How Sfp (or the native PPTase EntD) escapes inhibition by **6** remains unclear. The thioesterase inhibitors **4** and **5** show severe toxicity to the bacteria at

the high concentrations we employed (data not shown). However, at lower concentrations, both general inhibitors show slight toxicitiy, but also the presence of white colonies. Although only two of the inhibitors show promising results *in vivo*, this approach can be a useful addition to our toolbox for the interrogation of synthases.

Taken together, this *in vitro* and *in vivo* data show that using this small toolbox of inhibitors, we can quickly deduce the enzymatic activities of (and in) an unknown synthase. From these straightforward experiments, we learned that the interrupted A-domain[12] is functional and active, the Ox-domain is flavin-dependent, the PCP-domain can be loaded with various unnatural cargo *in vitro*, and the TE-domain is essential for blue pigment production and is inhibited by cysteine-targeting inhibitors. We, and others, can now speculate on the hypothetical enzymatic or non-enzymatic route to the final product (Figure 5.5). We are confident that our systematic approach opens up many new paths to interrogate the individual steps of a multi-domain synthase.

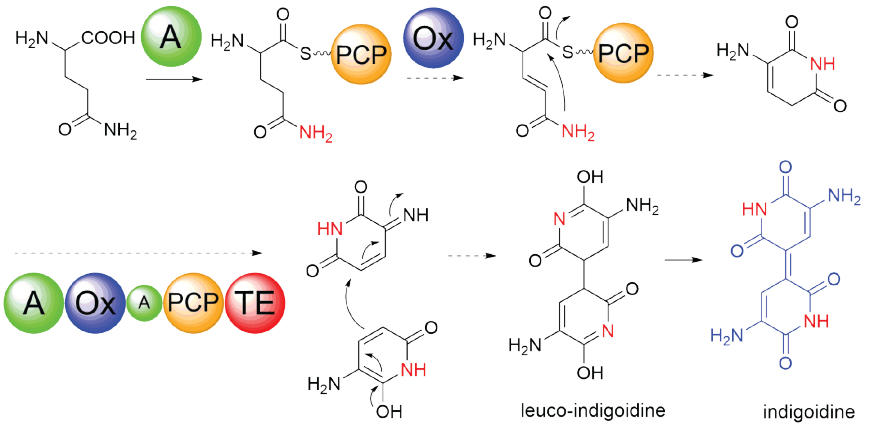

Figure 5.5: Proposed biosynthetic mechanism of indigoidine production.

Recent studies further demonstrated the applicability of blue pigment synthases as model system. Initially, they were utilized to develop blue-white screens in

streptomycetes.[24] Additionally, within an International Genetically Engineered Machine (iGEM) synthetic biology project, NRPS domain swapping recently led to production of novel indigoidine-containing peptides.[25] As part of this project, the PCP domain was replaced with various other PCPs, resulting in large variability in the amount of product. However, Owen et al. had previously co-expressed a PCP replacement of BpsA with various carrier proteins showing no (or severely reduced) indigoidine formation.[26] In contrast to this split system, Beer et al. found that many of the PCP replacement mutants do produce indigoidine, as opposed to the Walsh TdiA construct (SI). It appears that the linker regions between domains (here between Ox-A-PCP and PCP-TE) are crucial for productive catalysis and stable protein expression. However, the biological role of these synthases remains speculative, even so many years after their discovery. These synthases appear to be present in many different organisms, ranging from bacteria to eukaryotes, and their genes are often cryptic, such as in the example in the bacterial insect pathogen *Photorhabdus luminsecens*.[27]

Here we have shown a systematic chemical genomic approach for interrogating a synthase and its domains. Although current technology facilitates bioinformatical discovery of genes and proteins involved in biosynthesis of secondary metabolites,[28] there is a clear and urgent need to verify predictions with experimental data. Selective inhibition of synthase domains is one of the key implements in the toolbox of the chemical biologist, and the functional elucidation and mechanism of assembly-line synthases.

5.4 Acknowledgements

Funding was provided from NIH GM095970. We thank Prof. D. F. Ackerley for the BpsA plasmid construct, Prof. C. T. Walsh for the BpsA mutant plasmid construct, Dr. X. Huang and Dr. A. Mrse for assistance with NMR data collection, and Dr. Y. Su for mass spectrometry services.

Chapter 5 is a reproduced and reformatted version of a manuscript currently drafted for submission of publication:Vickery, Christopher; McCulloch, Ian; Jaremko, Matt; Sonnenschein, Eva; Beld, Joris; Noel, Joseph; Burkart, Michael. "Dissecting modular synthases through inhibition: a complementary chemical and genetic approach." The dissertation author shared primary authorship of this work.

5.5 References

1. (a) Walsh, C. T.; O'Connor, S. E.; Schneider, T. L. *J. Ind. Microbiol. Biotechnol.* **2003**, *30*, 448-455; (b) Schwarzer, D.; Finking, R.; Marahiel, M. A. *Nat. Prod. Rep.* **2003**, *20*, 275.

2. Meier, J. L.; Burkart, M. D.; *Methods Enzymol.* **2009**, *458*, 219.

3. Kuhn, R.; Starr, M. P.; Kuhn, D. A.; Bauer, H.; Knackmuss, H.-J. *Arch. Microbiol.* **1965**, *51*, 71.

4. Reverchon, S.; Rouanet, C.; Expert, D.; Nasser, W. *J. Bacteriol.* **2002**, *184*, 654.

5. Yu, D.; Xu, F.; Valiente, J.; Wang, S.; Zhan, J. *J. Ind. Microbiol. Biotechnol.* **2013**, *40*, 159.

6. Cude, W. N.; Mooney, J.; Tavanaei, A. A.; Hadden, M. K.; Frank, A. M.; Gulvik, C. A.; May, A. L.; Buchan, A. *Appl. Environ. Microbiol.* **2012**, *78*, 4771.

7. Rttig, M.; Medema, M. H.; Blin, K.; Weber, T.; Rausch, C.; Kohlbacher, O. *Nucleic Acids Res.* **2011**, 323.

8. Takahashi, H.; Kumagai, T.; Kitani, K.; Mori, M.; Matoba, Y.; Sugiyama, M. *J. Biol. Chem.* **2007**, *282*, 9073.

9. Lu, X.; Zhang, H.; Tonge, P. J.; Tan, D. S. *Bioorg. Med. Chem. Lett.* **2008**, *18*, 5963.

10. Beld, J.; Sonnenschein, E. C.; Vickery, C. R.; Noel, J. P.; Burkart, M. D. *Nat. Prod. Rep.* **2014**, *31*, 61.

11. (a) Jeremy, G. O.; Janine, N. C.; David, F. A.; *Biochem. J.* **2011**, *436*, 709; (b) Mller, M.; Auslnder, S.; Auslnder, D.; Kemmer, C.; Fussenegger, M. *Metab. Eng.* **2012**, *14*, 325.

12. Mofid, M. R.; Finking, R.; Essen, L. O.; Marahiel, M. A. *Biochemistry* **2004**, *43*, 4128.

13. Labby, K. J.; Watsula, S. G.; Garneau-Tsodikova, S. *Nat. Prod. Rep.* **2015**.

14. (a) Branchini, B. R.; Murtiashaw, M. H.; Carmody, J. N.; Mygatt, E. E.; Southworth, T. L. *Bioorg. Med. Chem, Lett.* **2005**, *15*, 3860; (b) Lu, X.; Zhou, R.; Sharma, I.; Li, X.; Kumar, G.; Swaminathan, S.; Tonge, P. J.; Tan, D. S. *ChemBioChem* **2012**, *13*, 129; (c) Engelhart, C. A.; Aldrich, C. C. *J. Org. Chem.* **2013**, *78*, 7470; (d) Sundlov, J. A.; Shi, C.; Wilson, D. J.; Aldrich, C. C.; Gulick, A. M. *Chem. Biol.* **2012**, *19*, 188; (e) Mitchell, C. A.; Shi, C.; Aldrich, C. C.; Gulick, A. M. *Biochemistry* **2012**, *51*, 3252; (f) Davis, T. D.; Gerry, C. J.; Tan, D. S. *ACS Chem. Biol.* **2014**, *9*, 2535; (g) Cisar, J. S.; Ferreras, J. A.; Soni, R. K.; Quadri, L. E.; Tan, D. S. *J. Am. Chem. Soc.* **2007**, *129*, 7752; (h) Ferreras, J. A.; Ryu, J.-S.; Di Lello, F.; Tan, D. S.; Quadri, L. E. *Nat. Chem. Biol.* **2005**, *1*, 29.

15. (a) Kim, S.; Lee, S.; Choi, E.-C.; Choi, S. *Appl. Microbiol. Biotechnol.* **2003**, *61*, 278; (b) Ueda, H.; Shoku, Y.; Hayashi, N.; Mitsunaga, J.-I.; In, Y.; Doi, M.; Inoue, M.; Ishida, T. *BBA Protein. Struct. Mol. Enzymol.* **1991**, 1080, 126; (c) Heacock, D.; Forsyth, C. J.; Shiba, K.; Musier-Forsyth, K. *Bioorg. Chem.* **1996**, *24*, 273; (d) Tao, J.; Schimmel, P. *Expert Opin. Investig. Drugs* **2000**, *9*, 1767.

16. Schneider, T. L.; Shen, B.; Walsh, C. T. *Biochemistry* **2003**, *42*, 9722.

17. McCulloch, I. P.; La Clair, J. J.; Jaremko, M. J.; Burkart, M. D. manuscript under revision **2016**.

18. Worthington, A. S.; Burkart, M. D. *Org. Biomol. Chem.* **2006**, *4*, 44.

19. (a) Yasgar, A.; Foley, T. L.; Jadhav, A.; Inglese, J.; Burkart, M. D.; Simeonov,

A. *Mol. Biosyst.* **2010**, *6*, 365; (b) Vickery, C. R.; Kosa, N. M.; Casavant, E. P.; Duan, S.; Noel, J. P.; Burkart, M. D. *ACS Chem. Biol.* **2014**, *9*, 1939.

20. (a) Pemble, C. W.; Johnson, L. C.; Kridel, S. J.; Lowther, W. T. *Nat. Struct. Mol. Biol.* **2007**, *14*, 704; (b) Zhang, W.; Chakravarty, B.; Zheng, F.; Gu, Z.; Wu, H.; Mao, J.; Wakil, S. J.; Quiocho, F. A.; *Proc. Natl. Acad. Sci.* **2011**, *108*, 15757.

21. Yeh, E.; Kohli, R. M.; Bruner, S. D.; Walsh, C. T. *ChemBioChem* **2004**, *5*, 1290.

22. Schneider, P.; Bouhired, S.; Hoffmeister, D. *Fungal Genet. Biol.* **2008**, *45*, 1487.

23. Bok, J. W.; Hoffmeister, D.; Maggio-Hall, L. A.; Murillo, R.; Glasner, J. D.; Keller, N. P. *Chem. Biol.* **2006**, *13*, 31.

24. Balibar, C. J.; Howard-Jones, A. R.; Walsh, C. T. *Nat. Chem. Biol.* **2007**, *3*, 584.

25. (a) Li, P.; Li, J.; Guo, Z.; Tang, W.; Han, J.; Meng, X.; Hao, T.; Zhu, Y.; Zhang, L.; Chen, Y. *Appl. Microbiol. Biotechnol.* 1; (b) Knirschova, R.; Novakova, R.; Mingyar, E.; Bekeova, C.; Homerova, D.; Kormanec, J. J. *Microbiol. Methods* **2015**, *113*, 1.

26. Beer, R.; Herbst, K.; Ignatiadis, N.; Kats, I.; Adlung, L.; Meyer, H.; Niopek, D.; Christiansen, T.; Georgi, F.; Kurzawa, N. *Mol. Biosyst.* **2014**.

27. Owen, J.; Robins, K.; Parachin, N.; Ackerley, D. *Environ. Microbiol.* **2012**, *14*, 1198.

28. Brachmann, A. O.; Kirchner, F.; Kegler, C.; Kinski, S. C.; Schmitt, I.; Bode, H. B. *J. Biotechnol.* **2012**, *157*, 96.

29. Medema, M. H.; Blin, K.; Cimermancic, P.; de Jager, V.; Zakrzewski, P.; Fischbach, M. A.; Weber, T.; Takano, E.; Breitling, R. *Nucleic Acids Res.* **2011**, *39*, W339-W346.

5.6 Supporting Information

5.6.1 Experimental Methods

Protein expression and purification

The bpsA gene was subcloned from pCDFDUET into pET28a. BpsA protein was expressed and purified using standard techniques.[S1] Briefly, BL21(DE3) cells carrying pET28a-BpsA were grown at rt to an OD_{600} of 0.6 and expression was induced with 0.5 mM IPTG at room temperature for 16 h. The inactive apo-protein was purified by Ni^{2+}-NTA (Novagen) affinity chromatography and the bright yellow (flavin containing) eluent dialyzed against 50 mM phosphate pH 7.8 containing 20% glycerol. Aliquots were stored at -80 °C. Mutant BpsA clones were expressed under the same conditions. CoaA, CoaD, CoaE and Sfp were expressed and purified as previously described.[S2]

Inhibition of A domain

A 50 μL serial dilution of 1 was made in concentrations ranging from 10 mM to 20 μM. A 50 μL mixture containing 1 μM BpsA, 75 mM potassium phosphate pH 7.8, 10 mM $MgCl_2$, 1 mM CoA, and 2 μM Sfp was added to each serial dilution and incubated at 37°C for 10 mins. The reaction was initiated by the addition of a 50 μL mixture containing 75 mM potassium phosphate pH 7.8, 5 mM **L**-Gln, and 250 μM ATP. The reaction was monitored by absorbance at 590 nm for 30 mins using a HTS 7000 Bio Assay Reader (Perkin Elmer).

Inhibition of TE domain

A serial dilution of either PMSF or AEBSF was made in 50 μL potassium phosphate pH 7.8 with concentrations ranging from 200 μM to 400 nM for PMSF and 2.5 mM to 10 μM for AEBSF. First, 1 μM BpsA was incubated in a 50 μL mixture containing 75 mM potassium phosphate pH 7.8, 1 mM CoA, 10 mM $MgCl_2$, and 2 μM Sfp. This mixture was incubated at 37 °C for 10 min. To these reactions were added the serial dilution of either PMSF or AEBSF and allowed to incubate at 37 °C for 5 min. The reaction was initiated by the addition of a 50 μL mixture containing 75 mM potassium phosphate pH 7.8, 5 mM **L**-Gln, and 10 mM ATP. Reactions were allowed to proceed for approximately 10 min.

Inhibition of PPTase by 6-NOBP

A serial dilution of 6-NOBP was made in concentrations ranging from 500 μM to 1 μM. 50 μL of a mixture containing 75 mM potassium phosphate pH 7.8, 10 mM ATP, 5 mM L-Gln, 10 mM MgCl2, 30 μM CoA, and 50 nM Sfp was added to each serial dilution. This mixture was allowed to stand at 25 °C for 10 min. The reaction was initiated by the addition of 1 μM BpsA and the reaction was monitored at 590 nm for approximately 30 min.

In vivo inhibition assay

BL21(DE3) cells carrying pET28a-BpsA and pUC8-Sfp^{S3} were grown overnight at 37°C and 200 μL was plated on an LB agar plate containing 50 mg/L kanamycin and 100 mg/L ampicillin. Filter discs (1 cm in diameter) were placed upon the surface and 10 μL of dissolved compound was added. The plates were incubated overnight

at 37°C or 24 h at rt.

Phylogenetic analysis of BpsA

(Supporting Figures 5.6, 5.7) The BpsA protein sequence from *Streptomyces lavendulae* (BAE93896) was subjected to DELTA-BLAST[S4] with default parameters increasing the aligned sequence number to 500. Sequences were aligned in MUSCLE.[S5] Using MEGA 5.2.2,[S6] a neighbor joining tree was generated using default settings. The subtree of highly conserved BpsA-like proteins was identified using Dendoscrope [7] and processed into a separate neighbor joining tree.

Phylogeny analysis based on BpsA domain homology

(Supporting Figures 5.12-5.15) Sequences were collected from the NCBI database using Psi-Blast. Domain borders were identified using Interpro and based on literature. Large sequence collections were sorted for duplicates using Duplicatefinder and names shortened using Speciesidentifier. Muscle was used to align sequences and Fasttree to assemble large phylogenetic trees. Dendropscope and Figtree were used to visualize trees.

5.6.2 Supporting Figures

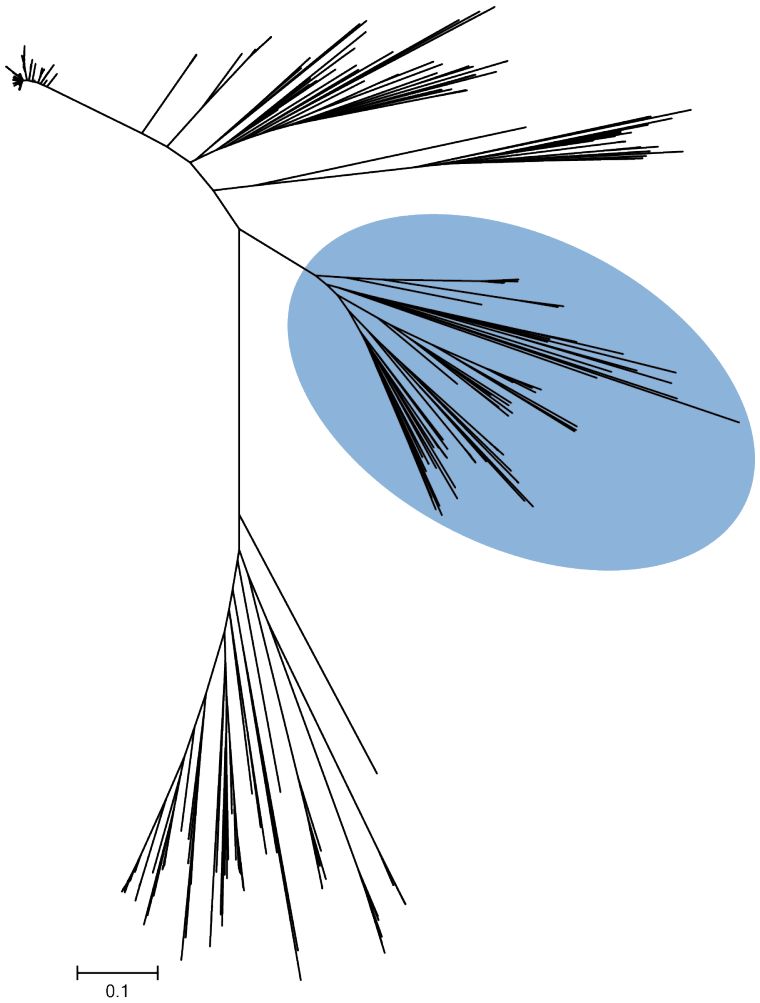

Figure 5.6: Phylogenetic tree of BpsA. Neighbor joining tree based on 500 protein sequences obtained by DELTA-BLAST of BAE93896 using MUSCLE (Edgar **2004** *Nucleic Acids Res.*) and MEGA 5.2.2 (Tamura **2011** *Mol. Biol. Evol.*).

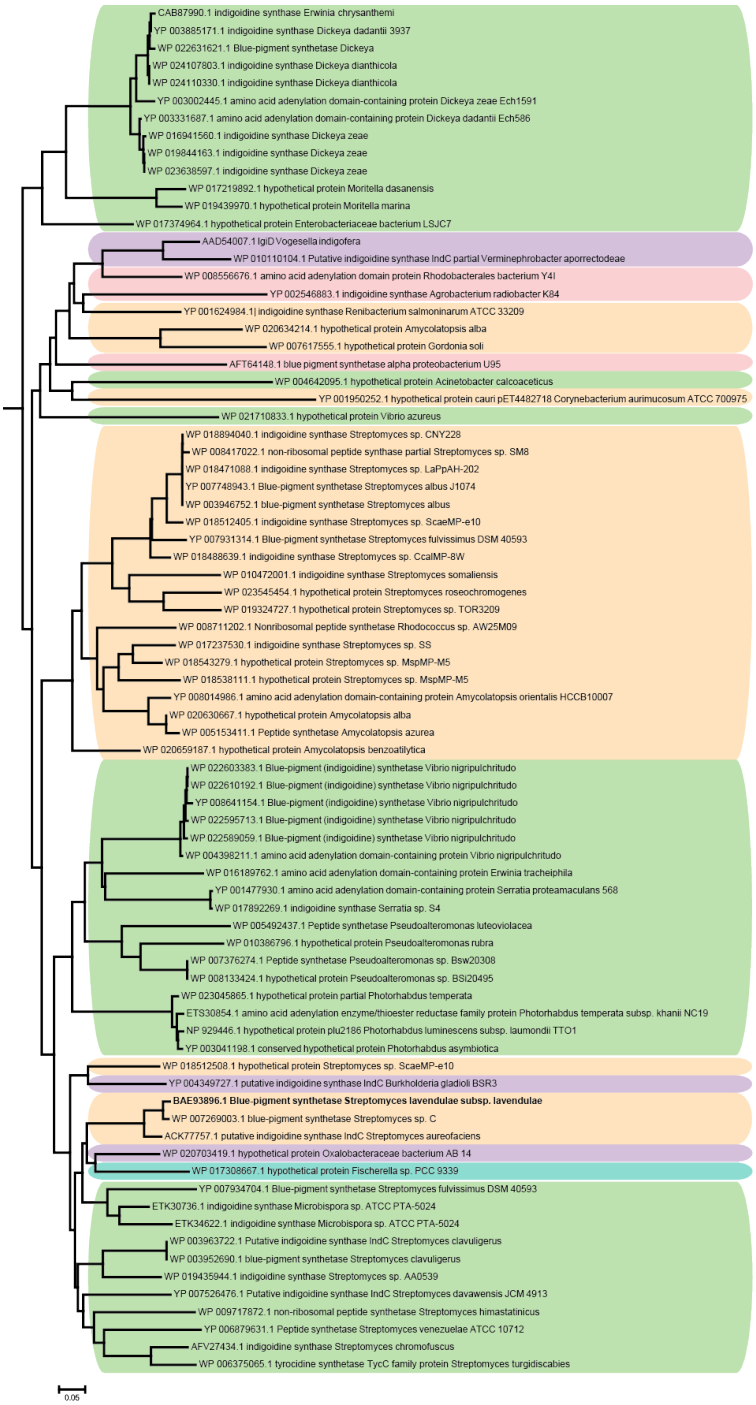

Figure 5.7: Phylogenetic tree of BpsA clade. Neighbor joining tree of BpsA-related protein sequences generated in Dendoscrope. Sequences were marked according to their taxonomic position (yellow: actinobacteria, pink: alpha-proteobacteria, purple: beta-proteobacteria, green: gamma-proteobacteria, blue: cyanobacteria, query sequence BAE93896 marked in bold).

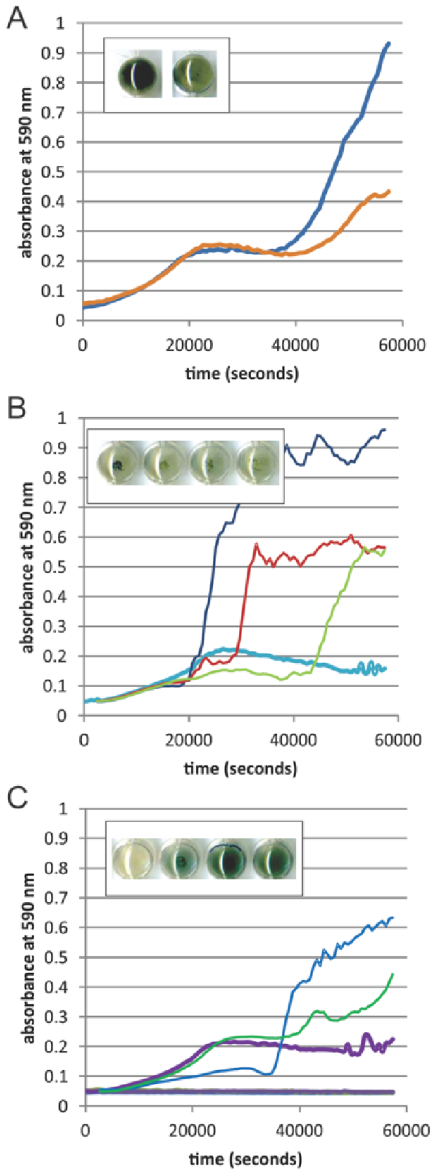

Figure 5.8: Representative growth curves of *E. coli* BL21 expressing BpsA and Sfp, under supplementation with glutamine, $MgCl_2$ and $MnCl_2$. A) A culture not supplemented with Gln (orange) and a culture supplemented with 3.3 mg/mL **L**-Gln (blue). Inset shows a picture of the two cultures. B) In blue, red and green and aqua cultures supplemented with a dilution series of $MgCl_2$ ranging from 3.3, 1.7, 0.8, 0.4 mg/mL. C) in blue, green and purple cultures supplemented with a dilution series of 0.2, 0.1 and 0.05 mg/mL $MnCl_2$, whereas 0.4 mg/mL appeared to be toxic to *E. coli* (flat growth curve and clear first picture).

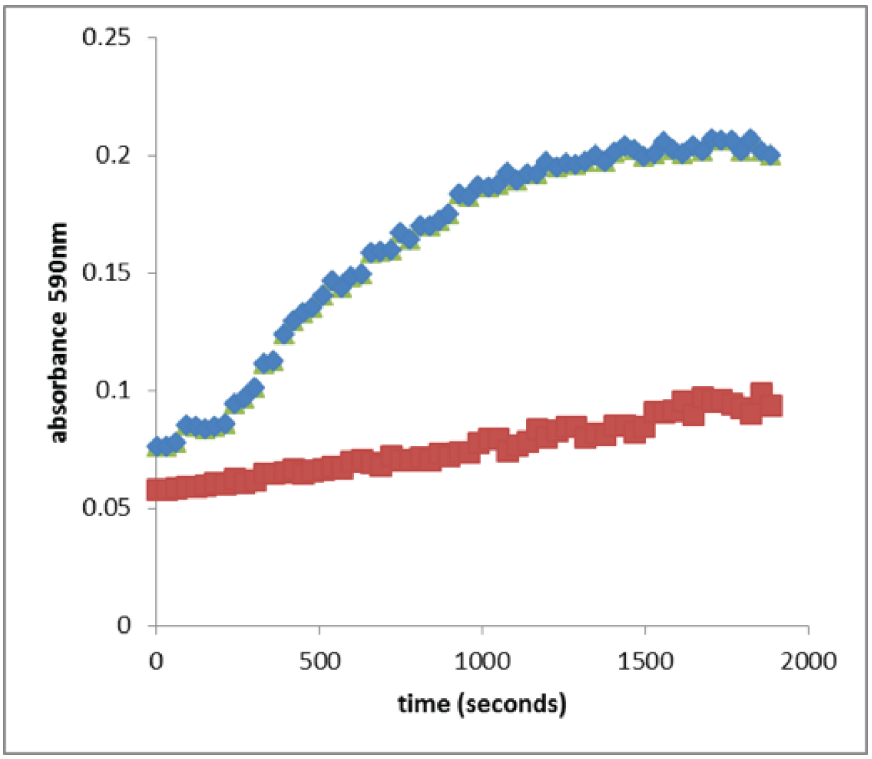

Figure 5.9: Glutamine pantetheinamide as inhibitor of BpsA. In vitro activity assay of BpsA activity by monitoring the formation of blue pigment. In blue, BpsA incubated with Sfp and CoA, followed by addition of **L**-Gln and ATP; in red, BpsA incubated with glutamine pantetheinamide, Coa-A,-D,-E and Sfp, followed by addition of **L**-Gln and ATP.

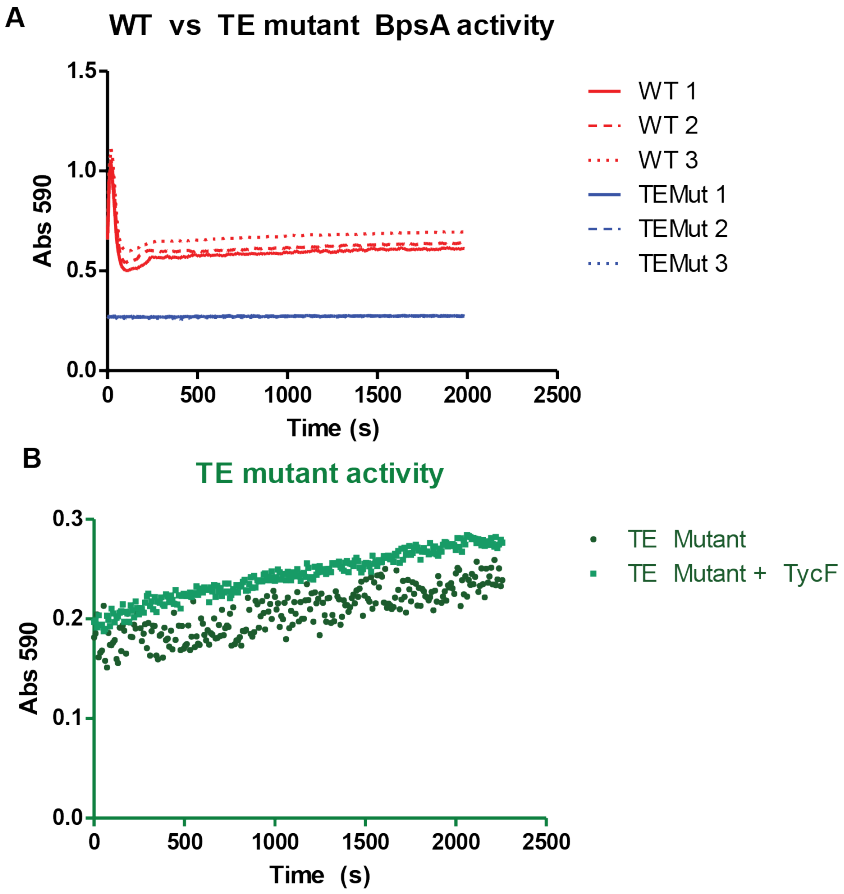

Figure 5.10: Activity BpsA mutant lacking TE domain. (A) Activity of WT BpsA compared to TE mutant. No activity was observed for the TE mutant. (B) Assay of the TE mutant with and without TycF, a type II thioestarase. No activity was observed when BpsA was incubated with TycF.

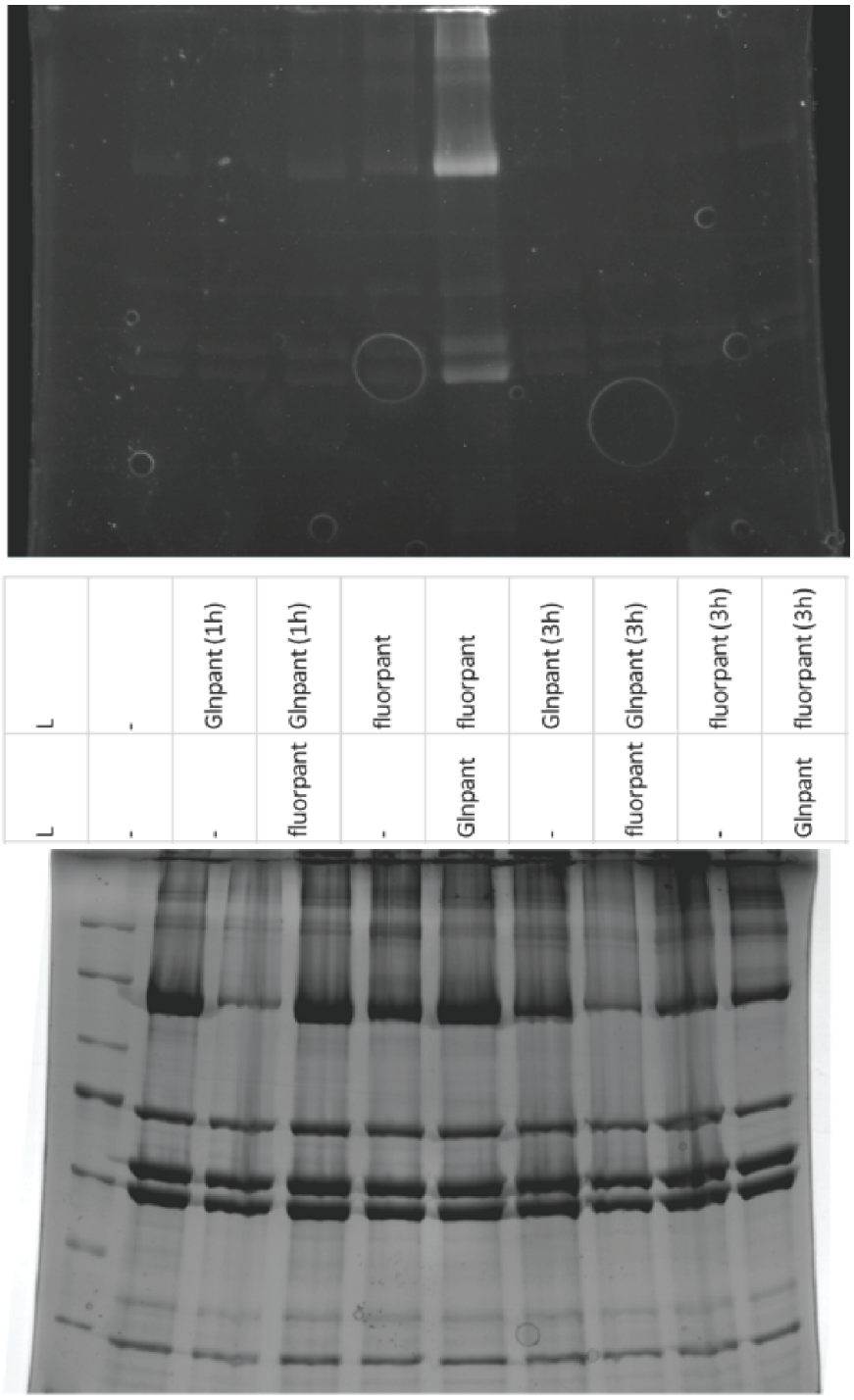

Figure 5.11: Chase experiment loading BpsA PCP with cargo. Top: fluorescent image of 8% SDS PAGE gel. Bottom: image of coomassie stained gel. BpsA was loaded with either glutamine-pantetheinamide probe or 4-DMN-pantetheinamide probe as previously described.[S9]

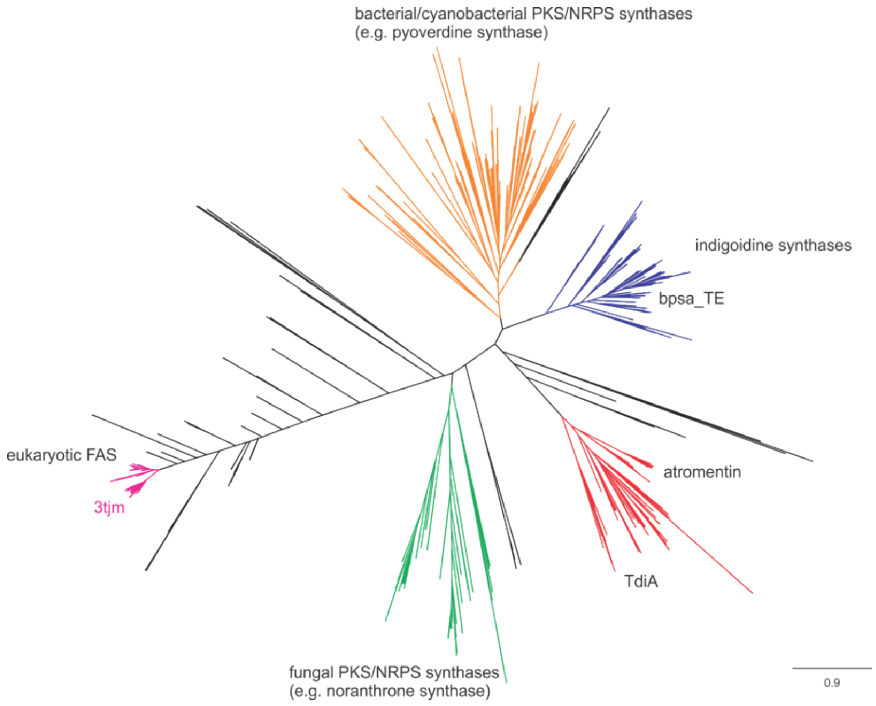

Figure 5.12: Phylogeny based on TE-domain homology. A phylogenetic tree was constructed based on a sequence alignment of the combined psi-blast results of the thioesterase domains of atromentin, tdiA and bpsa synthases (in total 2000 sequences). Within the atromentin/TdiA clade one other hit, besides many other putative hits, is annotated as PksJ from B. subtilis involved in bacillaene synthesis. Within the bacterial clade (orange), besides pyoverdine synthase, HctF, DidJ, surfactin and ZmaQ synthases can be found. Sequences were aligned using Muscle and tree constructed using Fasttree. The tree was visualized using Figtree and Dendroscope.

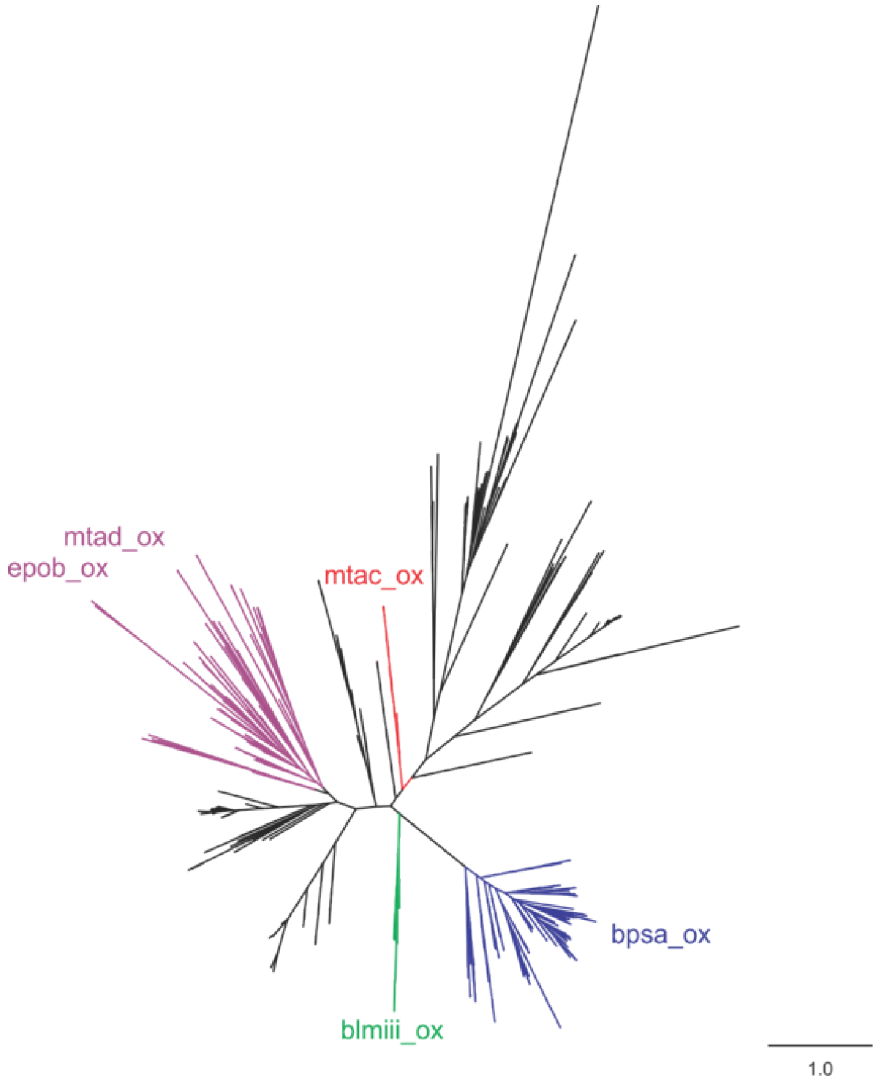

Figure 5.13: A phylogenetic tree was constructed based on a sequence alignment of the combined psi-blast results of the oxidase domains of Mtac, Mtad, Blmiii, EpoB and BpsA synthases (in total 1500 sequences). Sequences were aligned using Muscle and the tree was constructed using Fasttree. The tree was visualized using Figtree and Dendroscope.

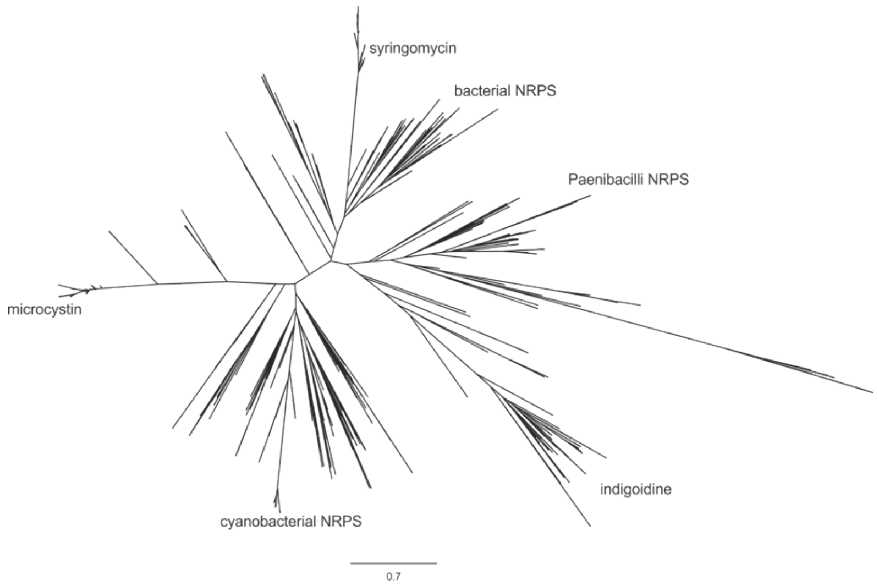

Figure 5.14: Phylogeny based on A-domain homology. A phylogenetic tree was constructed based on a sequence alignment of the psi-blast results of the A domain BpsA (in total 5000 sequences). Sequences were aligned using Muscle and tree constructed using Fasttree. The tree was visualized using Figtree and Dendroscope.

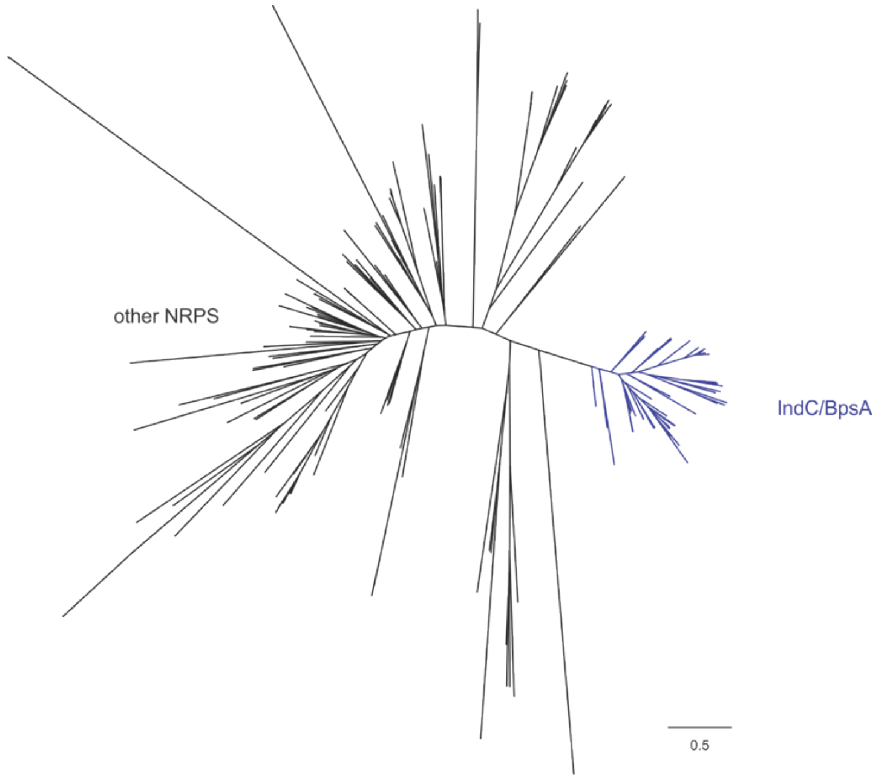

Figure 5.15: Phylogeny based on PCP-domain homology. A phylogenetic tree was constructed based on a sequence alignment of the psi-blast results of the PCP domain BpsA (in total 500 sequences). Sequences were aligned using Muscle and tree constructed using Fasttree. The tree was visualized using Figtree and Dendroscope.

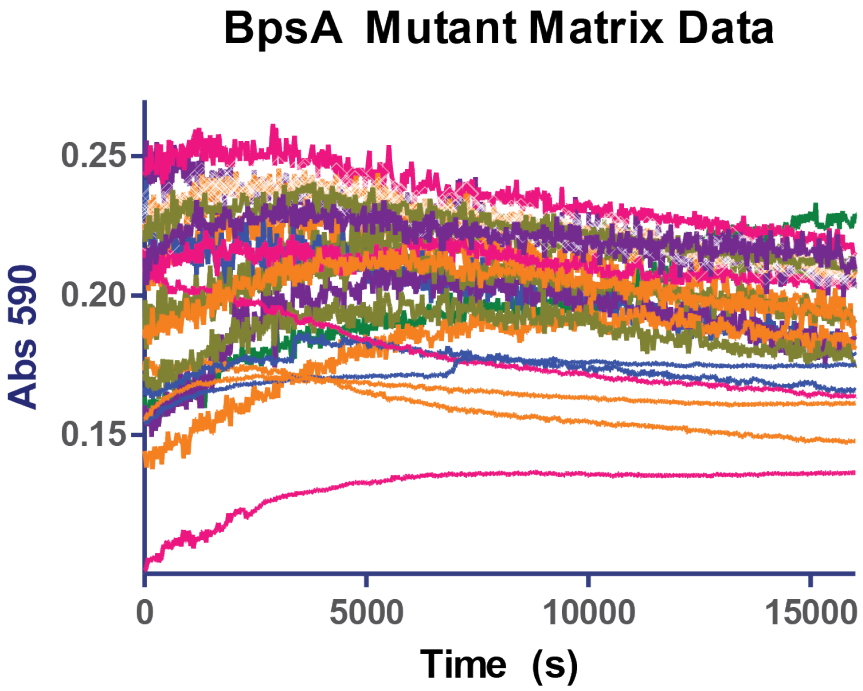

Figure 5.16: Absorbance curves of all BpsA mutants and mutant combinations. No significant measurable activity was recorded for any mutants when compared to WT. Variations in absorbance may be due to protein aggregation or cofactor degradation.

5.6.3 Synthesis of inhibitors

General Methods

Chemicals were obtained from various sources (Fluka, Sigma-Aldrich, Fisher, TCI and Acros). All reactions were carried out under an argon atmosphere in dry solvents and constant magnetic stirring. TLC analysis was performed using silica gel 60 F254 plates (EM Scientific) and visualized using an appropriate stain: 2,4-dinitrophenylhydrazin for PMB protecting group containing compounds, cerium molybdate for azides, ninhydrin for amines and potassium permanganate for pantetheine analogs. Flash chromatography was carried out with Silicycle 60 230-400 mesh. UPLC analysis was performed on a Waters Acquity system using an Acquity binary solvent manager, an Acquity column manager, a 2777c robotic autosampler, an Acquity TUV detector and a SQ detector. Compounds were separated on a BEHC18 1.7 μm 2.1 $\times$ 50mm UPLC column at 0.8 mL/min using a linear gradient of 95% H_2O containing 0.1% formic acid to 85% acetonitrile containing 0.1% formic acid in 2 min. The column was maintained at 55°C. High-res ESI mass spectra were obtained at the UC San Diego mass spectrometry facility using a Micromass Quattro Ultima Triple Quadrupole MS. Small molecue NMR spectra were obtained on a 400 Mhz Varian Mercury Plus spectrometer, a 500 Mhz JEOL ECA 500 spectrometer and a 500 Mhz Varian VX500 equipped with a XSens 2-channel cold probe.

L-Gln-sulfonamide-adenosine: **L**-Gln sulfonamide-adenosine was synthesized in four linear steps from adenosine. Adenosine was protected, reacted with synthesized sulfamoyl chloride, coupled with NHS-activated and Boc protected **L**-Gln, followed by global deprotection. **((3aR,4R,6R,6aR)-6-(6-amino-9H-purin-9-yl)-2,2**

-dimethyltetrahydrofuro[3,4-d][1,3]dioxol-4-yl)methanol[S10] **(S1):**

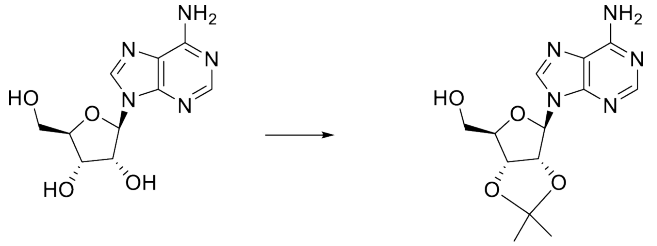

Figure 5.17: Synthesis of protected adenosine **S1**

Adenosine (1.0 g, 3.7 mmol) was suspended in 50 mL acetone under argon. Dropwise addition of 800 μL of $HClO_4$ gave a clear solution. After 2 h the solution was treated with concentrated NH_4OH until the pH was 7. The solvent was evaporated and the product **S1** was purified by flash chromatography using CH_2Cl_2/MeOH (95% yield). ^{1}H NMR (400 MHz, DMSO-d6) δ = 1.30 (3H, s), 1.53 (3H, s), 4.24 (2H, m), 4.47 (1H, m), 5.01 (1H, m), 5.25 (1H, m), 6.09 (s, 1H), 6.48 (1-2H, br s), 8.00 (1H, s), 8.16 (1H, s); ESI-MS *m/z* 310.4

Sulfamoyl chloride[S11] **(S2):**

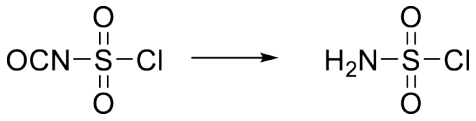

Figure 5.18: Synthesis of **S2**

Chlorosulfamoyl isocyanate (1.0 g, 7 mmol) was placed in a dry three-neck flask, equipped with a $CaCl_2$ drying tube. Formic acid (270 μL) were added dropwise by syringe, while cooling the flask with ice. A vigorous reaction occurred and the mixture turned turbid. The reaction was stirred for 30 min at rt and the reaction was diluted with benzene and evaporated to yield the desired product, which stained with ninhydrin (70%), and was used without further purification.

((3aR,4R,6R,6aR)-6-(6-amino-9H-purin-9-yl)-2,2 -dimethyltetrahydrofuro[3,4-d][1,3]dioxol-4-yl)methyl sulfamate (S3):

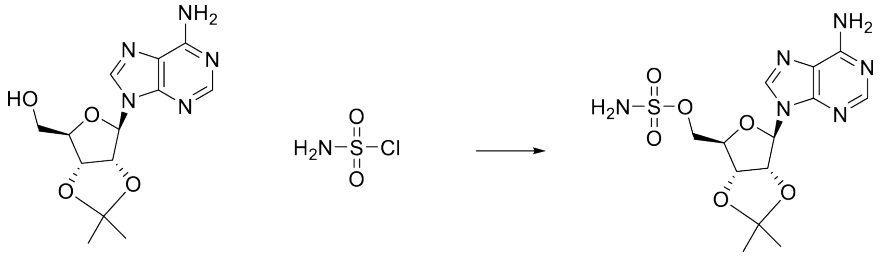

Figure 5.19: Synthesis of **S3**

To a magnetically stirred solution of NaH (84 mg of a 60% suspension in mineral oil, 2.5 mmol) in dioxane, under argon at 0 °C, was added 2',3'-*O*-isopropylideneadenosine **S1** (500 mg, 1.6 mmol) dissolved in dioxane. After 1 h, **S2** (3.2 mmol, 370 mg) was added and the mixture was allowed to warm to rt and stirred for 24 h. Methanol (mL) was added and the solvent was evaporated. The crude material was purified by flash chromatography using CH_2Cl_2/MeOH. (75%) ^{1}H NMR (400 MHz, DMSO-d6) δ = 1.29 (3H, s), 1.52 (3H, s), 4.22 (1H, m), 4.95 (1H, m), 5.31 (2H, m), 6.12 (1H, s), 7.36 (1H, bs), 7.43 (1H, bs), 8.15 (1H, s), 8.33 (1H, s); ESI-MS m/z 387.1

((3aR,4R,6R,6aR)-6-(6-amino-9H-purin-9-yl)-2,2 -dimethyltetrahydrofuro[3,4-d][1,3]dioxol-4-yl)methyl ((tert-butoxycarbonyl)-D-glutaminyl)sulfamate[S12] **(S4):**

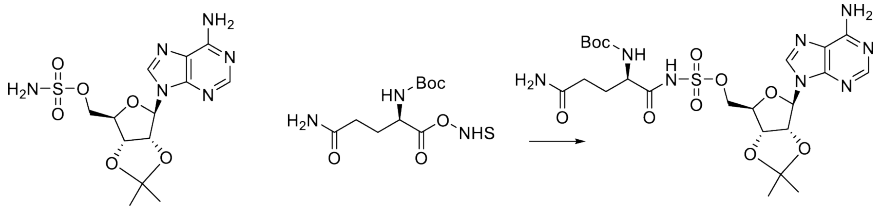

Figure 5.20: Synthesis of **S4**

Boc-**L**-Gln-OH (1 g, 4 mmol) was dissolved in CH_2Cl_2 (mL) at 0° C and N-hydroxysuccinimide

(500 mg, 4.3 mmol) and EDC (800 mg, 4.2 mmol) were added. The reaction mixture was maintained at 4°C for 16 h and the solvent was evaporated. The crude material was dissolved in dH_2O (mL) on ice, carefully acidified to pH 4 with 1M HCl, extracted with EtOAc (100 mL), and the aqueous layer basified to pH 10 with 1M NaOH, extracted with EtOAc (mL) and the combined extract was dried with Na_2SO_4 and evaporated. Compound **S3** (200 mg, 0.5 mmol) was dissolved in dry DMF and DBU (80 μL, 1eq.) added. The NHS-activated ester (151 mg, 1 eq.) was dissolved in DMF and was added dropwise to the solution, followed by stirring for 16 h at rt. The mixture was diluted with dH_2O (100 mL) and extracted with EtOAc (3 $\times$ 100 mL). The combined organic extracts were washed with H_2O (100 mL) and brine (100 mL), and the product was purified by flash chromatography using CH_2Cl_2/MeOH (70%). ^{1}H NMR (400 MHz, $CDCl_3$) δ = 1.21 (s), 1.29 (s), 1.48 (s), 2.17 (m), 2.55 (m), 4.12 (m), 4.34 (s), 5.82 (m), 5.95 (br s), 7.26 (s), 7.79 (s), 7.91 (s), 8.08 (s), 10.06 (s); ESI-MS *m/z* 615.2

((2R,3S,4R,5R)-5-(6-amino-9H-purin-9-yl)
-3,4-dihydroxytetrahydrofuran-2-yl)methyl
(L-glutaminyl)sulfamate[12] (1):

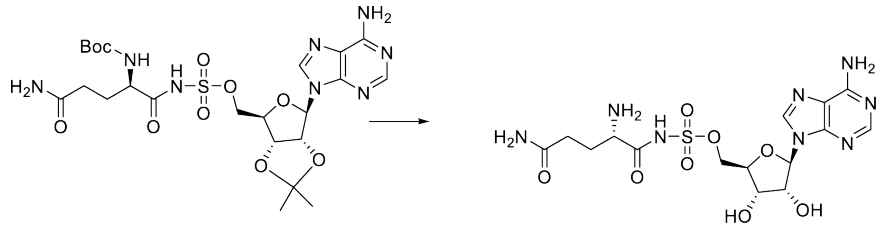

Figure 5.21: Synthesis of **1**

Compound **S4** (40 mg, 0.07 mmol) was dissolved in CH_2Cl_2 and chilled to 0°C. An equal amount of 20% TFA in CH_2Cl_2 was added and the reaction stirred for 2 h. The

reaction was evaporated and used as is. (90%) ^{1}H NMR (500 MHz, DMSO-d6) δ = 10.70, 8.31, 8.09, 7.33, 5.84, 4.57, 4.12, 3.93, 3.12, 2.55, 2.03, 1.93, 1.68; ^{13}C NMR (100 MHz, DMSO-d6) δ = 27, 31, 49, 51, 62, 71, 74, 88, 116, 118, 140, 149, 152, 156, 174, 176.

4H-benzo[d][1,3]oxathiin-2-one[13] (2):

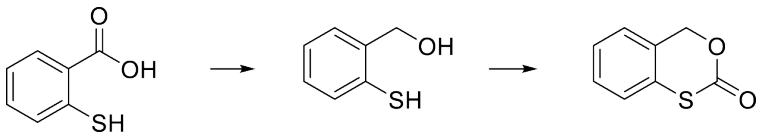

Figure 5.22: Synthesis of **2**

A solution of 2-mercaptobenzoic acid (0.5 g, 3.2 mmol) in THF (10 mL) was added dropwise to a mixture of $LiAlH_4$ (0.3 g, 7.9 mmol) in THF (20 mL) at 0°C. The mixture was stirred at rt under argon. After 3 h, dH_2O (10 mL) and 6M HCl (5 mL) were added dropwise at 0°C. The resulting mixture was poured into additional dH_2O (50 mL) and extracted with EtOAc (3 × 100 mL). The organic layer was dried over anhydrous Na_2SO_4, filtered, and concentrated to give the alcohol as a brown oil (0.44 g, 98%). To avoid oxidation of the thiophenol, the crude oil was carried on without purification and was dissolved in CH_2Cl_2 (50 mL). Carbonyl diimidazole (0.56 g, 3.44 mmol) was added to the mixture portionwise over 1 min. The reaction mixture stirred under argon at rt. After 14 h, dH_2O (50 mL) was added and the aqueous layer was extracted with CH_2Cl_2 (2 × 50 mL). The organic layers were collected, dried over anhydrous Na_2SO_4, filtered, and concentrated to give a crude yellow oil. Flash chromatography with silica gel and CH_2Cl_2 (R_f = 0.63 (CH_2Cl_2)) gave 4H-benzo[d][1,3]oxathiin-2-one as a white crystalline solid (0.39 g, 74% yield, 2 steps). m.p. 58-60°C. ^{1}H NMR (500 MHz, $CDCl_3$) δ 7.30-7.41 (m, 4H), 5.29 (s, 2H); ^{13}C NMR (125 MHz, $CDCl_3$) δ 166.6, 131.2, 129.9, 128.9, 127.8, 126.8, 126.5,

72.0; FT-IR: 1687, 1581, 1471, 1447, 1388, 1248, 1218, 1161, 1137, 1108, 1062, 1000, 971, 939, 870, 837, 751 cm^{-1}; HRMS (ESI-TOF) *m/z* [M+H]+ calcd. for $C_8H_7O_2S$, 167.0167; found, 167.0156.

Glutamine-pantotheinamide: The synthesis of PMB-protected pantetheine amine S5 has been described elsewhere.[S14] Here, we coupled Boc and trityl protected L-Gln to **S5** and deprotected the final product.

tert-butyl (1-((4R)-2-(4-methoxyphenyl)-5,5-dimethyl-1,3-dioxan-4-yl) -1,5,10,14-tetraoxo-16,16,16 -triphenyl-2,6,9,15-tetraazahexadecan-11-yl)carbamate (**S6:**)

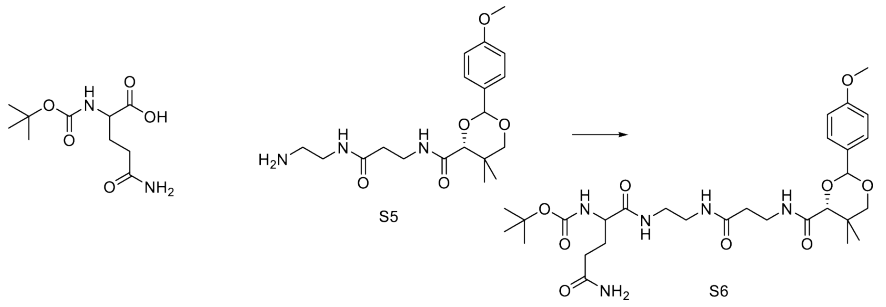

Figure 5.23: Synthesis of **S6**

Compound **S5** (100 mg, 0.2 mmol) was dissolved in 2 mL dry DMF at 0°C, and Boc-L-Gln-OH (80 mg, 0.2 mmol), HOBt (63 mg, 0.4 mmol) HOBt and EDC (80 mg, 0.4 mmol) were added. DIPEA (70 μL, 0.4 mmol) was added and the pH of the solution controlled by further small additions of DIPEA. The reaction mixture was allowed to warm to rt and was stirred overnight. dH_2O (100 mL) was added and the suspension extracted with EtOAc (3 × 100 mL). The combined organic layers were washed with dH_2O (100 mL) and brine (1000 mL), dried with Na_2SO_4, and evaporated. The crude material was purified by flash chromatography using CH_2Cl_2/MeOH. (90% yield).

2-amino-N1-(2-(3-((R)-2,4-dihydroxy-3,3-dimethylbutanamido)propanamido)ethyl) pentanediamide (3):

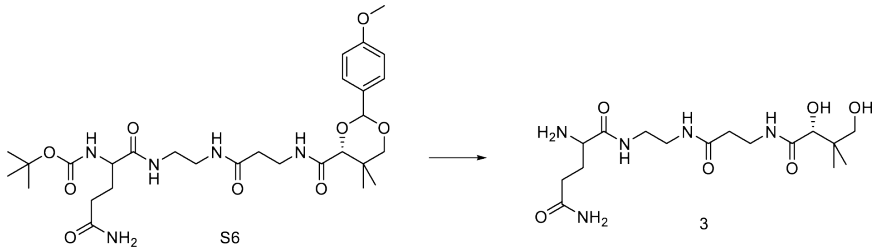

Figure 5.24: Synthesis of **3**

Compound **S6** (50 mg) was dissolved in CH_2Cl_2 (1 mL) at 0°C. 20% TFA in CH_2Cl_2 (2 mL) was added and the reaction stirred for 2 h at rt. The reaction was evaporated and **3** was used as is. (99% yield)

AEBSF-pantotheinamide: The commercially-available AEBSF (Pefabloc) with its amine-terminated extension, was used to synthesize a reactive pantetheinamide analog. For spacing, we extended pantothenic acid with aminobutyric acid.

2,5-dioxopyrrolidin-1-yl 3-((4R)-2-(4-methoxyphenyl)-5,5 -dimethyl-1,3-dioxane-4-carboxamido)propanoate[S15]**(S7):**

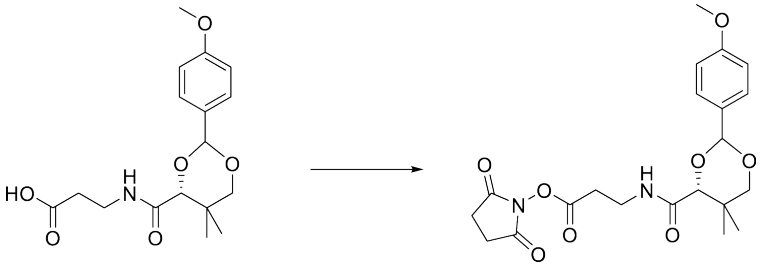

Figure 5.25: Synthesis of **S7**

PMB-protected pantothenic acid (300 mg, 0.9 mmol) and NHS (100 mg, 0.9 mmol) were dissolved in THF (2 mL) at 0°C. EDC (0.9 mmol) and DIPEA (0.9 mmol) were added and the reaction mixture was stirred overnight. The solvent was evaporated, and **S7** was purified by flash chromatography using CH_2Cl_2/MeOH (90%).

4-(3-((4R)-2-(4-methoxyphenyl)-5,5-dimethyl-1,3 -dioxane-4-carboxamido)propanamido)butanoic acid (S8):

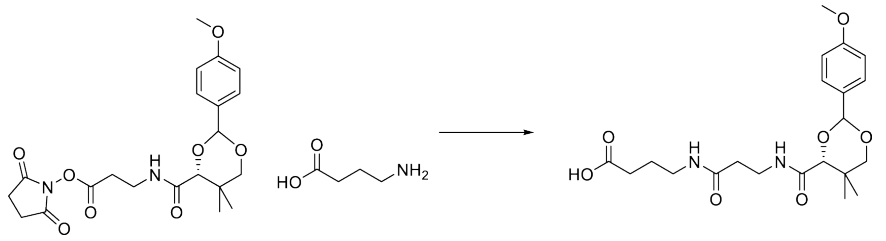

Figure 5.26: Synthesis of **S8**

Compound **S7** (200 mg, 0.5 mmol) was dissolved in CH_2Cl_2 (mL), aminobutyric acid (50 mg, 0.5 mmol) was added, and the reaction mixture was stirred overnight at rt. The product was purified by flash chromatography using CH_2Cl_2/MeOH (65% yield)

2,5-dioxopyrrolidin-1-yl 5-(3-((4R)-2-(4-methoxyphenyl)-5,5 -dimethyl-1,3-dioxane-4-carboxamido)propanamido)pentanoate (S9):

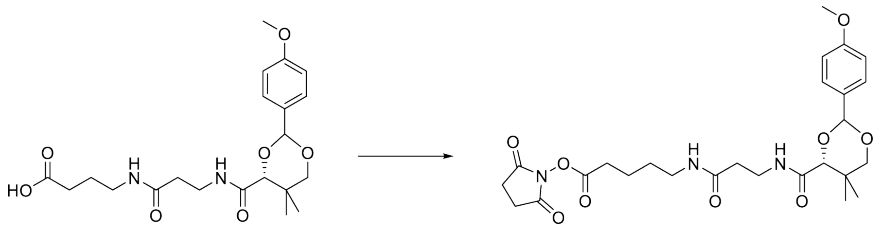

Figure 5.27: Synthesis of **S9**

Compound **S8** (200 mg, 0.5 mmol) and NHS (57 mg, 0.5 mmol) were dissolved in THF (2 mL) at 0°C. EDC (0.9 mmol) and DIPEA (0.9 mmol) were added and the reaction mixture stirred overnight. The solvent was evaporated and **S9** was purified with flash chromatography using CH_2Cl_2/MeOH (90% yield).

4-(2-(4-(3-((4R)-2-(4-methoxyphenyl)-5,5-dimethyl-1,3 -dioxane-4-carboxamido)propanamido)butanamido)ethyl)benzenesulfonyl fluoride (S10):

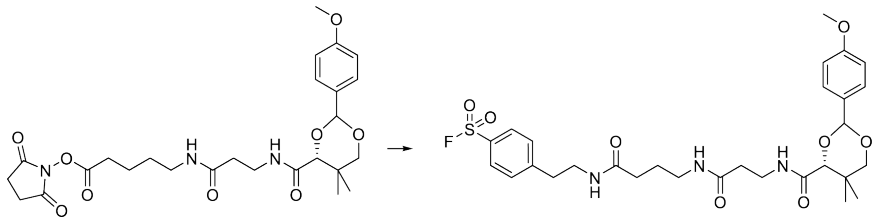

Figure 5.28: Synthesis of **S10**

Compound **S9** (40 mg, 0.08 mmol) was dissolved in CH_2Cl_2 at 0°C, followed by addition of AEBSF (15 mg) and stirred overnight, while being allowed to warm to rt. **S10** was purified by flash chromatography using CH_2Cl_2/MeOH (90% yield).

(R)-4-(2-(4-(3-(2,4-dihydroxy-3,3-dimethylbutanamido) propanamido)butanamido)ethyl)benzenesulfonyl fluoride (5):

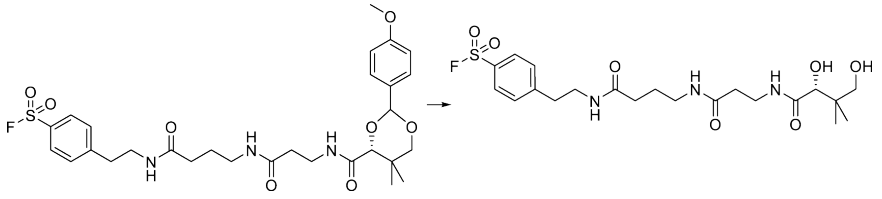

Figure 5.29: Synthesis of **5**

Compound **S10** (40 mg, 0.08 mmol) was dissolved in 80% aqueous acetic acid (5 mL) and stirred overnight at rt to afford **5** as a (90% yield).

5.6.4 Supporting References

S1. Jeremy, G. O.; Janine, N. C.; David, F. A. *Biochem. J.* **2011**, *436*, 709.

S2. Worthington, A. S.; Burkart, M. D. *Org. Biomol. Chem.* **2006**, *4*, 44.

S3. Nakano, M. M.; Corbell, N.; Besson, J.; Zuber, P. *Mol. Gen. Genet* **1992**, *232*, 313-321.

S4. Boratyn, G. M.; Schaffer, A.; Agarwala, R.; Altschul, S. F.; Lipman, D. J.; Madden, T. L. *Biol. Direct* **2012**, *7*, 12.

S5. Edgar, R. C. *Nucleic Acids Res.* **2004**, *32*, 1792.

S6. Tamura, K.; Peterson, D.; Peterson, N.; Stecher, G.; Nei, M.; Kumar, S. *Mol. Biol. Evol.* **2011**, *28*, 2731.

S7. Huson, D. H.; Scornavacca, C. *Syst. Biol.* **2012**, sys062.

S8. Thompson, J. D.; Gibson, T.; Higgins, D. G. *Curr. Protoc. Bioinformatics* **2002**, *2.3*. 1-2.3. 22.

S9. Beld, J.; Cang, H.; Burkart, M. D. *Angew. Chem. Int. Ed.* **2014**, *53*, 14456.

S10. Vertuani, S.; Baldisserotto, A.; Varani, K.; Borea, P. A.; Cruz, B. D. M. M.; Ferraro, L.; Manfredini, S.; Dalpiaz, A. *Eur. J. Med, Chem.* **2012**, *54*, 202.

S11. Kato, D.-I.; Tatsumi, T.; Bansho, A.; Teruya, K.; Yoshida, H.; Takeo, M.; Negoro, S. *J. Mol. Catal. B: Enzym.* **2011**, *69*, 140.

S12. Finking, R.; Neumller, A.; Solsbacher, J.; Konz, D.; Kretzschmar, G.; Schweitzer, M.; Krumm, T.; Marahiel, M. A. *Chembiochem* **2003**, *4*, 903.

S13. McCulloch, I. P. ; La Clair, J. J.; Jaremko, M. J.; Burkart, M. D. manuscript in review **2016**.

S14. a) Blatti, J. L.; Beld, J.; Behnke, C. A.; Mendez, M.; Mayfield, S. P.; Burkart, M. D. *PloS one* **2012**, 7, e42949; b) J. L. Meier, M. D. Burkart, *Methods Enzymol.* **2009**, *458*, 219.

S15. Patrone, J. D.; Yao, J.; Scott, N. E.; Dotson, G. D. *J. Am. Chem. Soc.* **2009**, *131*, 16340.

Chapter 6

Conclusion and Outlook

Aerobic flavoenzymes are crucial to the redox chemistry toolkit available to ogansims in the biosynthesis of a vast array of natural products. Deciphering the complex reactivity to perform these reactions can be an enigmagatic puzzle that endures as an important topic of investigation. From novel biosynthetic mechanisms that promote remarkable reactions, to targeted inhibitors and probes of activity, to studies that unravel the enzymology of biosynthetic domains, flavoenzymes provide a rich field of inquiry to pursue.

Addressed in this dissertation, were reviews of aerobic flavoenyzmes in biosynthesis and applications in chemical biology that discussed the current state of these topics. Within this context we described the synthesis of reactive benzothiocarbonate inhibitors, the first fluorescent probes that were demonstrated to react with an array of aerobic flavoenzymes, and an investigation into the enzymology of BpsA that featured the benzothiocarbonate inhibitor.

To consider the larger perspective, we can revisit the work flow diagram introduced in Chapter 3 that lays out the possible objectives that can be accomplished

with this inhibitor type, and is consistent with the inhibitor probe objectives of the Burkart laboratory (Figure 6.1). Described in this dissertation were studies that provided responses to the first two, often daunting, objectives, which were the successful design and synthesis of the benzothiocarbonate inhibitors and probes (objective 1) and the successful demonstration of enzyme activity with these tools (objective 2). These tools were illuminating from both an applications-based fluorescent tagging perspective (Chapter 4), and a biosynthetic mechanisms perspective (Chapter 5).

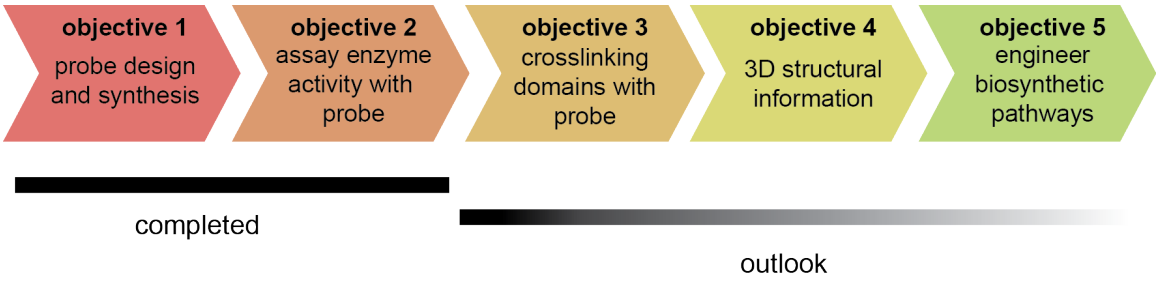

Figure 6.1: Completed and future objectives for investigation of the benzothiocarbonate mechanism-based inhibitor probe.

In consideration of the outlook for this ongoing area of study, objectives three to five are lofty goals, but are squarely within reach. Namely, objective three, which is to develop and demonstrate crosslinking of a flavoenzyme and its cognate protein, is of high interest. Consistent with the inquiries of our lab, crosslinking two such species can elucidate the protein-protein interactions that facilitate substrate processing, which provides a basis for understanding how these domains function and their potential for manipulation.

In fact, a model system for developing this crosslinker would consist of the previously mentioned halogenase, PltA, and its cognate carrier protein, PltL. Development of a probe with a pantetheine portion adjoined with the benzothiocarbonate warhead may prove useful in crosslinking PltA and PltL as a stable complex (Figure

6.1), completing objective three. A stabilized complex may be suitable for investigating three-dimensional structural properties that dictate this interaction.

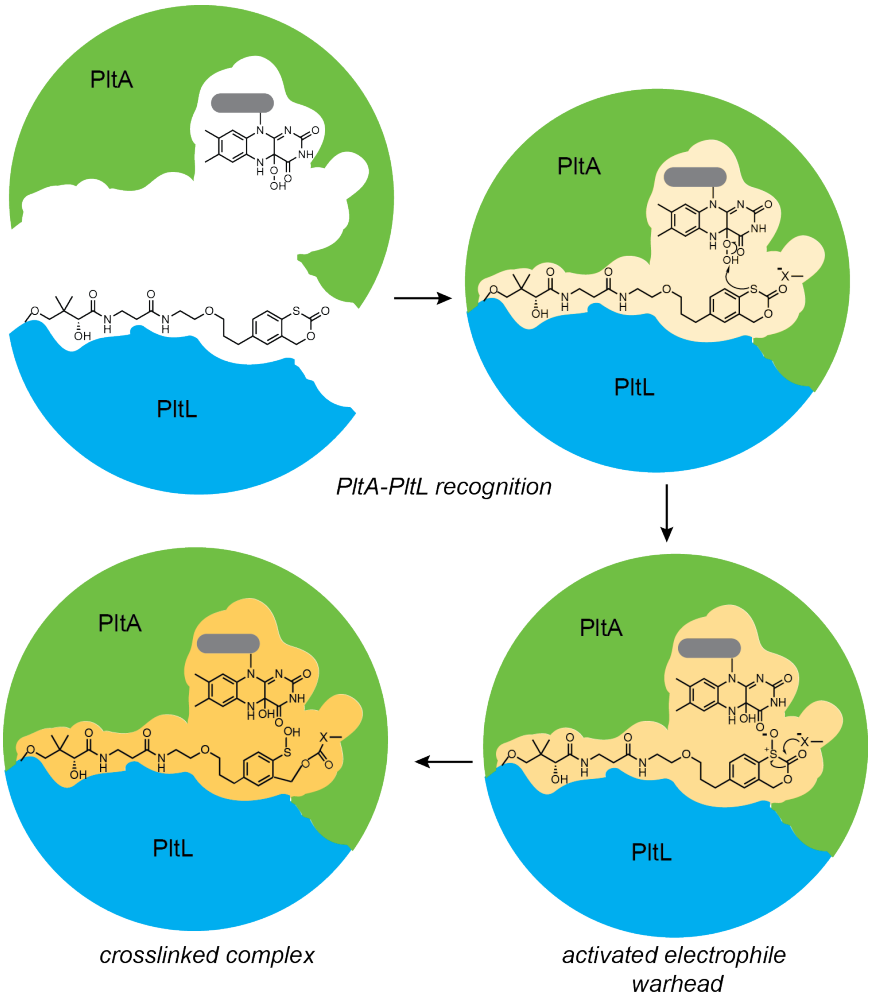

Figure 6.2: Crosslinking scheme of PltA and PltL.

With a better knowledge of systems such as PltA and PltL from the pyoluteorin biosynthetic pathway, we can endeavor to make use of them by application of our understanding, or by manipulation of the pathways that govern the complex synthetic chemistry that is inherent to life itself.